A Study of Injector Aging Eects on the Spray and Combustion in a Diesel Engine

Zhu, Xinda

2020

Document Version:
Publisher's PDF, also known as Version of record

A Study of Injector Aging Effects on the Spray and Combustion in a Diesel Engine

A Study of Injector Aging Effects on the Spray and Combustion in a Diesel Engine

by Xinda Zhu

LUND
UNIVERSITY

Thesis for the degree of Doctor of Philosophy in Engineering

Thesis main advisor: Professor Öivind Andersson
Thesis co-advisor: Professor Martin Tunér
Faculty opponent: Professor Ingemar Denbratt

To be presented, with the permission of the Faculty of Engineering of Lund University, for public criticism in the KC:A lecture hall at the Kemicentrum, LTH on Friday, the 5th of June 2020 at 10:15.

Organization
LUND UNIVERSITY

Department of Energy Sciences
Box 117
SE–221 00 LUND
Sweden

Document name
DOCTORAL DISSERTATION

Date of disputation
2020-06-05

Sponsoring organization

Author(s)
Xinda Zhu

Title and subtitle
A Study of Injector Aging Effects on the Spray and Combustion in a Diesel Engine:

Abstract

In this work a series of experimental studies are conducted to investigate the impacts of injector aging on the fuel injection and the combustion, with a focus on the soot process.

Reference tests are first conducted using new and aged injector sets on a multi-cylinder engine. A significantly higher fuel flow rate is observed when using the aged injectors, indicating that there is probably no influence from any deposits. Four fuels are tests to study the effects of certain fuel additives, which include a baseline fuel and three blends of the baseline fuel and additives representing different functions. It is found 2-ethylhexyl nitrate (2-EHN) is able to reduce the ignition delay without influencing the emission. Tripropylene-glycol methyl ether (TPGME) can work as a soot reducer even when the engine is operated at a very lean condition. A flow improver with quaternary ammonium salt(s) is supposed to be able to improve the fuel flow, but this phenomenon is not observed at the selected operating points.

Optical diagnostics are conducted on an optical engine to investigate the spray behavior and the soot process using one selected injector from each group. While the initial response of the injectors are similar, a longer injection duration is observed with the aged injector, meaning the closing stage of the injector needle causes the most difference. Shorter injection events are relatively more affected than a long injection. A higher amount of fuel dribbling after injection is also recorded with the aged injector. X-ray tomography results show smooth needle surfaces and nozzle holes without significant geometric difference, which excludes the effects of worn injector parts, meaning the flow difference is mainly caused by the needle actuation.

Laser induced incandescence and laser extinction are used for the late-cycle soot oxidation measurements. Soot oxidation rate at low load is more sensitive to the temperature difference while the TPGME additive shows a larger impact on the soot oxidation rate at medium load.

Key words
Diesel Combustion, Liquid Spray Formation, Injector Aging, Diesel Combustion, LII, LEM, Natural Luminosity, Mie-Scattering, TPGME

Classification system and/or index terms (if any)

Supplementary bibliographical information

Language
English

ISSN and key title
0282-1990

ISBN
978-91-7895-467-4 (print)
978-91-7895-469-8 (pdf)

Recipient's notes

Number of pages
172

Price

Security classification

A Study of Injector Aging Effects on the Spray and Combustion in a Diesel Engine

by Xinda Zhu

LUND
UNIVERSITY

A doctoral thesis at a university in Sweden takes either the form of a single, cohesive research study (monograph) or a summary of research papers (compilation thesis), which the doctoral student has written alone or together with one or several other author(s).

In the latter case the thesis consists of two parts. An introductory text puts the research work into context and summarizes the main points of the papers. Then, the research publications themselves are reproduced, together with a description of the individual contributions of the authors. The research papers may either have been already published or are manuscripts at various stages (in press, submitted, or in draft).

Funding information: The thesis work is financially supported by the European Union Horizon 2020 Research and Innovation Programme, grant agreement ID: 675528, and the KCFP Engine Research Center.

Faculty of Engineering, Department of Energy Sciences

ISRN: LUTMDN/TMHP-19/1159-SE
ISBN: 978-91-7895-467-4 (print)
ISBN: 978-91-7895-469-8 (pdf)
ISSN: 0282-1990

Printed in Sweden by Tryckeriet i E-huset, Lund University, Lund 2020

Contents

List of publications

This thesis is based on the following publications, referred to by their Roman numerals:

I **Performance of New and Aged Injectors with and without Fuel Additives in a Light-Duty Diesel Engine**
X. Zhu, Ö. Andersson.
Submitted to Transportation Engineering

II **High-Speed Imaging of Spray Formation and Combustion in An Optical Engine: Effects of Injector Aging and TPGME as a Fuel Additive**
X. Zhu, M. N. Mannazhi, N. Palazzo, P. E. Bengtsson, Ö. Andersson.
Submitted to Energies special topic edition on Advanced Modelling and Experimental Methods for Engine Combustion Analysis

III **Soot Oxidation Studies in an Optical Diesel Engine Using Laser-Induced Incandescence and Extinction**
M. N. Mannazhi, X. Zhu, Ö. Andersson, P. E. Bengtsson.
To be submitted to Fuel

Acknowledgements

Time really flies as this project is already approaching an end. It's a great pleasure to work and study here during these years. This journey wouldn't be so amazing without awesome companions.

First of all, I am grateful for having Professor Öivind Andersson as my main supervisor. Thank you for sharing your knowledge and especially your deep understanding of experimental methodology with me. They are extremely helpful. Your patient guidance and critical feedback make the learning curve much less steep for me. Many thanks to the other seniors Martin, Per and Sebastian as well for all the academic inputs and casual talks.

A great amount of help also comes from my colleagues at LTH. I'd like to thank the optical group Marcus, Mike, Sara, Ted, Slavey, Miao for sharing knowledge and experiences about engines and diagnostics. Thanks Lianhao, Xiufei, Pablo, Carlos and Vikram for all the help with LabVIEW. Thanks Peter, Sam, Marcus.T, Prakash, Yann, Jessica, Mengqin, Nika, Maja, Amir, Changle, Ola, Andre and if any I forget to mention here for sharing interesting topics in different research areas. Special thanks to my office mates Kenan, Erik, Nhut and our regular visitor Niko. You brought tons of interesting topics and most importantly, high energy, to the office. I really enjoyed being in those conversations. Thanks all for sharing your life and experiences during the Friday presentations and small talks.

Very special thanks to Manu and Professor Per-Erik Bengtsson in the physics department. I appreciate all the lab time and discussions with you. I've received a great amount of help from you. Thanks Alexios and Zhenkan for the occasional inputs. Thanks the LTT group: Javad, Vikrant, Natascia, Sebastian, Andreas, Lucas and Professor Michael Wensing for a warm host during my secondment at FAU Erlangen-Nuremberg. Thanks all colleagues in this EU project for the good time we shared.

Our great technician team certainly deserves a big thank you. Mats, Martin, Tomas, Tommy, Patrik.J, Patrik.L, Anders. Your work is the foundation of a functional lab. I've learned many practical skills from you. Thanks the administration team Catarina, Gity, Elna, Isabelle for organizing the general things and Robert for IT support.

Finally I must thank my family, friends and my girl friend for all the support.

Popular summary in English

The fast societal development in the past decades has driven the energy demand to record high levels. As we are enjoying various products from all over the world and travelling more often and further, the transportation sector is taking account of a large share in the total energy consumption and emissions.

Nowadays, the majority of the transportation sector still relies on internal combustion engines as a main power source. As a mature and robust energy conversion solution, it is widely used in many ways: from generators to construction machines, from cars to ships. Compression ignition engines, or so-called diesel engines, are particularly favoured thanks to their relatively high efficiency.

However, diesel engines have two major drawbacks: mainly the nitric oxides and the particulate emissions. Intensive research of the adverse effects of these emissions on the environment and human health have been conducted during the years. To mitigate the effects of these pollutants from an increasing number of vehicles in use, the legislations for the road transportation sector have been tightened significantly. This forces the engine technology to evolve to meet the requirements.

The fuel-air mixing process in a diesel engine is demonstrated to be the dominating factor for improving combustion efficiency and emissions, especially the particulate emissions. Modern fuel injection systems are capable of fast and precise fuel delivery. Coupled with exhaust after-treatment systems, the tailpipe emissions have achieved drastic reduction. On the other hand, efforts are made to search for alternative fuels, usually bio-based, to reduce the dependence on fossil products and to reduce greenhouse gas emissions. Thus, the fuel composition becomes more complex and the fuel quality may vary locally due to the blending of alternative components with fossil fuel.

These combined factors raise a challenge to the fuel system. As they consist of ultrafine components such as needles and nozzle orifices, they are less tolerant to aging and fuel variation. A disrupted fuel injection may influence the combustion significantly, leading to elevated emissions, lowered efficiency or even engine damage. Hence, it is important to investigate potential aging effects of the injection systems on fuel injection and combustion.

This thesis provides an insight into injector aging and additive effects by using optical diagnostics. The fuel spray formation, combustion heat release and soot formation/oxidation are investigated in detail. The results can be used as feedback to the future injection system design and control strategy development to

better cope with the aging problems.

To investigate the aging effects of injectors, an experimental approach is established, with special focus on the soot formation and oxidation. First, reference tests are conducted on a multi-cylinder engine at low to medium load, representing real-world driving conditions. New and aged injectors are tested in comparison and the results reveal a significantly higher fuel flow rate from the aged injectors using the same injection strategies. Consequently,the power output and emissions are influenced. Three fuel additives, including a soot reducer, a flow improver, and an ignition improver are blended with a baseline fuel for tests as well. Compared with the baseline fuel, these additives show marginal effects on the combustion and emissions.

Next, selected injectors are tested on an optical engine where in-cylinder processes can be studied. It is found that the higher fuel quantity from the aged injector is caused by the injector closing later than the new one. A larger amount of fuel dribbling at the end of the injection event is also observed. Shorter injection events in which the injector needle does not reach a full lift are particularly affected. The analysis shows a similar spray formation from both injectors, indicating that the nozzle geometry is not affected by aging. Thus, the hypothesis of injector deposits and worn nozzles are eliminated.

Finally, laser-based measurements are performed to investigate the late cycle oxidation of soot. The soot oxidation rates demonstrate a larger impact of temperature variance at low load while at medium load the soot reducer works better.

Populärvetenskaplig sammanfattning på svenska

Utvecklingen under de senaste decennierna har drivit efterfrågan på energi till rekordhöga nivåer. Då vi ständigt använder olika produkter från hela världen och reser oftare och längre, står transportsektorn för en allt större andel av den totala energiförbrukningen och utsläppen.

Transporterna drivs fortfarande med förbränningsmotorer som huvudsaklig kraftkälla. Då dessa utgör en mogen och robust energiomvandlingslösning används de på många sätt: från generatorer till anläggningsmaskiner, från bilar till fartyg. Motorer med kompressionständning, så kallade dieselmotorer, är särskilt populära tack vare deras relativt höga energieffektivitet.

Dock har dieselmotorn två stora nackdelar, nämligen utsläppen av kväveoxider och partiklar. Intensiv forskning av dessa utsläpps effekter på miljön och människors hälsa har bedrivits under åren. För att minska effekterna av ett ökande antal fordon har utsläppslagstiftningen också skärpts väsentligt. Detta tvingar fram en ständig utveckling av ny motorteknik för att uppfylla kraven.

Blandningsprocessen mellan bränsle och luft har visat sig vara den dominerande faktorn för att uppnå effektiv förbränning och låga utsläpp, särskilt av partiklar. Moderna bränsleinsprutningssystem kan tillföra bränslet snabbt och exakt och i kombination med avancerade avgasefterbehandlingssystem har utsläppen från avgasröret drastiskt reducerats. Samtidigt ökar användningen av alternativa bränslen, vanligtvis biobaserade sådana, för att minska beroendet av fossila bränslen och för att minska utsläppen av växthusgaser. Således blir bränslesammansättningen mer komplex. Bränslekvaliteten kan dessutom variera från plats till plats.

Dessa kombinerade faktorer utgör en utmaning för bränslesystemet, som idag har ultrafina komponenter i form av nålar och munstycken. Dessa blir därmed känsliga för åldringseffekter och variationer i bränslekvalitet. En störd bränsleinsprutning kan ha betydande påverkan på förbränningen, vilket ofta leder till förhöjda utsläpp, sänkt effekt och ibland till och med motorskador. Därför är det viktigt att undersöka effekterna av potentiella åldringseffekter i insprutningssystemet.

Denna avhandling ger en inblick i hur åldrade insprutare och bränsleadditiv påverkar förbränningen. Detta studeras med optisk diagnostik. Spraybildning, förbränning och bildning/oxidation av sot undersöks i detalj. Resultaten kan användas inom den framtida utvecklingen av insprutningssystem och styra strategierna för att bättre hantera problemen med åldring.

För att studera åldringseffekter hos insprutare tas här ett experimentellt angreppssätt fram som speciellt fokuserar på bildning och oxidation av sot. Först genomförs referenstest på en motor i driftspunkter med låg och mellanhög belastning, som motsvarar verklig körning. Nya och åldrade insprutare jämförs och resultaten visar att de åldrade ger betydligt högre bränslemängder med en given insprutningsstrategi. Härmed påverkas också motorns effekt och avgasutsläpp. Testen jämför också tre bränsletillsatser, nämligen en sotreduktionstillsats, en flödesförbättrare och en antändningsförbättrare. Dessa tillsatser visar sig dock ha begränsad effekt på förbränning och avgasutsläpp.

I nästa steg testas utvalda insprutare på en motor med optisk access, där bränslesprayer och sot kan avbildas i cylindern. Den högre bränslemängden från den åldrade insprutaren bekräftas bero på att den stänger senare än den nya. En större mängd bränsleläckage syns också efter stängningen. Kortare insprutningar, då insprutaren inte når full öppning, är särskilt påverkade. Analysen visar liknande spraybildning med båda insprutarna, vilket innebär att insprutarens inre form inte påverkats under åldringen. Slutsatsen är att åldringen varken leder till uppbyggnad av beläggningar eller slitage inuti hålen.

Slutligen utförs laserbaserade mätningar för att studera sotförbränningen sent under cykeln. Sotförbränningstakten påverkas mer av temperaturen vid lägre motorbelastning. Vid högre belastning fungerar additivet för sotreducering bättre.

Acronyms

aHRR apparent heat release rate

aTDC after top dead center

bTDC before top dead center

EGR exhaust gas re-circulation

EOI end of injection

ICE internal combustion engine

$IMEP_g$ gross indicated mean effective pressure

LEM laser extinction method

LII laser induced incandescence

NL natural luminosity

NO nitric oxide

NO_2 nitrogen dioxide

NO_x oxides of nitrogen

PAHs poly-cyclic aromatics

SOI start of injection

TDC top dead center

TPGME tripropylene-glycol monomethyl ether

2-EHN 2-ethylhexyl nitrate

Chapter 1

Introduction

In this chapter, the general background of this thesis work is given first. Then the research questions are revealed by motivating the the research purposes. The scope and approach are briefly described in the end.

1.1 Background

The energy consumption in the transportation sector takes a large share of the total global energy consumption. The growing demand of transporting goods and travelling lead to an estimation that the energy demand will keep increasing in the near future, with oil being the dominating resource [1].

Internal combustion engines (ICEs) are still the major power source in the transportation sector. From small passenger cars to mega ships, ICEs are widely applied because of their accessibility and robustness. Compression-ignition engines, or the so-called diesel engines, are usually favoured thanks to their relatively high efficiency and low-speed torque output, making them ideal for propelling medium to heavy duty vehicles. They are almost exclusively used in trucks, buses and ships.

The fundamental working principle of diesel engines, injecting liquid fuel into a chamber with compressed air and releasing the chemical energy in the fuels, decides that they have emissions from the tailpipes. One of the major drawbacks of diesel engines is emission of toxic pollutants, mainly oxides of nitrogen (NO_x) and soot. Over the years the impacts of these pollutants on human health and environment are studied extensively [2, 3, 4, 5]. The revealing of their pernicious

effects is driving the emission legislation increasingly stringent. Lots of effort is put into the development of modern diesel combustion systems focusing on lower emissions and higher efficiencies. A considerable evolution in the engine technologies has been achieved.

Rising concerns about air pollution and drastic climate change caused by greenhouse gases also make powertrain electrification a hot topic currently. Much attention is drawn towards the development of electric powertrains. However, it seems no scalable solutions that can fully replace ICEs in the coming years exist. Furthermore, whether an electrical powertrain is truly beneficial for the environment requires detailed life cycle analysis of the vehicles and highly depends on how the electricity is generated locally. Further research and discussion are necessary before making any conclusions. Meanwhile, renewable fuels with lower carbon footprint from bio-based components or renewable electricity are emerging in the market [6], which brings new challenges and opportunities to ICEs. Hence, more potentials of ICEs are to be explored, which makes research and development of ICEs remain highly relevant.

1.2 Motivation

One crucial point to achieve a better diesel combustion is the fuel-air mixing process. Diesel fuel is heavier than gasoline and is injected into the cylinder without premixing with air. It is difficult to break up, atomize, evaporate and mix fuel with air sufficiently in a short time. The unevenly distributed fuel and air is the main cause of the NO_x and soot emissions. The significant improvement of diesel emission is achieved by combining aftertreatment systems and advanced combustion systems, e.g.exhaust gas recirculation (EGR) and multiple injections, etc.

Aftertreatment systems are very effective for controlling the toxic emissions. However, they require a certain temperature to operate and usually rely on additional substances input for the catalyst, which inevitably reduces efficiency and increases cost. The evolution of fuel injection systems shows its potential to reduce emissions and to increase efficiency by simply providing a more flexible and precise fuel delivery [7, 8]. Injectors are particularly important in the fuel system since they have direct impact on the fuel spray.

High injection pressure and finer injector nozzle holes are demonstrated to be able to enhance the air entrainment in the fuel jets upstream of the combustion zone, which can reduce the soot emissions significantly [9, 10, 11]. On the other

hand, multiple-injection strategies also show great effects on emission reduction [12, 13].

Fossil fuels are refined products of crude oil which contain thousands of components. Their quality may vary slightly depending on the environment of storage, locations and seasons. Often fuel additives are necessary to improve the base fuels' chemical and physical properties. Furthermore, the progress of switching to low-carbon emission fuels, such as blending bio-contents in the fossil fuel or even using complete renewable fuels, makes the fuel composition more complex. The fuel systems should be able to cope with diverse conditions, keeping their performance and maintaining compliance with emission legislation through their lifespan.

The combination of the aforementioned factors increases the probability of injector aging as ultra-fine components in the injectors are less tolerant to aging effects, e.g.erosion and deposits. Faulty or aged injectors can have negative influences such as reduced efficiency, power loss, high emissions or even engine damage [14]. Considering passenger cars usually have a lifespan of at least 10 years and over 200 000 km while trucks can easily reach 1 000 000 km, injector aging effects cannot be neglected.

Thus, investigations of the injector performance at different stages in their lifespan are necessary to provide critical feedback to the control strategy development and to the future injection system design.

1.3 Scope and Approach

In this thesis work, an experimental approach is established to investigate some aged diesel injectors, with special focus on the fuel jet development, in-cylinder soot processes and effects of some common fuel additives. Comparison of same model injectors at different lifespan stages is performed.

A general reference test is conducted on a multi-cylinder engine first to find the performance and emission difference between the injector sets. One of the new injectors and one of the aged injectors, which show significant performance difference, are selected to be used in the subsequent experiments. Then optical measurements and laser-based diagnostics are applied on an optically-accessible version of the multi-cylinder engine to study the in-cylinder processes. Coupled with a high speed camera, Mie-scattering is used to image the fuel injection process. Then the combustion process is also imaged and the natural luminosity (NL) signal is interpreted in detail, which is used as an indicator of the in-

cylinder soot. Finally, combined laser induced incandescence (LII) and laser extinction method (LEM) measurements are used to further trace the in-cylinder soot process in the late cycle.

Chapter 2

Diesel Combustion

In this chapter, some detailed background relevant to this work is introduced. Conventional diesel combustion is discussed briefly first, followed by a close look at two quasi-steady reacting diesel jet models. Then the parameters that can influence the liquid fuel penetration and spreading angle are summarized in short. Since soot emissions are a particular focus, in-cylinder soot process is also introduced. Next, the structure of a typical diesel injector and some injector aging effects are illustrated. Finally, the roles of fuel additives are given in short.

2.1 Diesel Combustion General Background

2.1.1 Conventional Diesel Combustion Process

Nowadays most diesel engines are equipped with direct injection systems, in which the fuel is injected directly into the cylinder. For this reason, the conventional diesel combustion process illustrated here is based on direct injection diesel engines.

A typical conventional diesel combustion usually consists four stages as illustrated in Figure 2.1. The first stage is called the ignition delay period, which is the time gap between the start of injection (SOI) and the start of combustion. During this stage, high pressure fuel is injected into the cylinder where the air has been compressed and thereby heated. Momentum exchange occurs between the liquid fuel and the ambient air. The liquid fuel jet breaks into small droplets,

atomized and finally evaporates. When the evaporated fuel mixes with air and reaches a flammable equivalence ratio, and the temperature around the top dead center (TDC) is sufficiently high, auto-ignition occurs. Then the second stage called the premixed combustion starts. The elevated temperature and pressure from the initial ignition locations rapidly induces the ignition of the rest of the mixture. Hence, the heat release rate usually shows a sharp peak within a short period.

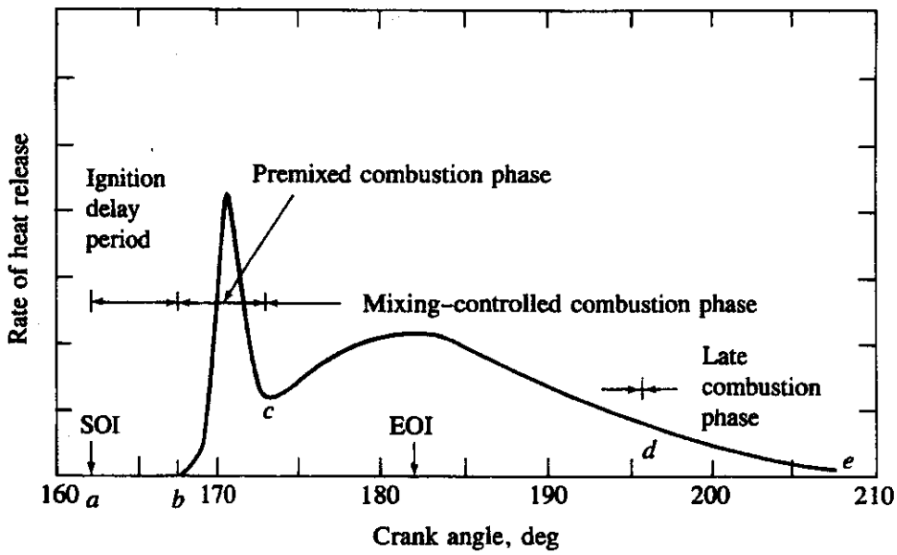

Figure 2.1: Heat release from a conventional diesel combustion. (Adapted from [15].)

After the premixed combustion, while most mixture formed during the ignition delay is consumed and the fuel injection is still going on, the mixing-controlled combustion stage appears. The heat release rate during this time is primarily limited by the fuel-air mixing process. Depending on different operating conditions, the shape of the mixing-controlled heat release rate may differ. There could be a second peak higher than the premixed combustion or there could be no peak. But generally it decays soon after the end of injection (EOI). After the EOI, the fuel-air mixing continues for some time and the rate is reduced significantly. Heat release is continued at lower rate into the expansion stroke where intermediate combustion products are being oxidised at a much slower rate mostly due to reduced mixing rate and temperature.

2.1.2 Quasi-Steady Diesel Jet Models

In the past decades, with the help of optical diagnostics, the structure of a reacting diesel jet could finally be revealed based on detecting different species at different moments of the in-cylinder processes.

A detailed in-cylinder process model from the SOI to a quasi-steady reacting diesel jet is established by Dec based on experimental researches using combined laser diagnostics on an optically accessible engine [16]. This model provides fundamental understanding of a diesel in-cylinder process, which is now widely accepted. The structure of a quasi-steady reacting jet is illustrated in Figure 2.2.

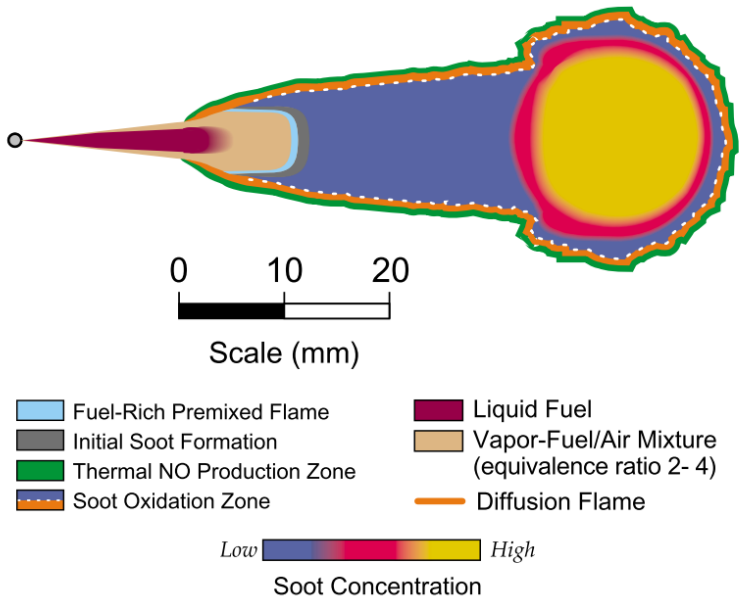

Figure 2.2: A conceptual model of quasi-steady reacting diesel jet by Dec. (Reproduced from [16].)

Immediately after leaving the injector nozzle, the liquid fuel starts to break up and ambient air is entrained. The hot air soon vaporises the liquid fuel droplets and a rich mixture layer surrounding the liquid jet is formed. As the fuel injection and air entrainment continue, the liquid fuel jet reaches its maximum penetration when the injection rate and vaporization rate reach a balance. Then fully evaporated mixture is driven further downstream to form a rich gaseous mixture zone, surrounded by a thin layer of premixed combustion. Initial soot

formation commences close to this premixed combustion region. The jet flow and diffusion effect drive the intermediate combustion products, including most of the early stage soot, outwards from the jet center where it mixes with ambient air to oxidise. Thus, a high temperature diffusion flame layer is formed where combustion is close to a stoichiometric condition. Thermal nitric oxide (NO) is also produced along this layer due to the high temperature. The unoxidized initial soot particles, together with other intermediate combustion products, travel further towards the tip of the jet where a vortex region is formed. Particle growth and agglomeration occur during this travel, making the jet tip a high soot concentration area.

Although this model is fairly complete, it has its limitations [16]. One is that the standing fuel-rich premixed flame and the thin soot layer along the diffusion flame is hypothesized, so verification is necessary. Another is that depending on the operating conditions, different fuels and injectors, the model needs to be extended to be valid in a various situations. Effects of wall interactions and swirl are the third point to be considered.

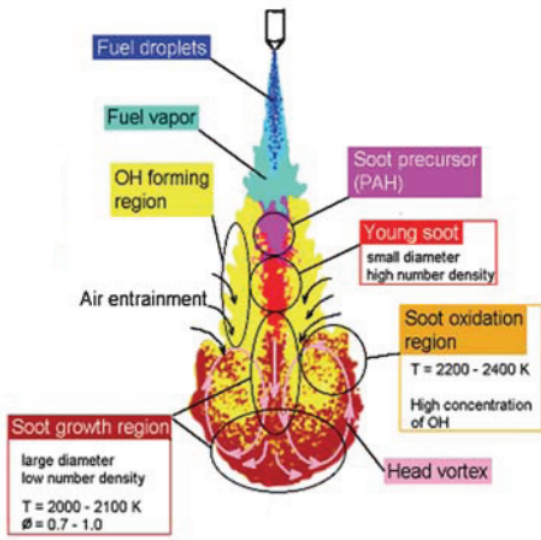

Figure 2.3: A conceptual model of quasi-steady reacting diesel jet by Kosaka. (Reproduced from [17].)

Later, another conceptual model based on experimental studies in a rapid compression machine (RCM) from Kosaka reveals the missing details just downstream of the fuel rich region [17, 18, 19]. The low-temperature oxidation and initial hot ignition process are investigated by identifying formaldehyde (H_2CO)

in the fuel spray. A more detailed soot process in a quasi-steady reacting diesel jet is built as shown in Figure 2.3. Poly-cyclic aromatic hydrocarbons (PAHs) and young soot are found just downstream the rich fuel vapor, replacing the thin premixed flame and the initial soot formation regions in Dec's model. Soot particles grow to larger forms while traveling to the jet tip and are redirected back to the sides of the jet periphery by the vortex in the tip region. Soot oxidation occurs when the redirected soot meets the entrained air from the side. The middle periphery of the jet is replaced with a more clear air entrainment illustration where OH is found, indicating the diffusion combustion areas [20].

2.1.3 Liquid Phase Fuel Penetration and Jet Spreading Angle

As indicated by the two conceptual models in the previous section, soot is initially formed in the middle of a reacting diesel jet. This makes the air entrainment critical phase since this process affects the equivalent ratio in the vapor phase significantly. A too long liquid penetration usually means a less ideal air entrainment, often leading to severe spray impingement and wall-wetting.

The liquid phase fuel penetration of the jet is defined as the distance between the injector nozzle hole and the point where all fuel is vaporized. Note although it is referred as 'liquid length' here, it is not an entire intact liquid form of fuel. Liquid breakup occurs really close to the nozzle [21, 22]. In a quasi-steady state this point is stabilized in a region where the vaporization rate is equal to the injection rate. Fluctuation inevitably exists due to influences from the turbulence [23].

The liquid penetration length can be affected by various factors. A wide range of in-cylinder parameters are investigated to find which can influence the liquid fuel penetration [24, 25, 26]. The orifice diameter of the nozzle is found to have a close-to-linear effect on the liquid penetration length. A reduced diameter decreases the liquid penetration. The pressure drop across the orifice shows very little impact on the liquid fuel penetration. With an increasing temperature or ambient density, the liquid length decreases in a non-linear manner. A denser and hotter ambient condition can increase the air entrainment in the liquid fuel phase and increase the vaporization rate, leading to a reduced liquid length. How much the liquid length can be reduced also depends on the properties of the fuel. A diesel-like fuel with lower 90% distillation point (or a lower boiling point for a single component fuel) has a shorter liquid penetration. However, the situation can be different if the fuels have a significant difference in their latent heats of vaporization.

The jet spreading angle depends on the densities of the fuel and the ambient air [27]. A denser ambient environment and a lower fuel density increases the jet spreading angle. The injector needle structure, sac volume design and orifice geometry have influences on the jet spreading angle as well [28, 29]. A larger spreading angle usually indicates a better air entrainment which decreases the penetration speed because of the conservation of momentum [30]. It needs to be noted that other parameters can probably also affect the jet spreading angle. There has not been any relatively complete understanding of the effects of those parameters established due to the highly turbulent multi-phase conditions. Furthermore, different definitions of the jet spreading angle exist due to lack of commonly accepted measurement procedure [27].

2.1.4 Flame Lift-off

The flame lift-off length is the distance between the injector nozzle and the most upstream combustion location in the reacting jet [30]. The lift-off position influences the upstream air entrainment since it decides the distance available for fuel-air mixing before the mixture reaches the combustion zone. Figure 2.4 shows how, depending on the operating conditions and nozzle size, the lift-off position can vary significantly. If combustion happens close to the nozzle, the reaction zone can block air from being entrained into the center region. And as discussed previously, the air entrainment is critical to the soot formation and oxidation process. It is estimated that the air entrained upstream of the lift-off point can count for about 20% of the total air required to oxidize all the fuel injected [9].

Key parameters that can affect the lift-off length significantly, including the injection pressure, orifice diameter, ambient air density, temperature and oxygen concentration, have been investigated extensively [31, 9, 32, 33]. An increasing ambient density or temperature decreases the lift-off length since combustion is accelerated in such conditions. Similarly, a higher oxygen concentration can also accelerate the combustion, which leads to a shorter lift-off length. An increasing pressure drop across the orifice or a larger orifice diameter increases the lift-off length. Despite these parameters, other factors such as fuel properties, piston bowl shape and jet-wall interaction may also have strong impact on the lift-off length. Further researches remain to be conducted to provide a more complete picture.

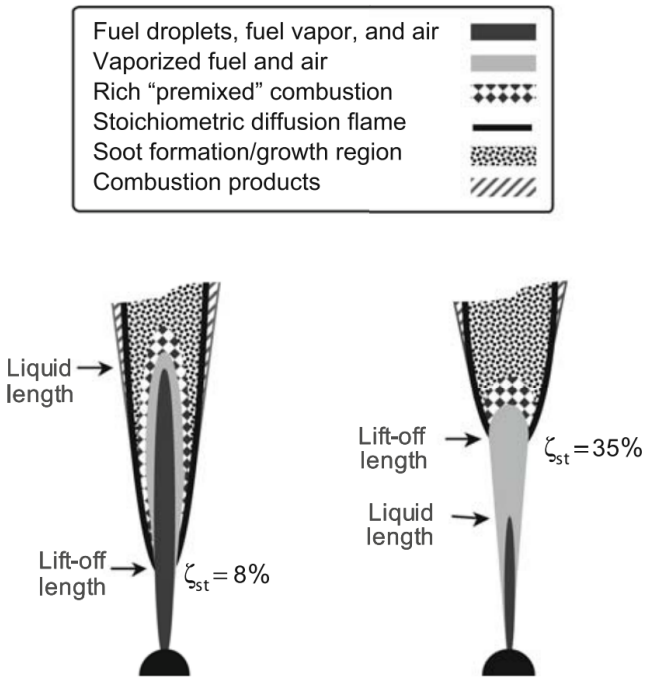

Figure 2.4: Schematics of different lift-off positions under different operating conditions. Left: ambient 1100 K, 23 kg/m^3, orifice pressure drop 40 MPa, diameter 250 μm. Right: ambient 1000 K, 20 kg/m^3, orifice pressure drop 200 MPa, diameter 100 μm. (Adapted from [30].)

2.1.5 Soot Processes in A Diesel Engine

Soot processes in a compression-ignition engine are rather complex, involving both formation and oxidation. Soot usually refers to solid particles consisting mostly of carbon while particulate includes soot, volatile species condensed on the soot and other particles attached. A schematic of soot formation steps is shown in Figure 2.5.

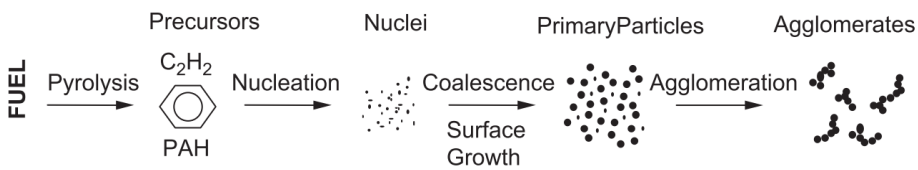

Figure 2.5: A schematic of soot formation process. (Adapted from [34].)

Hydrocarbons can react in a high temperature without oxygen or with very little oxygen. This reaction, called pyrolysis, breaks the original species' structure down and forms new products without significant oxidation. The main products are unsaturated gaseous hydrocarbons, which are considered as main building blocks to form PAHs. The rate of pyrolysis is highly temperature and concentration dependent.

The nucleation process is where gaseous pyrolysis products turn into solid particles. As the initial PAHs are formed and grow with increasing number of unsaturated radicals to a larger size, they are able to develop into solid particle nuclei. As soon as a nucleus is formed, the surface growth starts. The already formed small nuclei provide reactive surfaces which allow other hot gaseous radicals to be attached easily [35]. The majority of soot mass increase occurs during this phase [34]. Depending on the fuels and the formation environment, the structure of the soot in the surface growth phase can vary, which leads to different physical and chemical properties [36].

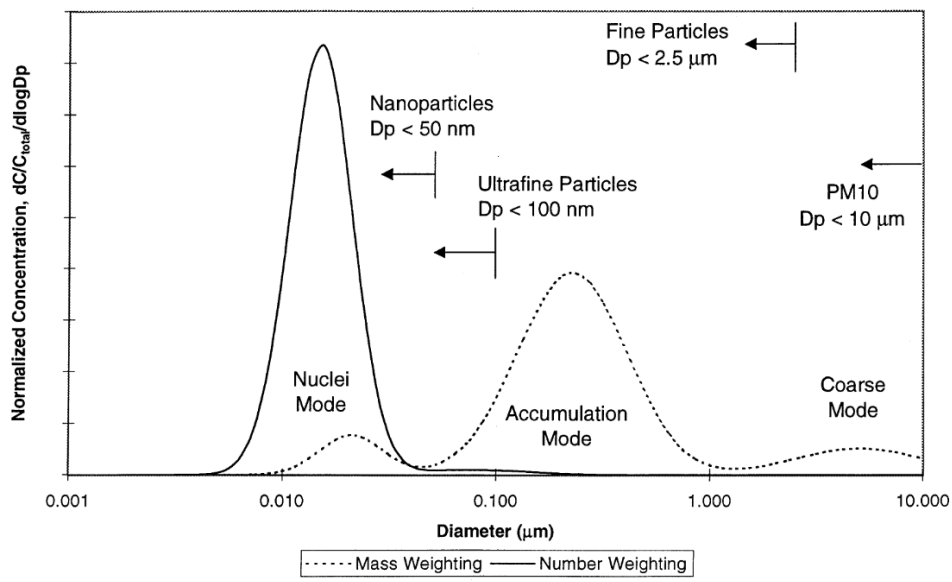

Figure 2.6: A typical engine exhaust soot size and mass distribution. (Adapted from [37].)

When two small soot particles collide and merge into one big particle, coalescence occurs. The total particle mass is conserved while the number is reduced. The coalesced particles, also called the primary particles, usually maintain their shape during the final agglomeration phase. The agglomerates are typically

chain-shaped attached or clumped primary particle groups. Depending on the oxidation process and residence time of the soot particles, the engine exhaust particles have a wide range of size and form, as shown in Figure 2.6.

While the soot formation process follows these steps, the soot oxidation can occur at any time and convert hydrocarbons to CO, CO_2 and H_2O from 1300 K and above [38]. The soot formation and oxidation are a pair of competing processes. Once the carbon in the soot is converted to CO, it is no longer available to be involved in any of the soot processes.

2.2 Diesel Injectors and Aging Problems

2.2.1 Basic Structure of Modern Diesel Injectors

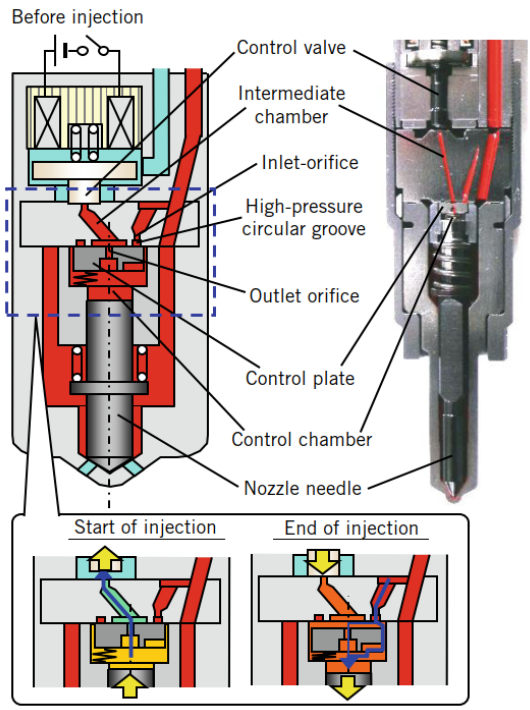

Figure 2.7: A schematic of the injectors used in this work. (Adapted from [39].)

Inside a modern day diesel injector, the design of the nozzle area is usually similar. The needle's position is controlled directly or indirectly by the actuation

components, either a piezoelectric unit or a solenoid, to open or close the fuel channels. Highly pressurized fuel passes the surfaces between the needle and seat and leaves the nozzle orifices in the form of a fuel spray. A schematic of the injectors used in this work is shown in 2.7.

Current diesel injectors usually have five to eight nozzle holes with diameters range from below 50 to 250 µm [40]. There are two common types of nozzle design. One is the sac type and one is the valve-covered-orifice type as illustrated in 2.8. The key difference is that the sac volume can act as a buffering zone during the fuel injection. On the one hand, it makes the sac type injector less affected by needle misalignment, which can cause large hole-to-hole variation in the valve-covered-orifice type. On the other hand, the sac volume makes fuel dribble inevitable after the fuel injection, which decreases the fuel injection precision and can increase the soot emissions.

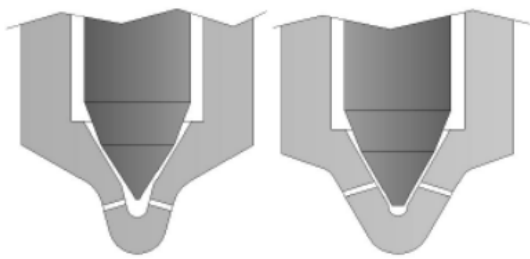

Figure 2.8: Typical nozzle design in diesel injectors. Left: sac type; right: valve-covered-orifice type. (Adapted from [41].)

2.2.2 Diesel Injector Aging and Aging Effects

All these fine injector components such as needles, nozzles and actuation parts ensure a precise fuel injection. At the same time, they make the injectors sensitive to deviations. Any aging effects can have large impacts on the combustion and emissions. Injector faults and related engine faults are among the most common diesel engine problems, including fouling nozzle holes by deposits formation, needle or actuation components stiction, nozzle erosion and leakage caused by other needle problems [14].

2.2.2.1 Deposits

Diesel deposits formation can happen both inside or outside the nozzle, even on the needle surface or on the control components in some cases. The fuel

properties and composition, injector temperature and nozzle geometry are the three key factors that can lead to deposit formation [42].

Small amount of metal contamination (from diffusion in the storage or transportation stages of the fuels) such as Zn and Cu are demonstrated to increase the nozzle coking [43, 44]. Additionally, fuel additives such as fatty-acid based fuel lubricants and some sodium-salt based corrosion inhibitors and drying agents also potentially cause deposition [45, 46]. The use of bio-diesel generally increases the deposits problem due to oxygen components in the fuel and their consequent self-reactions [47, 48]. On the other hand, high temperature around the nozzle area can lead to cracking reactions and reduced stability of bio-based contents, which both can intensify the coking problem [49]. Finally, using multiple nozzles hole with smaller diameters also increase the sensitivity of fouling [50, 51].

One of the key performance indices which can indicate the formation of deposits around the nozzle area is reduced fuel discharge rate due to partially blocked nozzles. Consequently the engine output power is also reduced [52]. Deposits also change the shape of the nozzles, which can reduce the spray quality. Jets can have asymmetric spreading angles, leading to a deteriorated air entrainment process [53]. The spray penetration is usually decreased and the jet distribution is non-uniform [54, 55]. However, depending on the fuel and nozzle geometry design, the spray penetration is found increased due to the impact of deposits in some gasoline injection studies [56, 57]. Deposits on the needle and actuation components can cause sticking problems, leading to a slowed response of the system or even a complete stop [58]. The emission is inevitably affected by injector deposits. Although hydrocarbon and NO_x emissions are usually less influenced, a disrupted fuel spray can degrade the fuel-air mixing quality significantly, leading to a high soot emission [59].

2.2.2.2 Erosion and Wearing

The deposits cause problems by adding material to the surfaces of the nozzle and the needle. It becomes an even bigger problem when material is removed from the injector components. Cavitation-induced erosion can cause severe damage to the surfaces of the nozzles and the needle [60]. Rough irregular surfaces and widened nozzles are usually caused by the shock waves after collapse of the vapor cavities. The jet pattern is thus affected by these changes. A shortened penetration length, a widened jet spreading angle and a reduced discharge rate are observed in some numerical studies [61, 62]. Needle wear can be caused by fuel as well. Such kind of wear usually leads to leakage problems [63].

2.2.2.3 Injector Needle Motion

The injector needle motion is another crucial factor which can affect the fuel injection significantly, especially during the needle lifting and closing phases. At low to medium lift the needle off-axis motion shows big impact on mass flow rate. Large hole-to-hole variation is also observed [64]. The internal flows and a higher number of nozzle holes are found to have larger effects on needle oscillation than the injection pressure and and fuel properties [65]. The so-called after-injection or fuel dribbling are more likely to happen if needle bouncing occurs during the closing stage. An increased gap between the needle and the seat surfaces or an increased stiffness in the valve spring can cause more needle bouncing, and thus a higher quantity of after injection [66].

2.3 Roles of Fuel Additives

To cope with the advancements of fuel system technology and help with emissions, standards for the fuels are also updated during the years. Diesel consists of thousands of individual components with properties varying in a wide range. Commonly, fuel additives are needed to modify certain fuel properties. Selecting a fuel additive requires comprehensive consideration since introducing a substance to a diesel blend can bring multiple changes to both physical and chemical properties. Sometimes not all these property changes are ideal.

The fuel stability is the most important factor to be considered during the transportation and storage stages. Physical properties, such as viscosity, should be stable in a wide temperature range. Pour point depressants are usually required to help diesel cope with low temperature conditions. To ensure a complete mixing of all components so that no separation occurs, dispersants and emulsifiers are often necessary. If there are oxygen components in the fuel, oxidation and bacteria formation problems need to be considered as well.

Additives are also needed when the fuel enters the fuel system. A certain level of lubricity needs to be ensured to protect the fuel system from wearing. Fuel lubricants are often necessary, especially when using ultra-low sulfur diesel with bio-based contents. Deposit formation can be prevented by using additives as well. To improve the ignitability of the fuel, cetane number improver is commonly used. Some additives are also capable of controlling in-cylinder emissions, such as soot reduction effects from some oxygenated additives [67].

Chapter 3

Research Methods

The first part of this chapter gives a brief background of the optical measurement techniques used in this work. Then the experiment related instrumentations and their settings are introduced in detail in the second part, including the injectors, the fuels and the operating conditions used. Finally in the third part, data processing procedures are described, including the heat release analysis and detailed imaging processing of the optical measurements.

3.1 Optical Measurement Techniques

3.1.1 Mie Scattering

Mie scattering is elastically scattered light from particles or droplets that have a diameter similar or larger than the wavelength of the incident light. In diesel jets, the droplet size is typically larger than 1 μm, which is larger than any of the visible light wavelengths usually used as an incident light source [68]. All droplets are assumed to have spherical shape and the same refraction index. Thus, the simple geometrical optical theory can be used to explain the scattering principle. The diffraction and other interference are neglected. The principle is illustrated in Figure 3.1. The refractive index of air n_a is smaller than that of the droplets n_d. Both refraction and reflection occur each time the light meets the air-droplet boundary. The direction of the refracted ray can be calculated using the Snell-Descartes law: $n_a * sin\theta_a = n_d * sin\theta_d$. The Mie signal intensity is dependent on the droplet number, size and diameter. When a large number of particles exist in the medium (optically dense), such as in a diesel spray near the

nozzle, the combined effects of the refraction and the reflection can cause multiple scattering, which can blur the detailed structure of the spray and increase the actual boundary of the spray in the imaging plane.

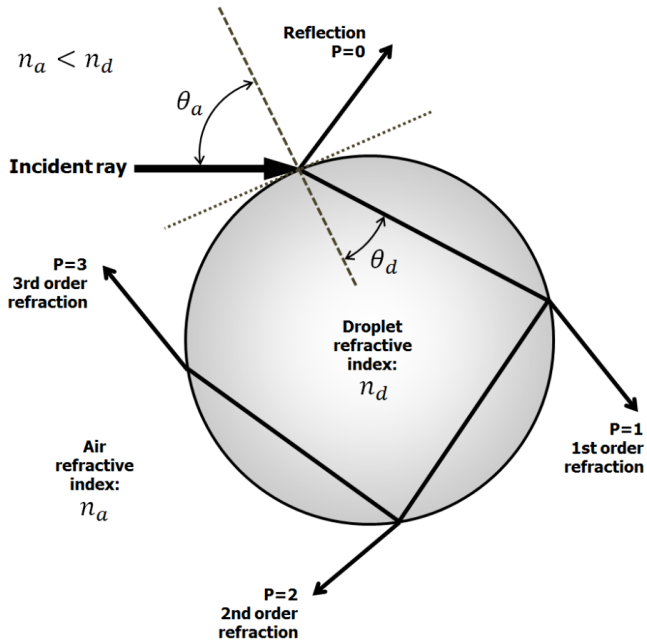

Figure 3.1: Light scattering by a spherical droplet.

3.1.2 Natural Luminosity (NL)

Natural luminosity is a simple yet very useful tool to study the in-cylinder processes. It is often used as a first step optical measurement to characterize the general features before applying any laser-based diagnostics for detailed analysis.

There are two primary components that contribute to the NL signals the most [69]: the chemiluminescence and the soot incandescence. The soot incandescence is usually the dominating part of the NL signals in a diesel combustion, which is from the thermal radiation emitted by hot burning soot. The emission is usually broadband, from ultraviolet to infrared region. On the other hand, the chemiluminescence is a much weaker non-thermal radiation emitted by gaseous intermediate reaction products. Excited by the reaction processes, molecules jump to excited states and come back to the ground state, emitting photons during this relaxation processes. Thus, chemiluminescence consists of various narrow-band emissions from specific species, whose wavelength are usually between 300 nm

and 600 nm.

Note that chemiluminescence must be spontaneous and not excited by energy from outside the system. Otherwise the corresponding signal is called fluoresces. In a highly premixed combustion process where little soot is formed, the chemiluminescence will be the dominating NL signal.

3.1.3 Laser-induced Incandescence (LII)

Although there is no substance that matches a perfect black body definition at the moment, soot particles are usually assumed to be black bodies [70]. Thus, Planck's law can be used to describe the spectral density of the radiation emitted by soot at different temperature:

$$B(\lambda, T) = \frac{2hc^2}{\lambda^5} \frac{1}{e^{\frac{hc}{\lambda k_B T}} - 1} \tag{3.1}$$

where λ is the wavelength of the emission, h is the Planck constant, c is the speed of light in the medium, k_B is the Boltzmann constant and T is the absolute temperature. An illustration of black body spectral radiation at different temperature is shown in Figure 3.2.

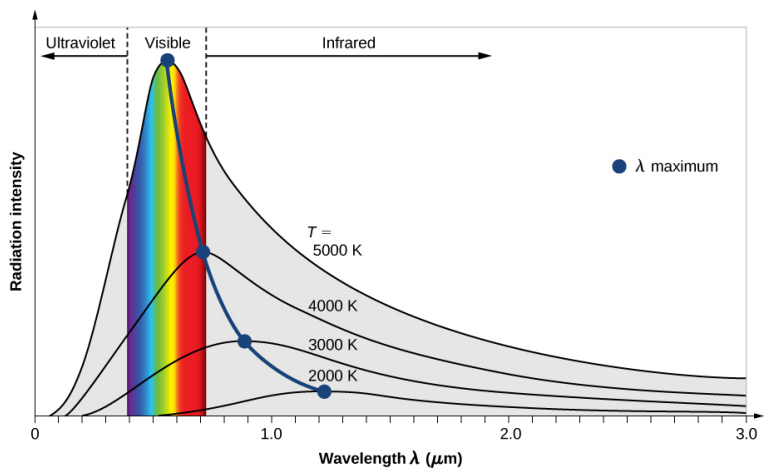

Figure 3.2: Black body spectral radiation at different temperatures.

Wien's displacement law, which states the black body radiation peaks at different wavelengths at different temperature, can be clearly observed. The LII technique

uses this very temperature dependence to distinguish the externally excited soot incandescence from the spontaneous soot incandescence of the NL signal. It is a nearly non-intrusive method which can be used in transient conditions for soot measurement.

The LII occurs when external energy from high-power lasers heats up the soot particles. After absorption of the laser energy, the particles' temperature can increase rapidly to around 4000 K, which is significantly higher than a common flame temperature of around 2000 K [71]. As the high temperature gives rise to very intense radiation at different wavelengths, the radiation of the LII hence can be distinguished by simple filtering of the signals. Multiple processes happen simultaneously during a short time, which can be summarized in an energy balance equation:

$$\frac{dU_{int}}{dt} = \dot{Q}_{abs} + \dot{Q}_{rad} + \dot{Q}_{cond} + \dot{Q}_{sub} + \dot{Q}_{ox} + \dot{Q}_{ann} + \dot{Q}_{therm} \tag{3.2}$$

where U_{int} is the internal energy of the soot, $\dot{Q}_{abs}$ is the heat absorbed from the laser energy, $\dot{Q}_{rad}$ is the heat transfer via thermal radiation, $\dot{Q}_{cond}$ is the conductive heat transfer, $\dot{Q}_{sub}$ is the heat loss via vaporization or sublimation, $\dot{Q}_{ox}$ is the heating rate by oxidation, $\dot{Q}_{ann}$ is contributed by annealing and $\dot{Q}_{therm}$ is the thermionic cooling. A detailed description of these terms can be found in [71].

The detectable LII signal is basically the thermal radiation part. For a single soot particle, its LII signal mainly depends on the particle temperature and detection wavelength [72, 73]. The temperature is dependent on various factors such as laser fluence and ambient conditions. For a soot cloud, it is usually assumed that the LII signal is proportional to the soot volume fraction when detected in the visible wavelength region. Although in fact the linearity can be effected by many parameters, as long as the laser fluence is in a proper region, in which case small variations in laser pulse energy and effects of absorption would not influence the LII signal significantly, and a prompt detection with short gate is used, this assumption can still stands in a high-pressure engine-like application condition [74]. Thus, the soot volume fraction can be semi-quantitatively measured by just using the LII technique. A 2-D imaging of the LII signal can also reveal the soot distribution qualitatively. Fully quantitative soot volume fraction and size measurement are achievable as well with the help from a calibration technique such as light extinction method [75, 76].

3.1.4 Laser Extinction Method (LEM)

As a light beam passes through a soot cloud, both absorption and scattering occur when the light encounters soot particles. The intensity of the light is thus decreased by these two extinction effects, which can be calculated using the Lambert-Beer's law [77], assuming a homogeneous and optically thin media:

$$I_t = I_0 * exp\left(-\int_0^L K_{ext} dx\right) \tag{3.3}$$

where I_t is the transmitted light intensity, I_0 is the incident light intensity, K_{ext} is the extinction coefficient for a particle cloud and L is the path length of the light beam through the cloud. The extinction coefficient can thus be calculated as:

$$K_{ext} = \frac{1}{L} ln\left(\frac{I_0}{I_t}\right) \tag{3.4}$$

Both absorption and scattering contribute to the extinction [78]. The scattering part can be considered in the Rayleigh scattering regime since both molecular intermediate products and primary diesel soot particles are mostly smaller than 100 nm [79], and the wavelength of the incident light normally used are in the visible range of 400 nm to 700 nm. Rayleigh scattering decreases in proportion to the sixth power of particle size [80], which means in the application of LEM, the scattering from both molecules and soot is often small enough to be negligible. In this case the extinction is assumed to be equal to the absorption part of the extinction.

Assuming that the primary soot particles are spherical and isotropic, d is the particle diameter and N is the particle number concentration, the soot volume fraction can be derived as [81]:

$$f_v = N\frac{4}{3}\pi\left(\frac{d}{2}\right)^3 = \frac{\pi}{6} N d^3 \tag{3.5}$$

The absorption coefficient can be defined as [78]:

$$K_{abs} = \frac{\pi^2}{\lambda} E(m) N d^3 = K_{ext} \tag{3.6}$$

where $E(m)$ = -Im $[(m^2-1)/(m^2+2)]$ is the soot absorption function, m is the complex refractive index of soot defined as $m = n - ik$. Using the Nd^3 term in Equation 3.5 and Equation 3.6, the soot volume fraction can be derived as:

$$f_v = \frac{\lambda}{6\pi} \frac{K_{ext}}{E(m)} \tag{3.7}$$

3.2 Experimental Set-ups

3.2.1 Multi-cylinder Engine Set-up and Emission Measurements

The initial reference tests of this thesis are conducted on a multi-cylinder light-duty diesel engine. The stock intake system is replaced with a direct supply of compressed air from the test cell. Stable intake pressure up to 7 bar and intake temperature over 100 °C can be achieved independently for the engine operating conditions. The stock exhaust is replaced with a straight pipe with a back pressure control valve to produce required exhaust gas re-circulation (EGR). The layout is shown in Figure 3.3 and some of the engine parameters are shown in Table 3.1.

The engine speed is directly controlled by an electrical dynamometer. The operating condition control, including intake air and fuel injection, are controlled by a NI LabVIEW-PXI-FPGA system. This system is also able to log all the sensor data. The high speed data such as crank angle and rail pressure are sampled at 0.2 CAD resolution while the slow data channels such as temperature and pressure monitoring are sampled every cycle.

The original high-pressure fuel system is kept while the low pressure circulation system is replaced with an in-house developed system. Fuel is first pumped into a canister which is connected with a high precision weighing scale and then driven by a low pressure pump into the circulation. The scale keeps logging the weight during the measurement, and from these data the fuel consumption rate during a certain period is calculated. Hence, a relatively accurate measure of fuel consumption is limited to steady state operating conditions.

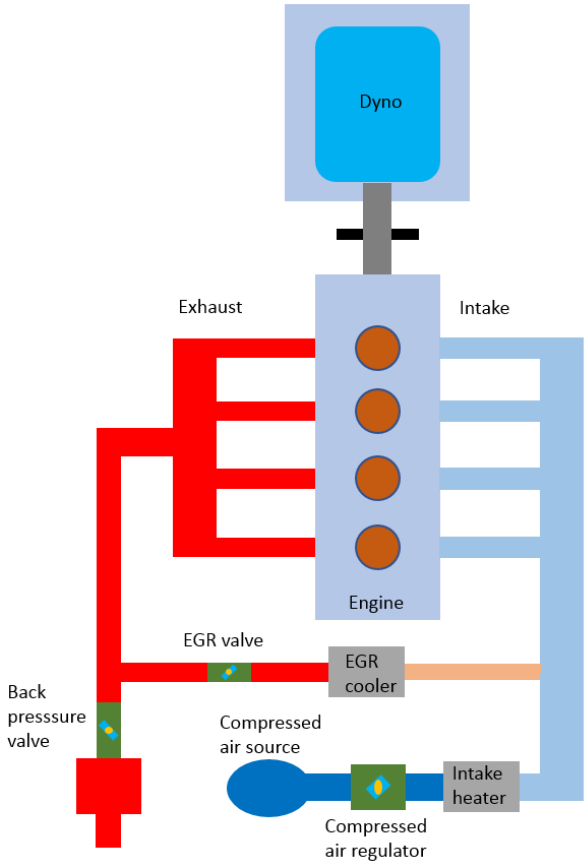

Figure 3.3: Multi-cylinder engine set-up.

Table 3.1: Key parameters of the multi-cylinder engine.

Stroke [mm]	93.2
Bore [mm]	82
Displacement [L]	2
Compression ratio [-]	15.8
Connecting rod length [mm]	147
Combustion chamber design	Re-entrant bowl-in piston

Gaseous emissions are measured by an AVL AMA i60 exhaust analysis system while soot particles are measured by an AVL 483 micro soot sensor. The soot sensor is based on the photo-acoustic principle and is able to detect transient soot concentration at maximum 100 Hz sampling frequency. A wide range of 0.001 - 50 mg/m^3 soot concentration is detectable [82].

3.2.2 Nozzle Imaging Using X-ray Tomography

To investigate if there is damage or metal-based deposits in the injector nozzle, the internal structure of the nozzle needs to be revealed. A couple of methods can achieve this goal. Silicone moulding can obtain the nozzle geometry fairly well [83]. However, the injector must be disassembled and the detection is limited to the nozzle area. Imaging methods can obtain more structure including the needle area and the data is usually easier to process. A direct imaging of the nozzle exits can be achieved using optical microscopy with the limitation that only the close to the nozzle exit part can be visualized. The phase-contrast X-ray imaging can retrieve the internal structure of a injector nozzle very well in a 2-D form. It can even be coupled with high speed camera for imaging transient conditions such as injector needle actuation or internal flow visualization [84].

3-D X-ray tomography is a powerful tool which can extract internal structures. It has been applied to detect injector nozzle successfully [85, 86]. A detailed principle of this method and instrumentation can be found in [87].

In this work a 3-D X-ray tomography is performed on both the selected new injector and the aged injector. A ZEISS Xradia 520 3D X-ray microscope is used with maximum source voltage of 160 kV and a power of 10 W. The region from the nozzle tip to around 5 mm above is scanned, which includes the nozzle holes, the needle head and the needle seat areas. The voxel size is set to be 8 μm, meaning the spatial resolution in each frame is 8 μm/pixel and the distance between two neighbouring slices is also 8 μm. Around 680 slices are acquired in total during each scan. 3-D reconstructions using these image slices are performed later in the 3D slicer software to extract the surfaces of the nozzles.

3.2.3 Optical Engine Set-Up

The optical engine is a Bowditch-type conversion of the multi-cylinder engine which gives optical accesses from both the side and the bottom of the combustion chamber [88]. The design is illustrated in Figure 3.4. The original cylinder head is replaced with a specially built single cylinder head with identical intake manifolds and valve system. An extension structure holds the original engine block and the single cylinder head together. The optical piston, which has a geometry identical to the stock piston, sits on a retainer mounted on the piston extension. The optical liner is mounted on the cylinder head, holding four side windows. Due to a significantly larger crevice volume created by the design,

the geometric compression ratio is reduced to 13.5. Both the windows and the optical piston are made of non-crystalline fused silica to ensure high transmission in the UV region. The mirror underneath the piston is also capable of reflecting UV light.

The intake system consists of two compressors and a diesel burner as an external EGR source. One compressor takes air from the test cell directly and one compressor takes the EGR flow form the burner. Both flows are cooled after compression to remove water first, and mixed to acquire desired oxygen level in the mixture. Finally the mixture is heated up by a heater just before entering the intake manifold. The oxygen level can be as low as 5% so a non-reacting environment can be achieved.

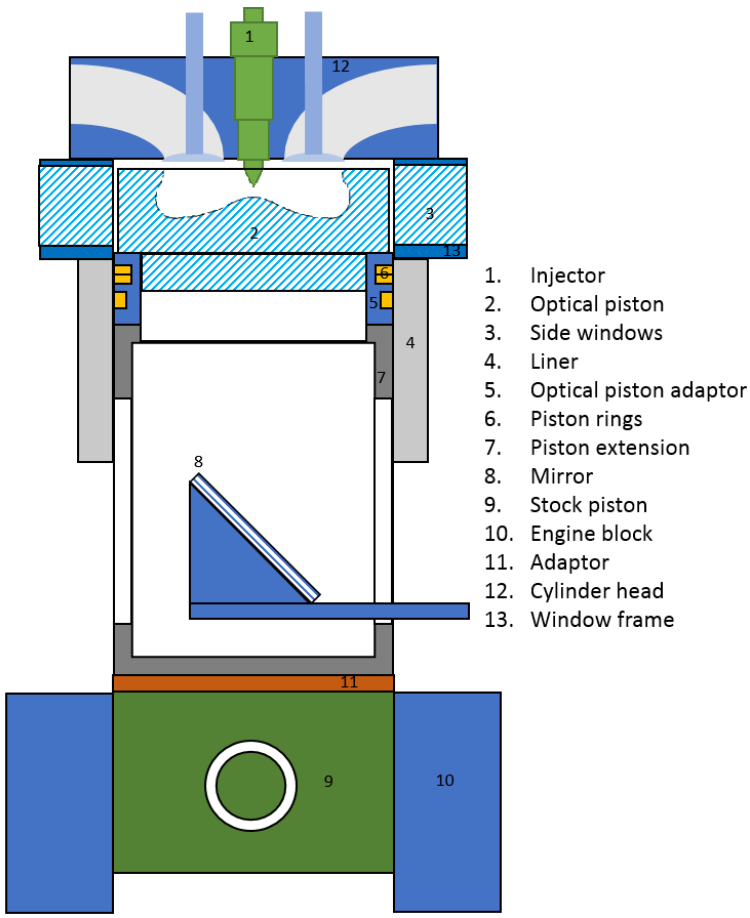

Figure 3.4: Optical engine set-up.

3.2.3.1 Set-up for High-speed Mie Scattering and Natural Luminosity Imaging

Mie scattering is first used to image the liquid phase of the fuel jet. A 452 nm laser diode aims at the front side window. A group of cylindrical lenses transform the point light source to fully covers the entrance of the side window. A Photron SA-5 high speed camera is aligned towards the mirror on the side of the engine. The sensor of the camera is capable of recording 12-bit uncompressed raw data. The recording speed is set at 25 000 fps with a gate time just below 40 000 ns. The resolution at this speed is limited to a maximum 512x512 pixels. A 100 mm focal length B.Halle lens is used as the objective lens. An additional manual aperture is used since the lens has a fixed aperture at f/2. The aperture is set at f/2 for the spray imaging for maximum signal collection. A band-pass 452 nm (+/-22 nm) filter is place in front of the objective lens. The recorded files are saved in 16-bit TIFF format for a complete preservation of dynamic range.

Natural luminosity imaging is performed to capture the soot processes in the cylinder. Most of the set-up is identical to the Mie-scattering measurement. However, due to a significantly stronger luminosity from the soot radiation, natural density filters are necessary to prevent the sensor from saturation. An additional ND-05 and ND-07 filter is used for the low load measurement and the medium load measurement, respectively. The reduction factors are then multiplied with the recorded signals to retrieve original signals.

The thermal conductivity of the quartz material is usually two order of magnitude smaller than steel or aluminium. Although its thermal expansion coefficient is also much smaller, a steep temperature gradient in the quartz material still increases the probability of cracking significantly. Thus, all the operating conditions on the optical engine use a skip fire strategy, meaning that there are nine motored cycles after one fired cycle.

3.2.3.2 LII and LEM Set-up

The set-up of the LII and the LEM measurements is shown in Figure 3.5. A Nd:YAG laser is used at 10 Hz with 1064 nm wavelength to avoid fluorescence from PAHs as much as possible. The laser beam is transformed to a 16 mm high vertical laser sheet just before entering the front side window. The laser pulse energy after passing one side window is measured externally to ensure a laser fluence of 0.7 J/cm^2 inside the cylinder. The focus of the laser sheet is located in the center of the cylinder. The injector is adjusted so two of the sprays are in

the same plane with the laser sheet.

A Princeton Instruments PI MAX IV ICCD camera is aligned to the right side window, perpendicularly to the laser sheet. The same 100 mm f/2 lens is used as the objective lens. The field of view is adjusted to just cover the whole side window. Due to the severe distortion caused by the piston geometry when imaging from the side, it is difficult to achieve sharp images inside and above the bowl simultaneously due to the optical piston displaces the focal plane in the depth-direction. Thus, a manual aperture is set at f/8 for the objective lens to obtain optimum depth of field. A 4x4 binning is used to obtain a better signal-to-noise ratio, which also decreases the resolution to a 512x512 pixels. Two short-pass 450 nm filters are placed in front of the camera to help distinguishing the LII signals from the natural soot luminescence.

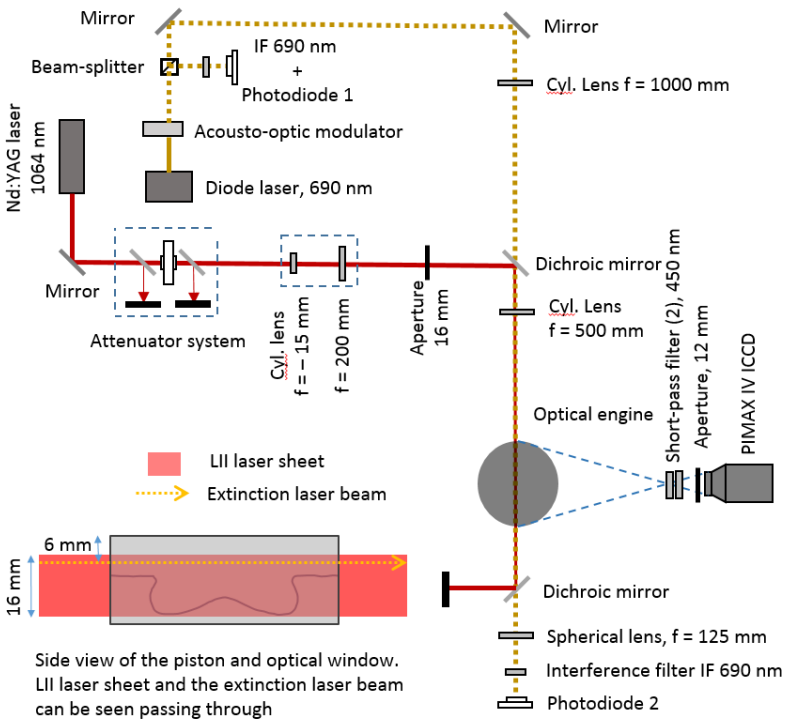

Figure 3.5: LII and LEM set-up.

An illustration of the triggering sequence of the whole system is shown in Figure 3.6. The gate width for the LII signal capture is set at 20 ns. A background image is also acquired just before this gate starts, which is later used to subtract

the noise from the LII image. The gap between these two frames is approximately 2.4 µs, which corresponds to less than 1/50 CAD of time at 1200 rpm engine speed. Hence, the in-cylinder motion can be considered as at the same moment. LII is measured from 25 CAD aTDC to 70 CAD aTDC with a step size of 5 CADs. 70 cycles at each measurement point are recorded and averaged.

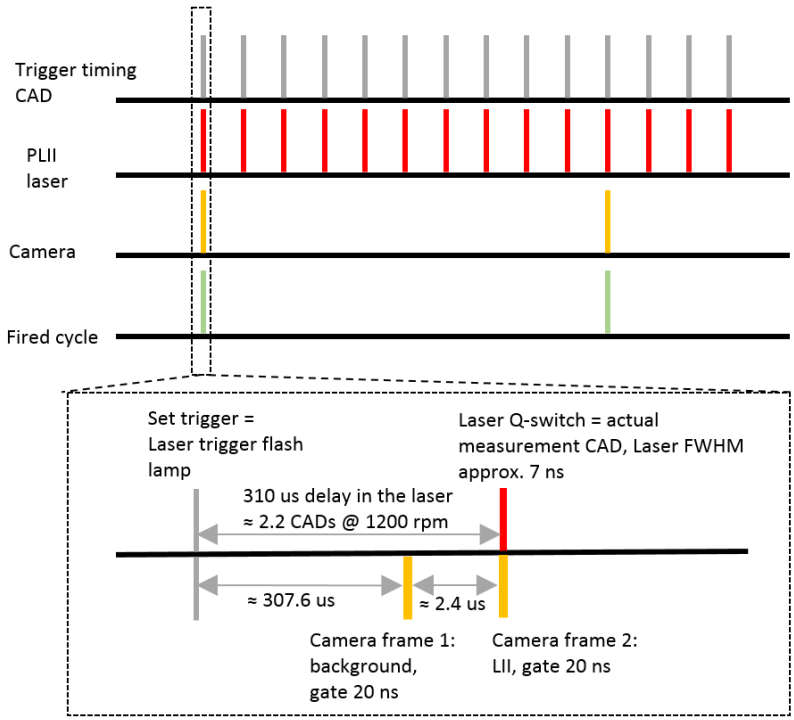

Figure 3.6: The triggering sequence of the LII imaging system.

A 690 nm diode laser (continuous wave) is used as the light source for the LEM due to the risk of interference from PAHs absorption at a longer wavelengths [89]. Using visible light also makes it easier to align. A high frequency acousto-optic modulator (AOM) is placed in front of the laser diode to shape the light intensity into a 72 kHz square wave signal. A beam splitter splits the modulated laser into two signals. One is recorded by photo diode 1 just after the splitter while the other passes through the optical cylinder and is received by photo diode 2. To minimize the interference from NL signals, a 690 nm interference filter is placed just in front of photo diode 2.

The extinction laser beam is in the same plane as the LII laser sheet, located about 9 mm from the ceiling of the cylinder to avoid interference from injector

nozzle tip and valves. With this distance, there is no interference from the piston after 25 CAD aTDC, allowing the calibration of the LII signal in the late cycle. A Dichroic mirror is used to reflect the LII laser and let the LEM laser pass initially. However, there is strong interference from the high power LII laser pulse which disrupts the LEM signals on photo diode 2. Hence, the LEM and the LII are conducted separately. 150 fired cycles are used for the LEM signal analysis at each operating point.

3.2.4 Injectors, Operating Conditions and Fuels

3.2.4.1 The Injectors

The injector used in this work is Denso's 4th generation solenoid injectors for light-duty diesel engines. They all have 8 tapered nozzle holes with 125 µm outlet diameter and a 155° umbrella angle. Two sets of in total 8 injectors are used for the reference test on the multi-cylinder engine. One set consists of new injectors which have only been used for a couple of hours of test run. The other set is the aged ones, which have been used over 100 000 km of field test.

3.2.4.2 The Operating Conditions

Two reference points are adapted from [90], representing real-world low to medium operating conditions. Both consist of two pilot injections, one main injection and one post injection. The operating conditions are kept as similar as possible on the multi-cylinder engine and on the optical engine. However, due to hardware limitations, such as different compression ratios, some adjustments need to be done on the optical engine. The operating conditions are summarized in Table 3.2. The swirl levels are kept at minimum on both engines for an easier optical analysis.

Table 3.2: A summary of the operating conditions.

Multi-cylinder engine		
	Reference point 1 – low load	Reference point 2 – medium load
Injection pressure [bar]	450	850
Intake pressure [bar]	1.1	1.6
Intake temperature [°C]	30	30
Engine speed [RPM]	1500	1500
Engine load IMEPg [bar]	Approx. 4	Approx. 9
Oxygen concentration [%]	20	20
Optical engine		
	Reference point 1 – low load	Reference point 2 – medium load
Injection pressure [bar]	450	850
Intake pressure [bar]	1.27	1.83
Intake temperature [°C]	75	75
Engine speed [RPM]	1200	1200
Engine load IMEPg [bar]	Approx. 4	Approx. 9
Oxygen concentration [%]	20	20
Estimated TDC density [kg/m^3]	Approx. 15	Approx. 22
Estimated TDC temperature [K]	Approx. 880	Approx. 890

3.2.4.3 The Fuels

There are four fuels used in this work. One is the certified CEC RF-79-07 reference fuel. It has low fatty acid methyl ester content and no special additives are blended, which is usually used as a baseline for additive insertion tests [91]. The other three fuels are blends using this baseline fuel with different representative additives for reducing soot, increasing ignitability and improving nozzle flow, respectively.

Tripropylene-glycol monomethyl ether (TPGME, $C_{10}H_{22}O_4$) is used as one representative of the oxygenated compounds, which are found to have a clear soot reduction effect [92, 93, 94]. The oxygen in the fuel not only affects the soot formation and oxidation rate, but also influences the soot structure in some conditions [95, 96].

2-ethylhexyl nitrate (2-EHN, EHN, $C_8H_{17}NO_3$) is a common ignition improver for diesel fuel. It has a relative low decomposition temperature of 450-550 K, which can increase the hydroxyl (OH) radical concentration significantly [97, 98, 99]. The OH radicals are usually used as an indicator for ignition since they are the reactants in the chain propagation of hydrocarbons. An elevated concentration of OH radicals prompts the ignition. Due to the existence of

nitrogen molecules, side effects such as increased NOx emission is found in some cases [100, 101].

Quaternary ammonium salts are not common fuel additives. They are normally used in industrial applications as antimicrobial agents [102, 103] or phase-transfer catalysts [104]. Some recent research tries to use quaternary ammonium salts as a fuel additive, finding that the turbulence level throughout the orifice is reduced and cavitation is suppressed [105, 106]. For this reason, these types of fuel additives may have potential to improve fuel flow in ultra-fine diesel injector nozzles.

Some measured fuel properties are listed in Table 3.3. Though the composition and concentration of the flow improver additive are confidential and thus unknown, in general they are quaternary ammonium cations with positively charged ions in a structure of NR_4^+, R being an alkyl group or an aryl group.

Table 3.3: Some of the measured fuel properties

Fuel names	Baseline	Ignition improver (II)	Soot reducer (SR)	Flow improver (FI)
Fuel composition	100% baseline diesel	99.5%vol baseline diesel + 0.5%vol 2-EHN	95%vol baseline diesel +5 %vol TPGME	Baseline diesel + quaternary ammonium salts (composition and concentration unknown)
Density @ 15 °C [kg/m^3]	833.8	834.4	837.6	833.8
Net heating value [MJ/kg]	43.2	43.07	42.76	43.2
Flash point °C	84	84	84	84
Cetane Number [-]	53.3	66.3	54.9	53.3

All four fuels are tested on the multi-cylinder engine for reference, while in the optical measurements only the baseline and the soot reducer fuel are tested.

3.3 Data Processing

3.3.1 Heat Release Analysis

General combustion information can be obtained using cylinder pressure data. Apparent heat release rate (aHRR) is commonly used in the combustion analysis. Assuming the cylinder is a single zone of ideal gases, ignoring mass exchange such as blow-by through the piston rings and valves, the first law of thermodynamics can be applied. The net aHHR is then derived as [15]:

$$\frac{dQ_n}{dt} = \frac{dQ_{ch}}{dt} - \frac{dQ_{ht}}{dt} = \frac{\gamma}{\gamma - 1} p \frac{dV}{dt} + \frac{1}{\gamma - 1} V \frac{dp}{dt} \tag{3.8}$$

where dQ_n is the net heat release which equals to the difference between the apparent gross heat release rate dQ_{ch}/dt and the heat transfer rate to the wall dQ_{ht}/dt, $\gamma = C_p/C_v$ is the heat capacity ratio and p and V are the cylinder pressure and volume, respectively.

The pressure data are acquired from the pressure sensor and the cylinder volume can be calculated using the geometry of the cylinder. The γ value depends on the gas compositions and their temperature, which can not be calculated precisely. Since the majority of this work is comparative analysis, an accurate aHRR is not of importance. Thus, the γ value is approximated using a relatively simple method based on the global temperature estimation [107]. For the very same reason, the heat transfer term is neglected in the analysis.

Once the aHRR is calculated, the cumulative heat release can be obtained, so the combustion phasing CA50, ignition delay and combustion duration can be calculated.

It needs to be noted that although the calculation of aHRR is quantitative, it is an approximation to the real heat release rate which cannot be measured accurately.

3.3.2 Processing of the Spray and the Combustion Images

When imaging from the bottom of the piston, image distortion inevitably occurs due to the geometry of the piston, which needs to be corrected before applying any analysis. A grid target image with 2 mm squares is used to show the distortion as illustrated in the left of Figure 3.7. The grid is placed on the pis-

ton top directly and the piston is cranked to 5 CAD aTDC position, which is approximately the middle point of the fuel injection events. Since the piston is close to the TDC position, a couple of degrees of movement doesn't change the focusing significantly. Then the grid is imaged directly by the camera without the piston. Both the distorted grid image and the original grid image are sent to MATLAB for correction. It is done by fitting control points on these images and using geometric transfer function with local weighted mean method.

The corrected image is shown in the right of Figure 3.7. Some blurring is introduced by the distortion correction in the periphery of the image. Since the majority of the fuel injection and combustion occurs within the bowl area, a circle of around 45 mm in the center, this blurring does not affect the analysis. A slight rotation is also introduced during the correction procedure, which does not affect the analysis either. The spatial resolution is calculated as 10 pixels/mm.

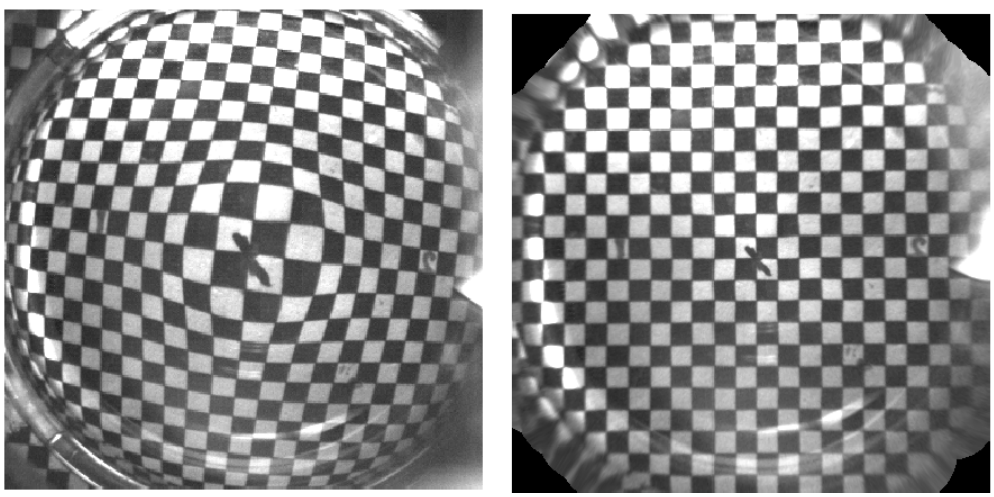

Figure 3.7: Target image at 5 CADs ATDC. Left: original image with distortion. Right: image after distortion correction.

After the distortion correction, the combustion images are ready for analysis while the spray images need some further processing. Due to there only being one laser coming from one side of the cylinder, and the serious beam steering occurring when the laser comes through the side window and half of the piston, the luminosity is not uniform when the laser encounters the sprays. The sprays closer to the incoming laser also attenuate the laser, making the laser on the far side of the sprays even less uniform and weaker. The beam steering also causes strong reflection from the ceiling of the combustion chamber. Five motoring

cycles are recorded and averaged as a background signal, which is then subtracted from the spray images to reduce the noise. Only one spray which shows the best scattering signals is selected for analysis.

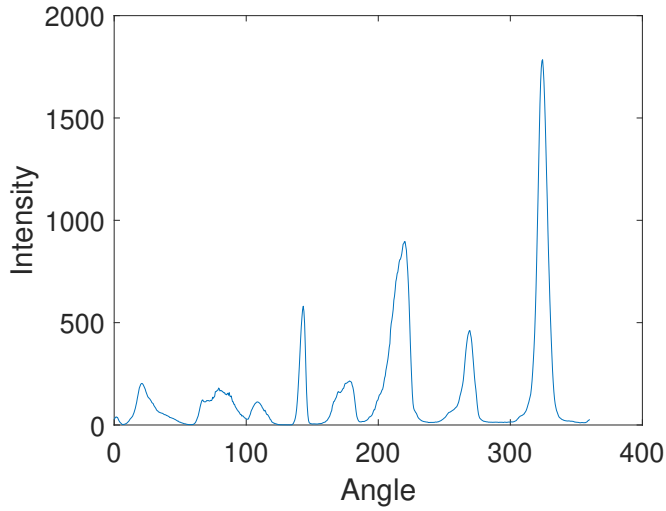

Figure 3.8: Spray scattering intensity distribution as a function of angular position

The selection procedure starts with manually setting a center point of the injector nozzle. A series of concentric circles starting from 50 pixels radius (5 mm) to 210 pixels radius (21 mm) are created to sample the pixel intensity on the circle. The angular position of the intensity on the circles can thus be retrieved. An averaged results from the samplings is shown in Figure 3.8. The spray with the strongest scattering signal and its angular position thus can be found. Finally a pie-shape mask is made to crop out the selected spray and the cropped images are rotated to a horizontal position using the angular position of the spray axis, as shown in Figure 3.9.

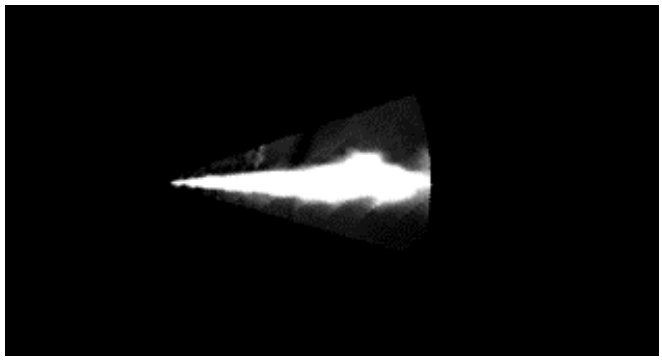

Figure 3.9: Cropped and rotated spray

3.3.3 Processing of the LII and LEM signals

3.3.3.1 Distortion Correction for the LII Images

When imaging from the side windows, the combined image distortion from the piston and the side window is even more serious. In this case, the distortion correction is applied individually to different areas. An illustration is shown in Figure 3.10. Two special LED targets are made to fit the 'left' half or the 'right' half of the piston bowl. The 'left' target is shown in (a) and (b) shows the distortion when the 'left' target is placed in the piston bowl. The top two lines above the piston top doesn't suffer any distortion induced by the bowl boundary while there is severe reflection and distortion inside the bowl area. The reflection part is removed and the remaining part is distortion corrected using the same method as mentioned before. The corrected part is than stitched together with the upper part as shown in (c).

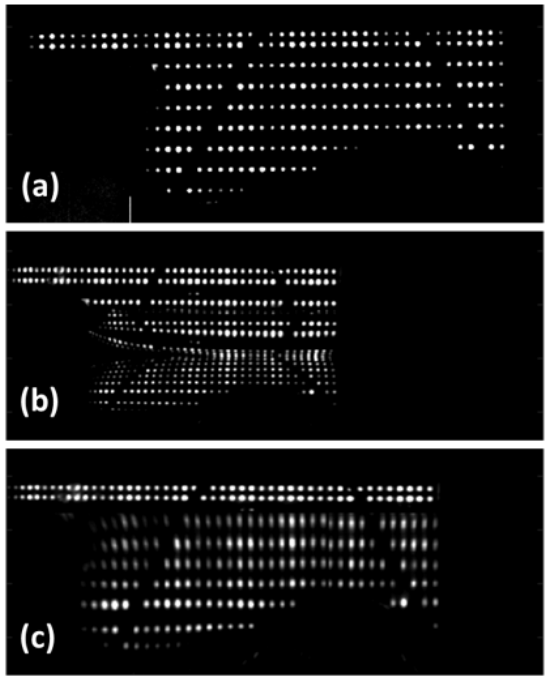

Figure 3.10: Distortion correction for the LII images. (a) a direct imaging of a specially made LED dots target which fits the 'left' half of the bowl. (b) image of the same target in the piston bowl behind the side window. (c) distortion correction applied to (b).

The distortion correction has some limits when it comes to the sharpness of the corrected part. Some blurring is observed just below the top of the piston. However, considering only comparative measurements are required, these flaws are neglected. The similar procedure is also applied to the 'right' half. Finally, the corrected images are stitched together to recover a complete image.

3.3.3.2 Calibration Using the LEM signals

The general principle of calculating the soot volume fraction f_v using the LEM is already introduced previously. To apply the LEM measurement on the optical engine, the signals are measured firstly in motored cycles when no fuel injection or combustion occurs as shown in Figure 3.11. In a combustion case the valley signals are increased due the NL from the combustion while the peak signals are reduced by soot and other combusting products as shown in Figure 3.12.

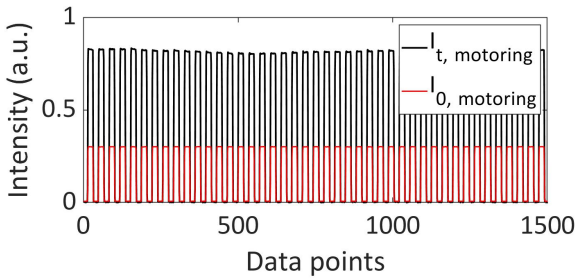

Figure 3.11: An example of a LEM signal in a motored condition. where I_0 is the reference signal recorded by photo diode 1 before the cylinder and I_t is transmitted signal recorded by photo diode 2 after the cylinder.

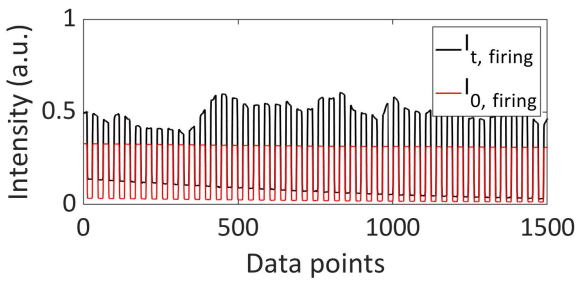

Figure 3.12: An example of LEM signals in a combustion condition. I_0 is the reference signal recorded by photo diode 1 before the cylinder and I_t is transmitted signal recorded by photo diode 2 after the cylinder

The high frequency square wave shape intensity signals generated by the AOM enable background subtraction by simply subtracting the neighbouring valleys from the peaks. A derived example is shown in Figure 3.13

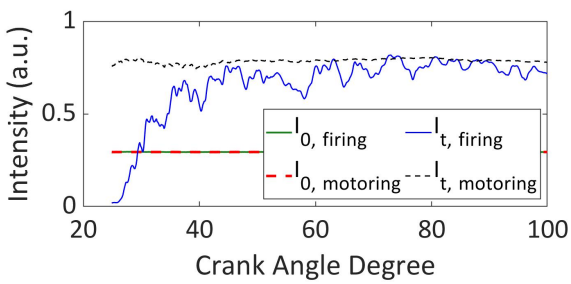

Figure 3.13: An example of LEM signals after background subtraction.

Using Equation 3.4, the $K_{ext}L$ value can be calculated, which represents the line-integrated soot volume fraction. L is calculated using the LII signal intensity distribution along the x direction in the LEM laser beam region. Figure 3.14 illustrates the relative position of the LEM laser to the cylinder. The LII signals in LEM laser beam region can be obtained since the position of the LEM laser beam is acquired during the calibration. Figure 3.15 shows the integrated and normalized LII intensity distribution along the x direction in the LEM laser beam region. A 5% maximum threshold is applied to cut the noise region. Finally the effective absorption length L is obtained.

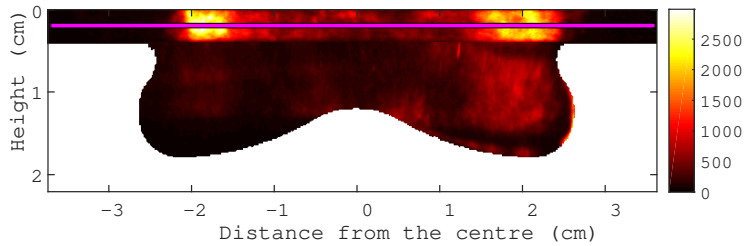

Figure 3.14: An example of LII signal intensity (a.u.) distribution after averaging and distortion correction. The purple line above the piston represents the LEM laser beam position.

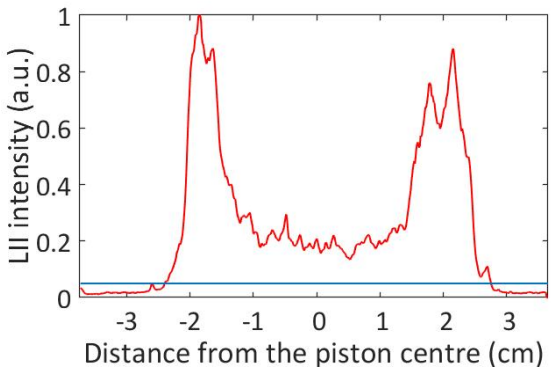

Figure 3.15: An example of LII signal intensity distribution along the x direction in the LEM laser beam region (red line) and the applied threshold level (blue line).

Finally, The LII signals can be calibrated to absolute f_v values using the representative value in the LEM laser beam area as shown in Figure 3.16.

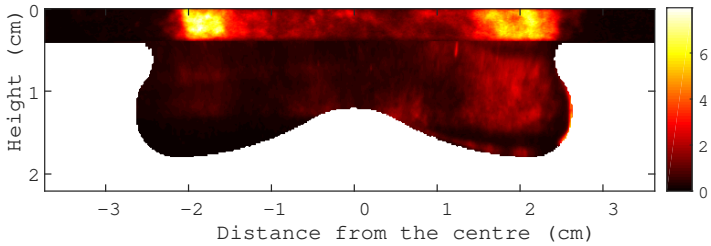

Figure 3.16: An example of calibrated soot volume fraction distribution. The LII signal intensity is converted to ppm.

Chapter 4

Results and Discussion

4.1 Multi-cylinder Engine Reference Tests

The first thing noticed during the reference tests is the difference of fuel flow rate when using different injectors. The total diesel fuel consumption rates at the two operating conditions are shown in Figure 4.1. With fixed injection pressure and injection strategies, the aged injectors show a 25% higher total fuel injection rate at low load and a 10% increase at medium load. This is verified by checking the gross indicated mean effective pressure ($IMEP_g$) of each cylinder, showing that the difference between the new and the aged injector sets are larger than the difference between individual injectors in the same group. Based on these observations it is thus hypothesized that there are no deposits inside the injector nozzles which are blocking the fuel injection. Needle actuation, worn injector parts or leakage are more likely the causes of increased flow rate.

No significant difference is found between the fuels. The flow improver (FI) fuel may have some effects on the fuel flow rate, but the precision of the fuel flow measurement system is probably not sufficient for monitoring very slight flow change caused by a limited amount of fuel property modification.

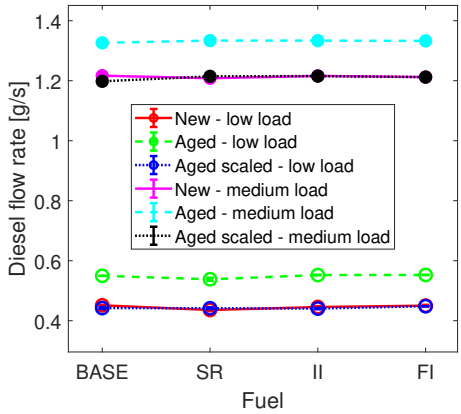

Figure 4.1: Comparison of fuel flow rates.

The large difference in fuel flow has an obvious impact on the combustion and emissions. Thus, a scaled injection strategy for the aged injectors is also tested at each operating condition. The main injection duration in these scaled points is reduced to equalize the $IMEP_g$ between the new and the aged injectors, while the other three injection events are kept the same.

To compare the injectors, the cylinder pressure and derived aHRR are shown in Figure 4.2 and Figure 4.3 at low and medium load, respectively. These are the average results from all four cylinders over 150 cycles. Only the baseline fuel is used in this comparison. At both load points, the heat released in the pilot combustion is about 50% higher with the aged injector. This not only increases the $IMEP_g$, but also changes the combustion process. A higher heat release rate in the pilot combustion advances the main combustion and reduces its peak because of a higher temperature and reduced premixing time. This is more obvious at the low load. Due to a longer ignition delay, the pilot combustion events merged as one heat release feature at the low load. At medium load, each pilot injection is followed by a separate pilot combustion heat release. In either case, the combustion does not show an obvious mixing-controlled combustion heat release phase typically found in diesel engines. The overall combustion mode is highly premixed in this light-duty engine at these load levels.

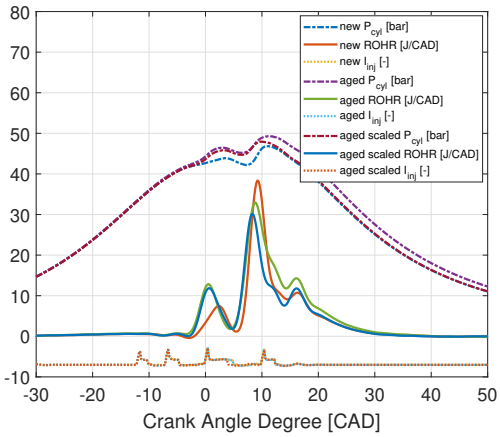

Figure 4.2: Comparison of different injectors at low load using the baseline fuel.

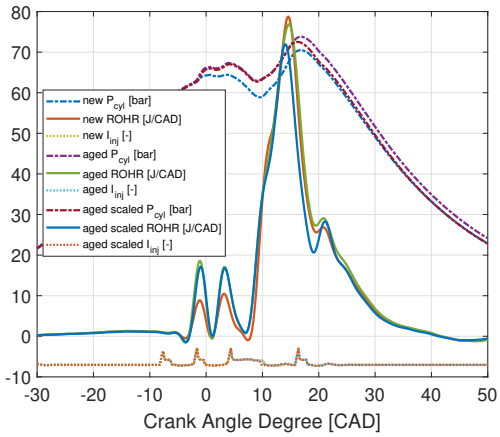

Figure 4.3: Comparison of different injectors at medium load using the baseline fuel.

Figure 4.4 and Figure 4.3 show the comparison between different fuels when using the new injectors at different loads. The general difference is very small, despite some ignition delay difference in the first pilot combustion. The phasing and the magnitude in the main combustion heat release rate show a high similarity at both load points.

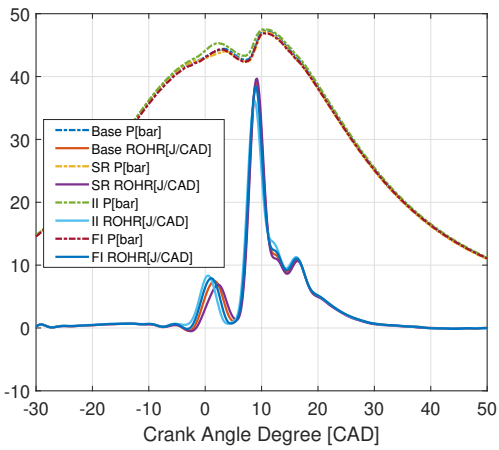

Figure 4.4: Fuel comparison using new injectors at low load.

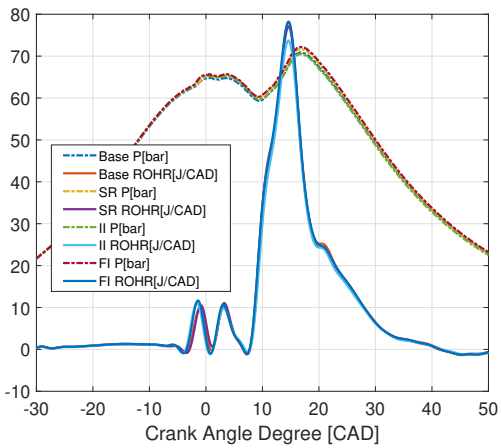

Figure 4.5: Fuel comparison using new injectors at medium load.

The ignition delay is usually defined as the time between the SOI and the start of combustion. The SOI used here is the start of the injection command signal

since the actual needle lifting moments are difficult to obtain. The start of combustion is determined from the accumulated heat release. In a low to medium load combustion condition, the initial fluctuation of the aHRR curve can have impact on the accumulated heat release, especially with multiple pilot injections. Thus, the ignition delay in this work is defined as the gap between the SOI and the first point where the aHRR surpasses 3 J/CAD. This threshold is selected based on that the noise level of the aHRR before the pilot combustion does not surpass 2 J/CAD. A 50% margin is added to ensure a robust detection of the ignition timing. The ignition delay is summarized in Figure 4.6.

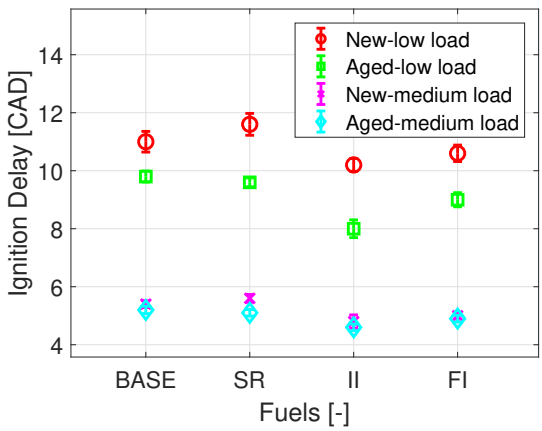

Figure 4.6: Comparison of ignition delay when using different fuels with different injectors.

The fuel quantity difference at low load shows an obvious impact on the ignition. With the extra fuel injected by the aged injectors, there is a one to two CAD advance of ignition. In a highly diluted condition with relatively low TDC temperature, a richer fuel-air mixture increases the probability of chain branching and propagating reactions induced by the initial radicals, which facilitates ignition [38]. At medium load, the fuel quantity difference in the pilot injections is smaller. Combined with the elevated TDC temperature, very little ignition delay difference between the injectors is observed, with the aged injectors showing just a slight advance in ignition. The cycle-to-cycle variation is also marginally reduced at medium load since a smaller standard deviation is observed.

The ignition improver (II) fuel is most prone to auto-ignition, followed by the FI fuel. Compared to the base fuel, the soot reducer (SR) fuel shows a bit more ignition delay when using the new injectors while a bit less ignition delay when using the aged injectors. This is probably caused by the fuel quantity difference.

But overall the difference is very small since the standard deviations show a certain amount of overlap. At this point, the ignition is equally sensitive to the fuel quantity and the ignition quality.

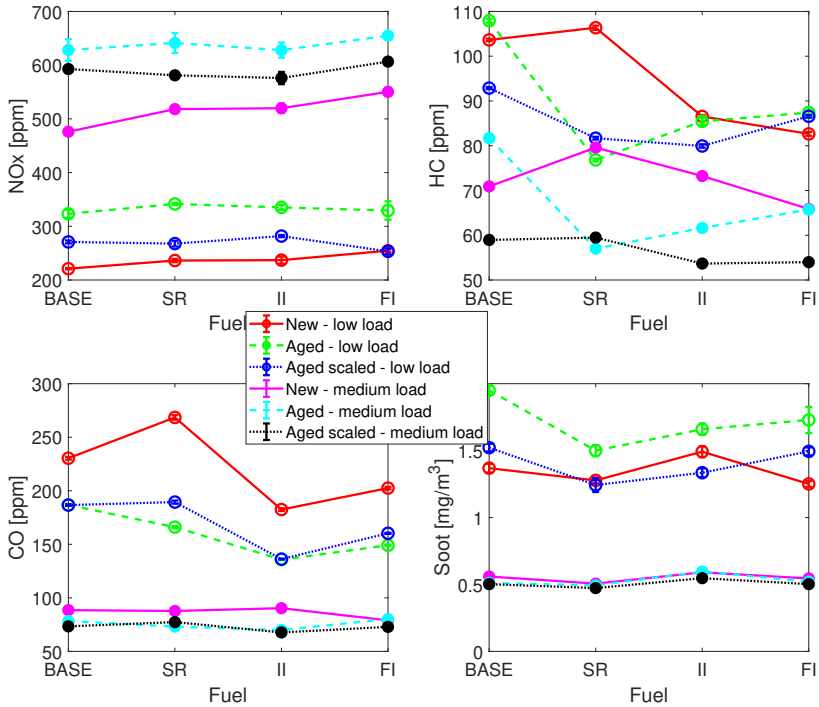

Figure 4.7: Engine-out emissions from reference tests.

The emissions are shown in Figure 4.7. The top left figure shows the NO_x emissions. At both load points, the new injector emits the lowest NO_x, followed by the aged injector with scaled injection strategies. The aged injectors using normal injection strategies emits the highest NO_x. Under engine conditions with a given nitrogen level, the NO_x formation is simply related to high temperature and high oxygen concentration. The NO_x difference is mostly contributed by the fuel quantity difference from the injectors. With a same amount of intake charge, more fuel means a higher temperature, which leads to a higher NO_x formation.

At low load, there is on average a 42% increase of NO_x from the aged injectors when using the same injection strategy, while at medium load there is a 22% increase. When the $IMEP_g$ is scaled to the same level, the higher amount of

heat release in the pilot combustion with the aged injectors is closer to the TDC position, which increases the overall temperature. The difference becomes about 19% and 13% at low and medium load, respectively. The strong non-linear increase of the NO_x formation rate with increasing temperature can be noted.

The general difference between fuels is much smaller with just around 5% difference. Parameters such as fuel density, heating value and ignition delay can all have impacts on the NO_x. However, the difference between fuels is too small to conclude any obvious trend.

The hydrocarbon (HC) emissions are shown at the top right in Figure 4.7. Generally, the HC emissions at medium load are slightly lower than at the low load. However, the difference is very small, within a 40 ppm range. The difference between the fuels in a similar operating condition is even smaller, within a 10 ppm range.

A higher combustion temperature and a stronger in-cylinder flow certainly help to increase the oxidation of unburned HC. HC emission is usually low in a diesel combustion. A couple of factors can have impact on the HC emission: 1) the impingement of liquid fuel on the combustion chamber wall; 2) asymmetric spray patterns; 3) fuel trapped in the squish area; 4) the nozzle sac volume and the needle behaviour in the injector [108].

In a common multiple injection diesel combustion mode, factors 1) and 3) can be excluded first since there is no excessively long injection duration and most of the fuel is injected into the bowl area when the piston is close to the TDC position. Factors 2) and 4) can produce local fuel-rich or fuel-lean zones such as unevenly distributed fuel pockets in the spray or dribbles at the end of injection, which in a highly diluted environment can cause incomplete oxidation, leading to an increase of HC emission.

The CO emissions are shown at the bottom left in Figure 4.7. The new injectors constantly emit more at both load points, with a larger difference compared with the new ones at low load. At medium load the overall CO emissions are around half of those at low load. In a diesel combustion mode where there is always excessive oxygen available, the CO emissions are mostly linked to temperature. CO is an important combustion intermediate product, with the conversion of CO to CO_2 taking place during the later stage [38]. A higher temperature during a longer period can lead to better oxidation of CO. As can be seen in the figure, fuel effects on the CO emissions are also very small, with around 50 PPM of difference at low load and just 10 PPM of difference at medium load.

The soot emissions are shown at the bottom right of Figure 4.7. At low load,

they are more than twice as at medium load, which is caused by an overall lower temperature and a shorter high temperature window for oxidation. The aged injectors emit more soot, most likely due to the fuel quantity difference. Although the extra fuel amount can increase the temperature, this increase is probably not sufficient for a more complete oxidation. The fuel-air mixing is also limited by the low injection pressure, which usually leads to a high soot formation. Uneven fuel distribution caused by asymmetrical spray pattern and fuel dribbling could also add to the soot emissions. At medium load, elevated temperature and denser ambient conditions can accelerate the soot oxidation process while an enhanced mixing by a higher injection pressure reduces the soot formation. The difference between the injectors becomes barely noticeable at this point.

The SR fuel shows a marginal soot reduction effect compared with the base fuel at medium load, with a larger influence at low load. Although the oxygen is sufficient in the ambient air, without sufficient temperature and mixing, soot precursors can still be produced by the pyrolysis process. The oxygen content in the fuel reduces the overall probability of the formation of typical soot precursors. Oxidation could also be increased by the oxygen content. The substantially increased temperature and mixing at medium load eliminate most of such effects. However, in a less oxygen-rich condition it may show its advantages again.

4.2 X-ray Tomography of Injectors

The material density difference between the injector nozzle and the needle gives different intensity in the tomography images because of different levels of X-ray absorption, making it simple to use a threshold method to distinguish the boundaries. Figure 4.8 and Figure 4.9 show the X-ray tomography results for the new and the aged injector, respectively. Both the nozzle holes and the transition area from the sac volume to the nozzle holes have smooth surfaces. The injector needle and the needle seat show well-matched surfaces without any abnormal conditions. These observations can eliminate the hypothesis of corrosion or worn in the nozzles and needle head area. Thus, the nozzle flow during fuel injection events are considered being not affected by the nozzle surface conditions.

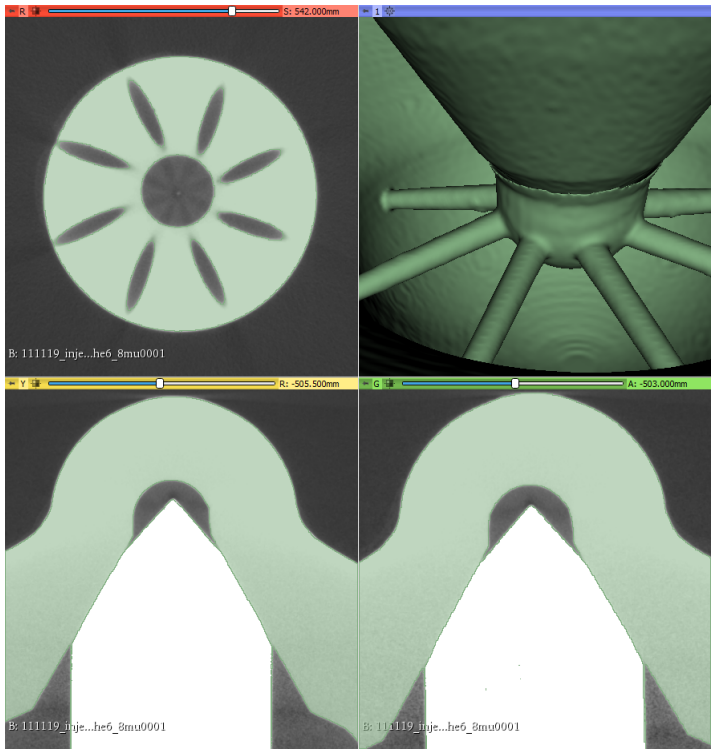

Figure 4.8: X-ray tomography of the new injector. Top left: a cross section image in the nozzle area. Top right: reconstructed surfaces of the sac volume, the nozzle holes and the needle tip. Bottom: side views of the nozzle and the needle region.

Figure 4.10 shows a overlapped comparison of the new and the aged injector in the nozzle area. The left image illustrates a cross section at a position farther from the nozzle tip while the right image is at a closer position to the nozzle tip. Some geometric difference caused by manufacturing tolerance can be observed such as the angular orientation of the nozzle channels, but overall these differences are small and no significant dimension difference is observed.

Carbon based deposits cannot be observed in this case because high energy X-rays will pass through them with very little absorption. Based on the observation in the reference tests that the aged injectors generate a high fuel flow rate, deposits are very unlikely formed inside the nozzle because the flow rate would be reduced in this case. Asymmetric spray pattern might also be observed if internal deposits exist. This is revealed in the following spray imaging part. Metal based deposits should be able to be seen in the tomography due to their high density and hence a higher absorption of X-ray. Thus, it can be confirmed

that there is no aging effects from any deposits in the aged injector.

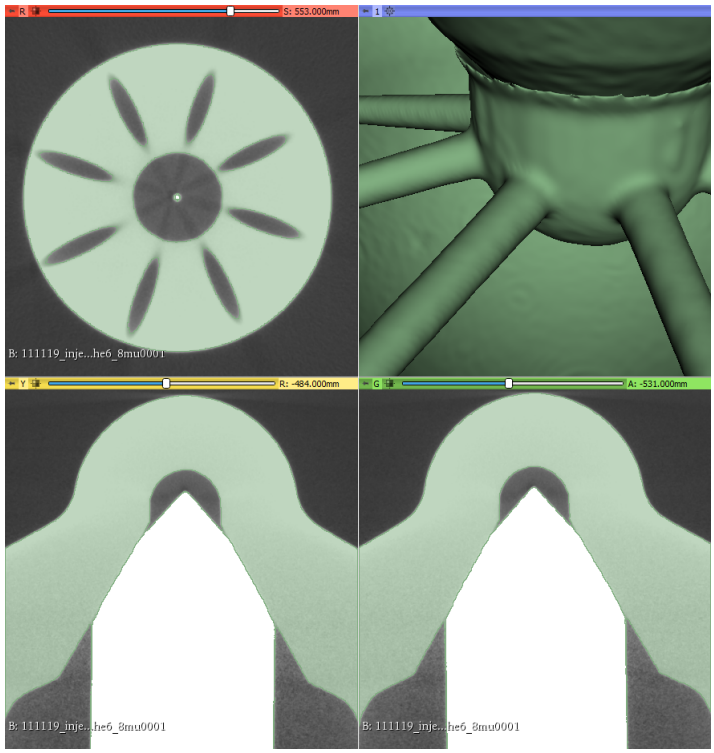

Figure 4.9: X-ray tomography of the aged injector. Top left: a cross section image in the nozzle area. Top right: reconstructed surfaces of the sac volume, the nozzle holes and the needle tip. Bottom: side views of the nozzle and the needle region.

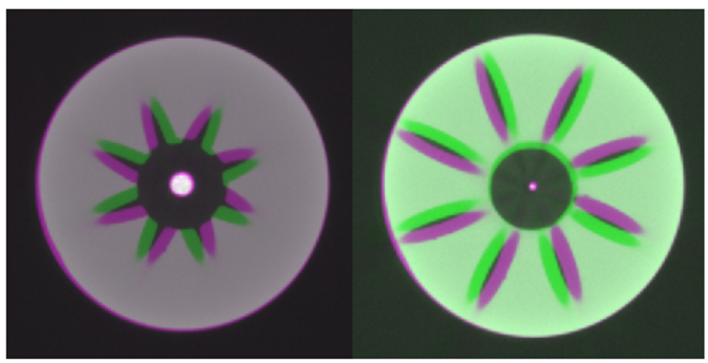

Figure 4.10: Overlapped cross-section images in the nozzle area of the new and the aged injector. Left: far from the nozzle tip. Right: close to the nozzle tip

4.3 Spray Measurements Using Mie Scattering

The spray measurements are conducted on the optical engine using Mie-scattering technique. The intake oxygen concentration is controlled below 5% to create a non-reacting environment. Fifteen cycles are recorded and averaged to acquire the results.

The total intensity in the spray images is the sum of the signals on all pixels. It can be used as an indicator of the fuel quantity, albeit the actual fuel quantity may have a very non-linear relation to the total scattering signal. Note that some background reflection is inevitably included. Considering that it is much weaker than the scattering signals, its influence can be neglected. The results are shown in Figure 4.11 and Figure 4.12 for the low and medium load, respectively.

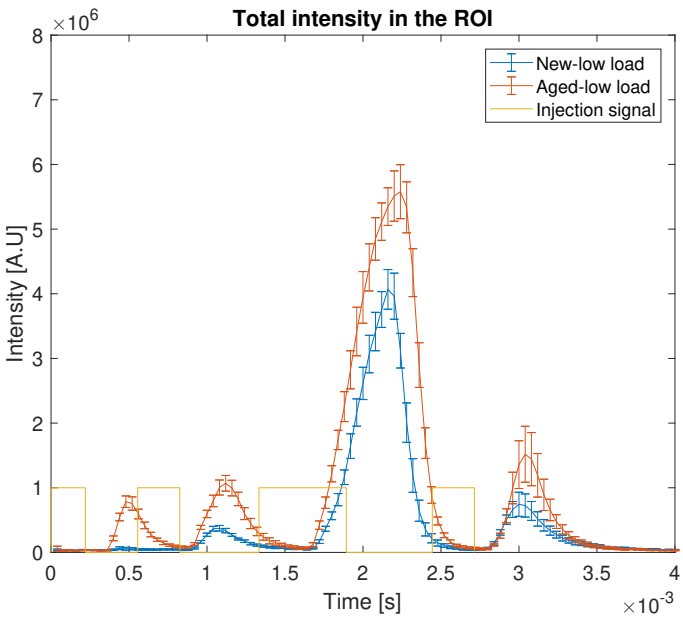

Figure 4.11: Total scattering signal intensity in the spray images at low load condition.

At low load, all four fuel injection events show an approximately Gaussian-shaped signal intensity, indicating that the injections are mostly in a transient state where the needle lifting and closing procedure can have a big impact on the fuel flow. If the needle is fully lifted and the injection reaches a steady state, there would be a plateau in the intensity signal where the liquid fuel length is stabilized and the injection rate equals the vaporization. The aged injector shows

a substantially higher total scattering signal in all injection events, especially in the pilot injections. This demonstrates the fuel quantity difference observed in the heat release analysis during the reference tests.

At medium load, the main injection starts to show a profile similar to a top-hat shape, meaning the needle is fully lifted and a steady state is reached during the injection. The spray is fully developed in this condition and is stabilized for a short time. The mean peak value of the intensity in this period from both injectors are very similar, as well as the shoot-to-shoot variation. This indicates that the discharge rate of these two injectors are similar when the needle is fully lifted, which verifies that the nozzles of the aged injector doesn't affect the discharge rate significantly.

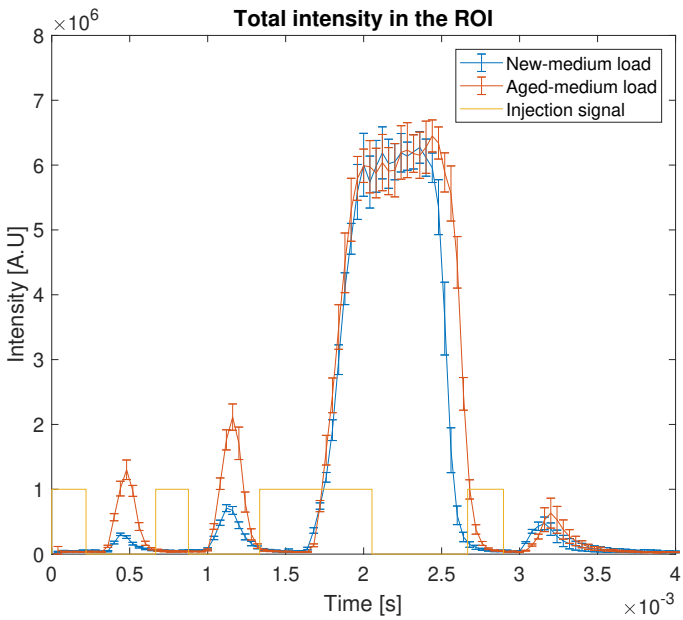

Figure 4.12: Total scattering signal intensity in the spray images at medium load condition.

The time derivatives of the total scattering signals, which can reflect the response of the fuel injection during transient conditions, are shown in Figure 4.13 and Figure 4.14 for the low and medium load, respectively. The moments of the scattering signal occurs have a consistent delay of about 0.35 ms to the SOI signals, which corresponds to 2.5 CAD at 1200 rpm engine speed. This delay is similar for all injection events at both load conditions, as seen at the points where the derivatives start to increase above zero. This means the initial

needle response during the start of the fuel injection has no significant difference between the injectors and the injection pressure does not affect their response either. The largest difference is during the end of injection period, the moments the derivatives turn from positive to negative. The scattering signal from the aged injector lasts longer than that of the new injector. This delayed needle closing is suspected to contribute the most of the fuel quantity difference.

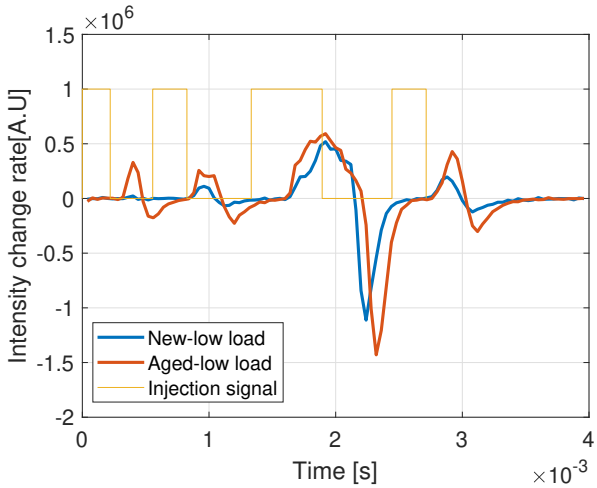

Figure 4.13: Time derivative of the total scattering signal of the injectors at low load.

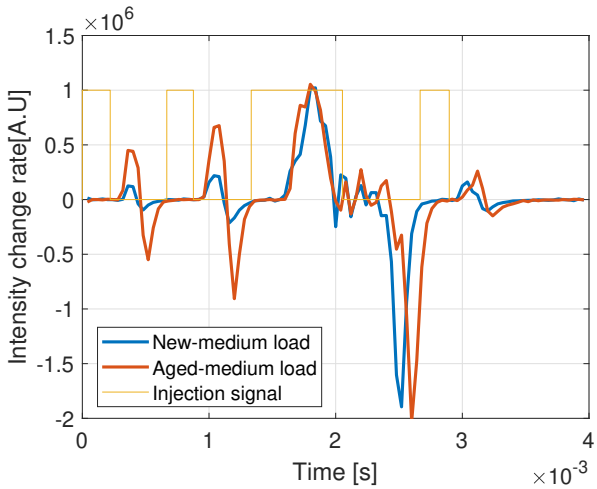

Figure 4.14: Time derivative of the total scattering signal of the injectors at medium load.

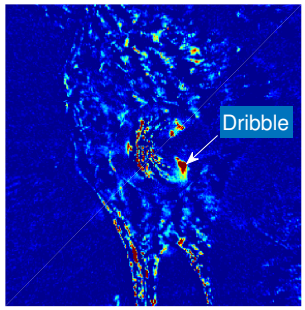

Figure 4.15: Fuel dribble of the new injector after one second pilot injection at low load.

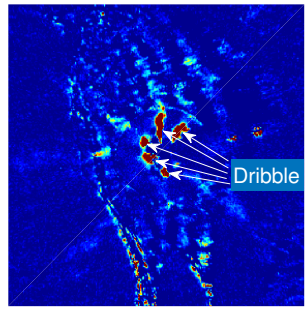

Figure 4.16: Fuel dribble of the aged injector after one second pilot injection at low load.

With the aged injector, it is also noticed that on average there is a larger amount of fuel dribble after the injections, particularly the pilot injections. Illustrations in Figure 4.15 and Figure 4.16 show a typical difference between the injectors. The nozzles are located in the center of the images. Only one piece of fuel dribble with strong scattering signal is observed when using the new injector while there are five pieces of obvious fuel dribble from the aged injector. Though fuel dribble is inevitable with a sac type injector nozzle, such substantial difference can cause larger fuel quantity difference in a small injection event and increase emission such as unburned HC and soot.

The spray penetration is calculated using a threshold method. The liquid length is calculated as the count of the pixels which have a signal greater than 5% of the maximum signal on the axis. The results are shown in Figure 4.17 and Figure 4.18 for the low and medium load, respectively. Generally, in the small injection events, the aged injector shows a longer liquid penetration length due to a delayed needle closing that gives more time for the spray to develop. In the main injection events, both can reach an approximate maximum length which is close to the wall of the piston bowl. The similar liquid length indicates that there is no major difference in the air entrainment between the sprays, as the liquid length is the distance over which the air needed to evaporate the fuel that has been entrained.

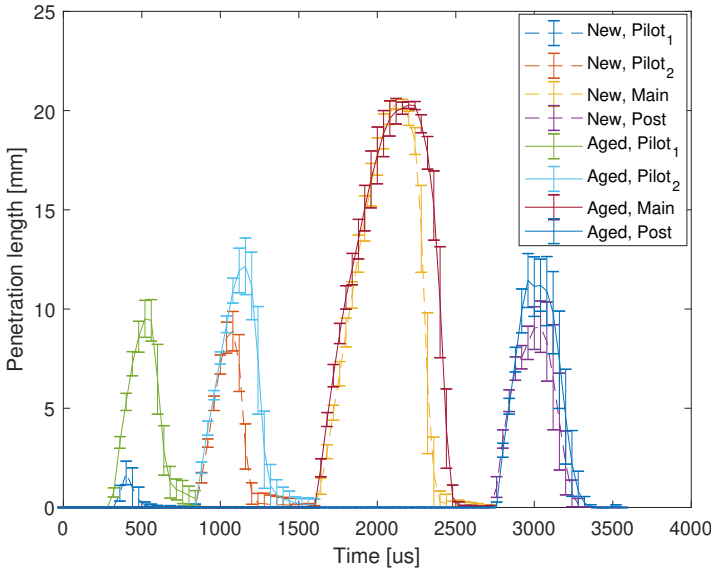

Figure 4.17: Liquid fuel penetration length at low load.

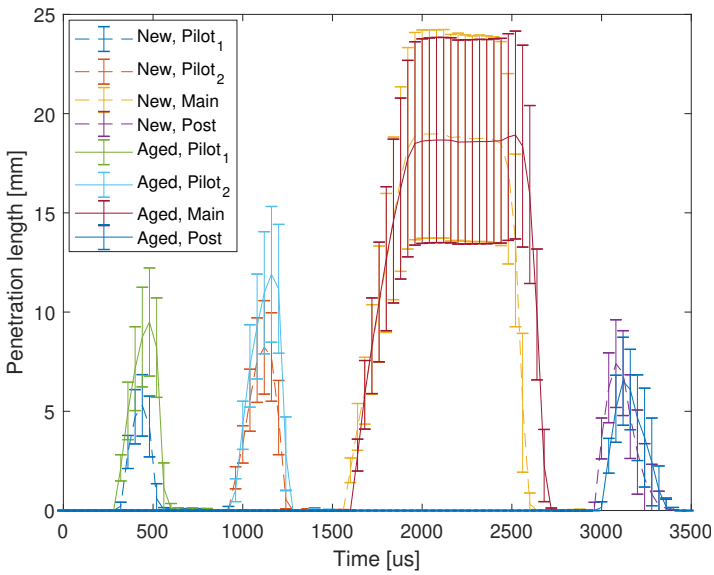

Figure 4.18: Liquid fuel penetration length at medium load.

At medium load the liquid penetration length of both injectors show a larger variation when they reach the steady state. The tip of the liquid spray stabilizes in a region where a dynamic balance between the injection rate and the evapor-

ation rate is achieved. Turbulence causes the liquid spray tip to move slightly back and forth along the axis as well as swing left and right, leading to this large standard deviation during the main injection. The overall penetration length at medium load is marginally shorter than that of the low load. As pointed out in Chapter 2, that liquid penetration length is mainly related to the ambient density when using the same fuel. A denser and hotter ambient increases the entrainment of air upstream of the spray. The increased air mass and temperature lead to a faster evaporation in the downstream and hence, a shorter liquid penetration.

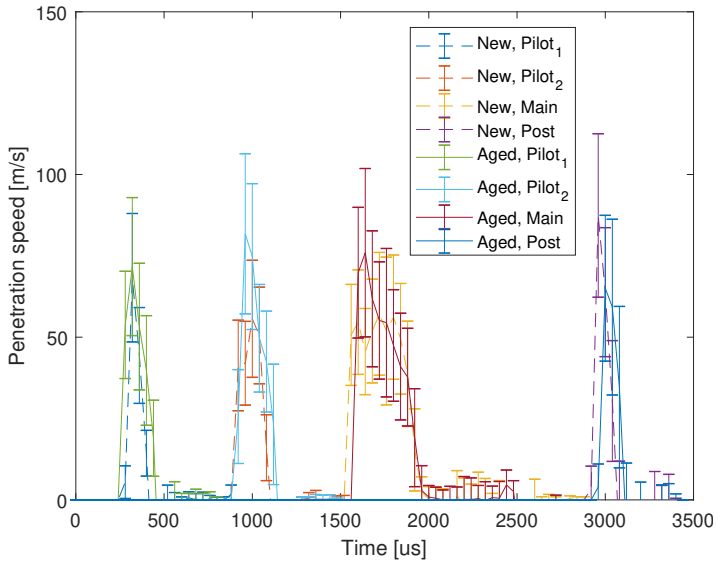

Figure 4.19: Spray penetration speed at low load.

The time derivatives of the penetration length are shown in Figure 4.19 and Figure 4.20. It can be seen that during the main injection, the penetration speed is similar at the same operating point for both injectors, with the aged injector giving just slightly faster spray penetration on average in the beginning of the injection. Due to the limited time resolution, the moment that a spray starts to scatter signal may occur anytime between two recorded frames. Depending on this moment, the spray could have traveled a different distance, which leads to the large variation in spray speed estimation at the starting point. The increamental penetration speed after this point shows a smaller difference. The overall penetration speed at medium load is slower due to the short penetration length during a similar time period.

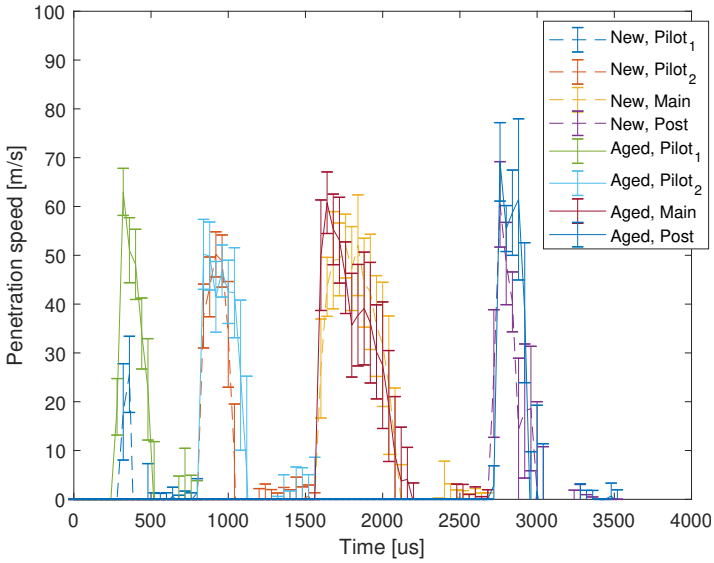

Figure 4.20: Spray penetration speed at medium load.

As discussed in Chapter 2, spray spreading angle is defined differently in different sources. To avoid the influences from definitions, the spray width at different distances from the nozzle is calculated instead of a spreading angle. A threshold is applied to all the pixel intensities in a line perpendicular to the spray axis at different distances from the nozzle. The pixel number of pixels having an intensity stronger than 5% of the maximum intensity on the spray axis defines the spray width at that distance. If there are large fluctuations, it can also indicate the existence of asymmetric sprays. Thus, the morphology of the spray can be revealed. The results are shown in Figure 4.21 and Figure 4.22 for the low load and the medium load, respectively.

The injectors do not show much difference at the two load points. The variation increases as the sprays travel farther. Increased evaporation and influences of turbulence could be the main causes. Liquid droplets far downstream the jet are smaller with less mass and their speed is significantly reduced. Thus, turbulence has a larger impact on the spray tip regions. The spray width are similar in both load conditions, despite the density difference. At low load, there is strong background noise in the location of around 7 to 8 mm downstream the nozzle for the new injector, which leads to a large deviation of the spray width estimation in this region. Generally the images show symmetric spray patterns, which verifies that there is no strong impact from the nozzle geometry. The similar penetration and spreading angle again indicates a similar air entrainment for both injectors.

In conclusion, the aging does not alter the internal nozzle geometry. Thus, the spray formation is not affected. The major difference is the characteristics of the closing flank of the needle, which could be caused by servo components in the injector.

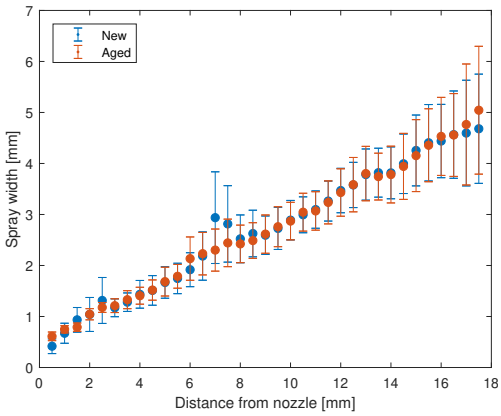

Figure 4.21: Spray width at different distances from the nozzle at low load.

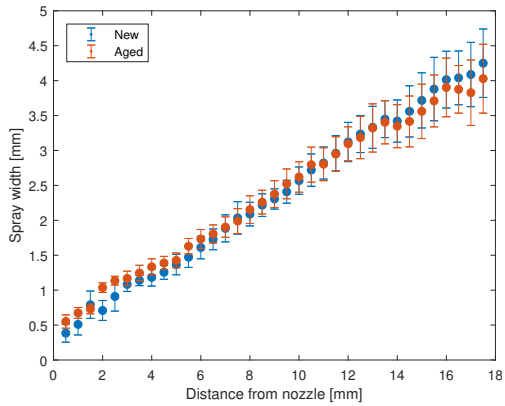

Figure 4.22: Spray width at different distances from the nozzle at medium load.

4.4 Natural Luminosity Measurements

As the thermal radiation part in the NL is related to the soot volume fraction and the temperature, it can be used as a soot indicator. However, it is difficult to use it quantitatively due to interferences: 1) the intensity of the chemiluminescence; 2) soot particle size, spectral emittance, refractive index and temperature; 3) quantum efficiency and linearity of the detection system; 4) adiabatic flame temperature; 5) in-cylinder temperature; 6) spatial distribution of luminous soot; 7) optical thickness effects [69].

As mentioned in Chapter 3, the chemiluminescence is often much weaker than the soot luminosity in a diesel combustion mode. The 452 nm band-pass filter used in front of the camera also blocks most of the typical chemiluminescence bands from OH*, CH* and C_2* [109]. Thus, the measured NL signal is assumed not to be affected by chemiluminescence. Note that this 452 nm selection allows the high temperature burning soot signal to pass while the colder soot might not be shown.

The band-pass filter ensures only a narrow-band signal is recorded, which minim-

izes the influence of the wavelength dependent quantum efficiency of the camera sensor. The response of the camera is assumed to be linear, as the ND filters avoids sensor saturation while maximizing the usage of the dynamic range of the camera.

The difference of the optical thickness in a line-of-sight measurement must also be considered. In this work, the optical thickness of the measurement system is assumed to be the same. However, if different injectors cause significant difference in the soot formation, the thickness of the soot cloud can lead to a considerably different optical thickness, which could lead to deviated estimations.

After eliminating some potential interference, the NL signals are assumed to only be affected by the soot particles and the temperature difference caused by the fuel quantity and properties. The injection strategy is kept the same at each load point for all cases during the NL imaging.

Sequences of the combustion images taken at low load are shown in Figure 4.23. The corresponding cylinder pressure, aHRR, and integrated NL are shown in Figure 4.24. The first NL signal appears at around 3 CAD aTDC when the aHRR just starts to climb. It originates from the burning soot in the pilot combustion. At around 7 CAD aTDC, the main injection fuel is shot into the pilot combustion area and is ignited by the high temperature. With a larger fuel quantity injected during the pilot injections, there is more soot signal close to the bowl periphery and the overall signal is stronger when using the aged injector. The NL signal develops stronger in the the jet regions while the main combustion goes on, reaching a peak at around 11 CAD aTDC as shown in Figure 4.24. The NL signal from the aged injection is slightly higher than that from the new one due to the fuel quantity difference. No significant difference is observed from the SR fuel yet.

As the jet tips reach the wall of the piston bowl, part of the reacting gases expands to the squish volume while the rest is redirected by the bowl into the center of the piston. At around 15 CAD aTDC, just after the post injection, the redirected expanding gases move towards the center. The unconsumed air in the center region is mixed with the reacting products and combined with the post injection combustion, to boost the final oxidation of the remaining soot. The hot soot is still more abundant in the outer region of the bowl since the momentum in the flow is ceased after the injection events.

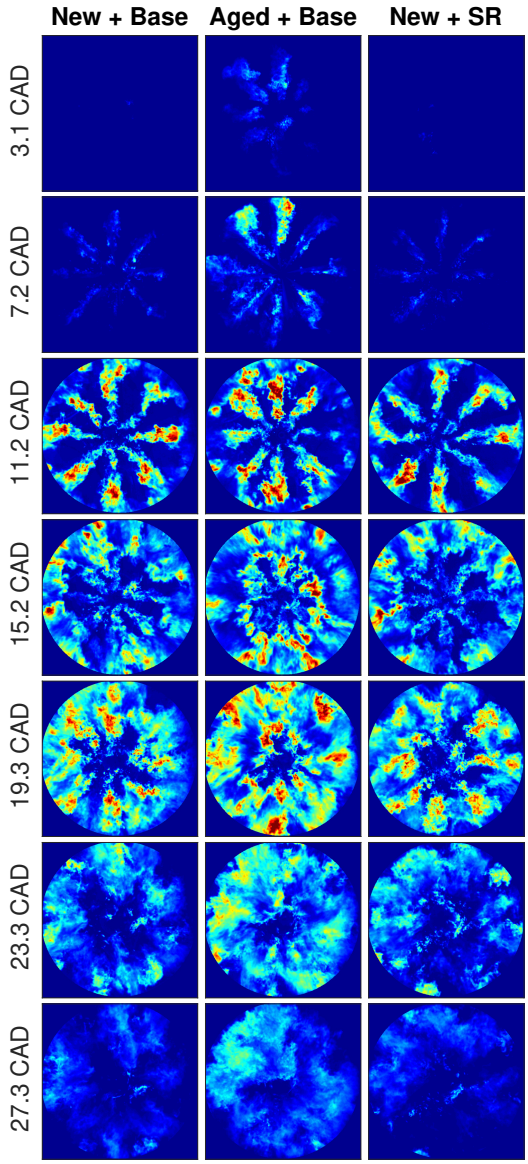

Figure 4.23: Natural luminosity signals of combustion processes at low load.

As can be seen in Figure 4.24, at around 19 CAD aTDC, the heat release is approaching the end while the integrated NL reaches a second peak. As the piston

travels further down and the flow becomes much weaker, the soot oxidation is limited to where the cold soot is left. The plots at 19.3 CAD in Figure 4.23 reveal that the NL signal becomes more evenly distributed since the effect of diffusion. The NL intensity from the aged injector is the highest simply due to the fuel quantity difference. More soot is formed initially and the combustion temperature is also higher. Figure 4.24 shows that the NL when using the new injector peaks at around 20 CAD aTDC and then decays rapidly whereas the NL from the aged injector reaches its peak slightly later. As the temperature and pressure decrease sharply at this stage, the soot oxidation is also significantly lowered until it stops due to insufficient temperature. It takes a longer time for the NL to decrease to zero in the aged injector case because the higher temperature allows a longer time window for soot oxidation. The SR fuel shows very little difference compared with the base fuel, indicating at this low load point with adequate ambient oxygen, the soot oxidation is not limited by the overall oxygen concentration.

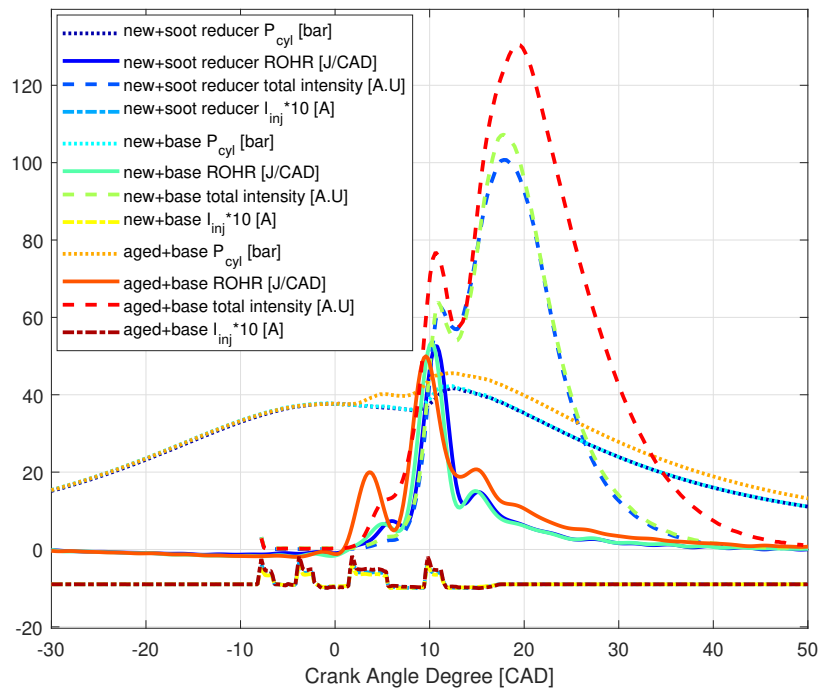

Figure 4.24: Cylinder pressure, heat release and total natural luminosity at low load.

The combustion process at medium load is shown in Figure 4.25 and the corresponding aHRR and the integrated NL signal are shown in Figure 4.26. As the ignition delay is reduced at this load point, the first NL signal appears at

around 3 CAD aTDC, which is from the first pilot injection. Then fuel from the second pilot injection is injected into the already reacting mixture at around 5 CAD aTDC (Figure 4.25), which gets ignited almost immediately and increases the NL signal to the first peak at around 8 CAD aTDC (Figure 4.26). The NL signals remain in the spray region with a higher signal in the tip areas. The aged injector's larger pilot injection quantity transports the soot a bit farther towards the center compared with the the new injector, as shown in the plots at 9.6 CAD of Figure 4.25.

Then the main injection passing through the hot soot clouds quenches the reaction slightly at around 10 CAD aTDC. But it is also ignited immediately by the heat from the pilot combustion, leading to the rapid main combustion heat release after 10 CAD aTDC as seen in Figure 4.26. With a higher injection pressure, the spray shaped soot luminosity after the main injection at low load is not observed at medium load. A shorter ignition delay leaves less time for the soot formation. Enhanced premixing by a higher pressure fuel injection also reduces the soot formation in the early stage. The longer main injection generates continuous momentum exchange between the fuel and the air which allows the soot to be oxidized in a more uniform distribution in the cylinder. The integrated NL signal starts to increase sharply just before the start of the post injection at around 18 CAD aTDC, which is illustrated in Figure 4.26, when the redirected gases are mixed with the residual air in the center region. At around 22 CAD aTDC it reaches its peak.

It can be seen in Figure 4.26 that the soot oxidation still lasts longer with the aged injector. The peak integrated NL signal from the aged injection is lower than that of the new injector but it becomes the highest after around 27 CAD aTDC among all the cases. One possible reason for this is the optical thickness difference. The aged injector delivers more fuel which lead to a higher soot formation. Soot cloud close to the bowl wall is colder due to temperature loss to the wall. Access to Oxygen is also inevitably limited. Thus, soot oxidation might be reduced and this optically thicker soot cloud layer could attenuate the NL signal recorded by the camera. Another possible explanation is that there is less soot formed with the aged injector because its prolonged injection duration provides a better fuel-air mixing. Additionally, the reduced ignition delay leaves less time for the early soot formation process, leading to an more prompt and complete combustion. Because of the higher temperature and a longer high temperature window, soot oxidation can continue longer in the late cycle with a slower reducing oxidation rate.

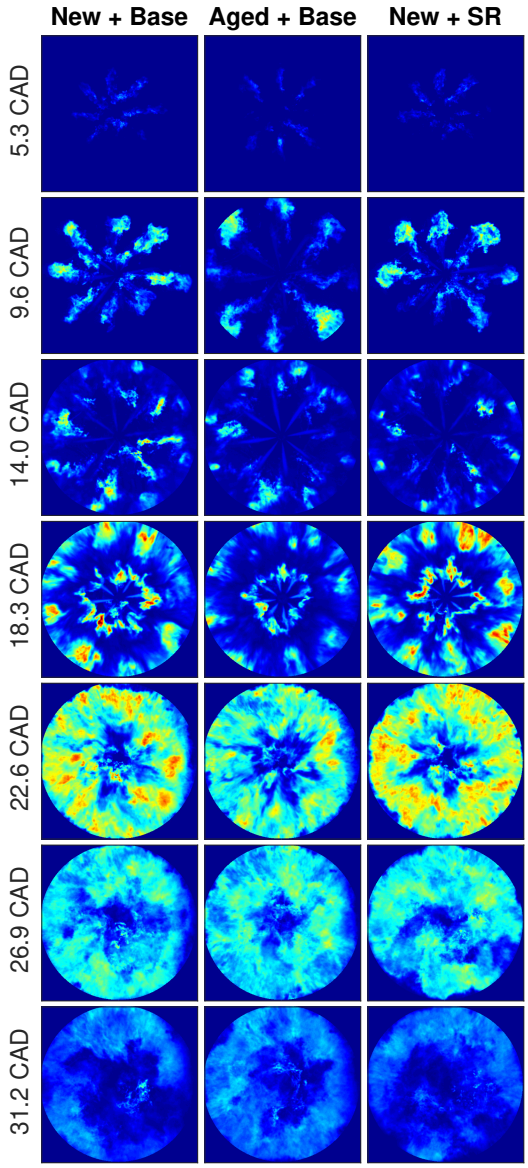

Figure 4.25: Natural luminosity signals of combustion processes at medium load.

Studies conducted on heavy-duty engines using single injection strategies have shown that the integrated NL signal is inversely correlated with the local oxygen

level at the flame lift-off position [110, 69]. The oxygenated fuel shows obvious reduction of the soot formation in such a diffusion flame, usually leading to a much lower NL. However, the SR fuel, compared with the baseline fuel, produces a much higher peak integrated NL in this multiple injection condition. This is probably caused by a thinner optical thickness as less soot is formed in the early cycle. More NL signal can pass through the soot cloud and be recorded by the camera. The pyrolysis of fuel is reduced and the soot oxidation is increased when the fuel is oxygenated [111]. As the soot luminosity increases exponentially with the local soot temperature [69], it is possible to obtain a higher NL signal even with a smaller soot volume fraction. It is noteworthy that the 452 nm filter may block a certain amount of NL signal from less hot soot in the longer wavelength. If the NL signal is integrated in a broadband way, the results could be different.

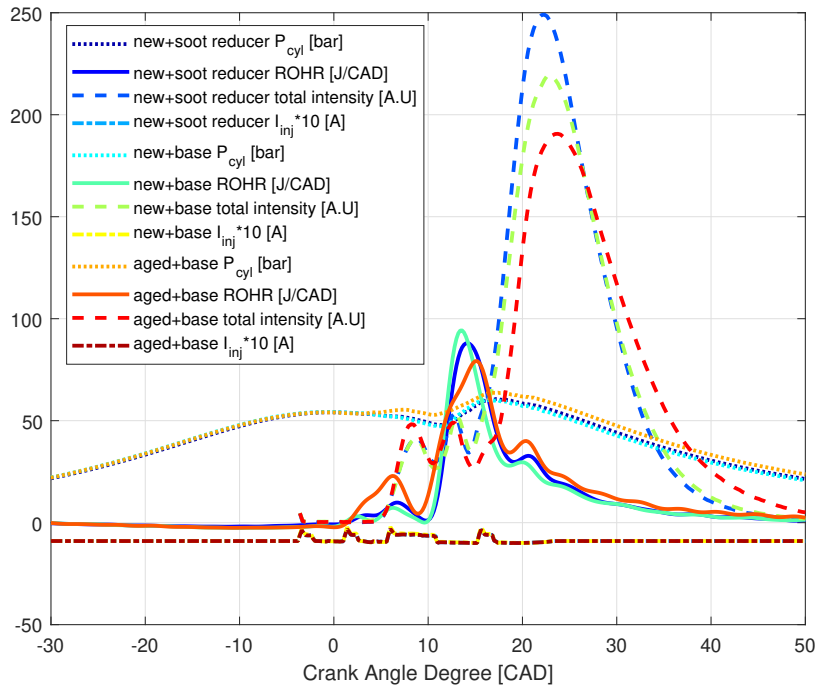

Figure 4.26: Cylinder pressure, heat release and total natural luminosity at medium load.

4.5 LII and LEM Measurements

Since LII is a 2-D technique and LEM is a 1-D method, the soot distribution in the cylinder volume becomes critical when trying to estimate the total soot. Based on observation from Figure 4.23 and Figure 4.25, the assumption is made

that the soot distribution is relatively even throughout the cylinder volume and axially symmetric after 25 CAD aTDC.

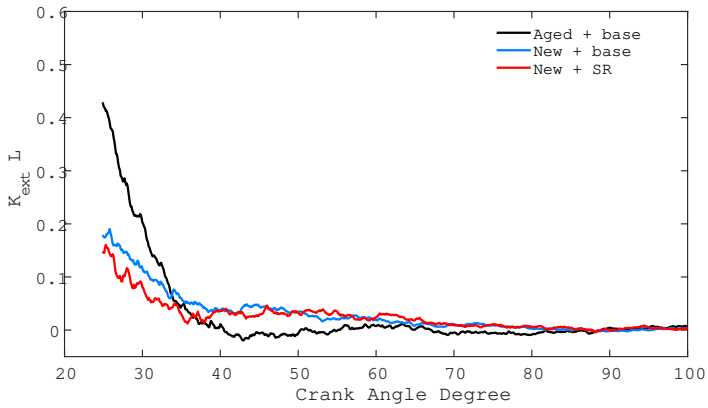

Figure 4.27: $K_{ext}L$ value calculated from the LEM measurement at low load.

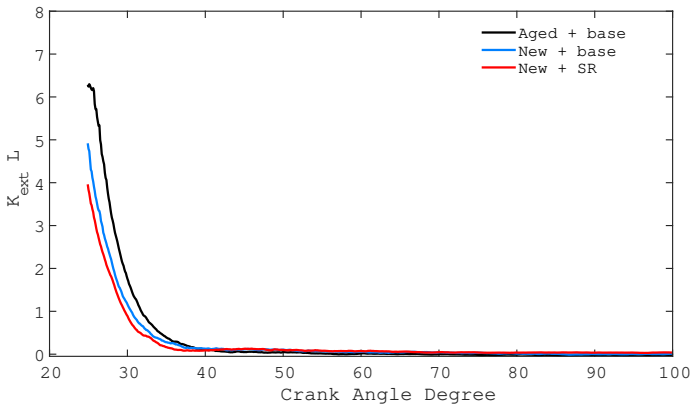

Figure 4.28: $K_{ext}L$ value calculated from the LEM measurement at medium load.

The $K_{ext}L$ values, which reflect the line-integrated soot concentration along the LEM laser beam, can be calculated using the method introduced in Chapter 3. The results are shown in the Figure 4.27 and Figure 4.28 for the low and medium load, respectively. At low load, $K_{ext}L$ is relatively noisy due to beam steering and lower soot concentration. In this case the transmitted signal I_t in the combustion condition is closer to the I_t in the motored condition, making $K_{ext}L$ more sensitive to small fluctuations.

At both load conditions, the aged injector shows a higher $K_{ext}L$ between 25 and 35 CAD aTDC. The larger fuel quantity injected by the aged injector, including a larger amount of dribble, causes the increase of soot formation in the early stage. However this extra amount of fuel also increases the temperature which accelerates the soot oxidation. To extract a more straightforward view of the change of $K_{ext}L$ values, the half-life of the $K_{ext}L$ is calculated by fitting an exponential decay function to it.

The calculated half-life of the $K_{ext}L$ is shown in Table 4.1. Large impact of the fuel quantity difference on the half-life is observed at low load. The 25% higher fuel quantity from the aged injector almost halves the half-life of the $K_{ext}L$ while there is only a very limited reduction at the medium load where there is a 10% of fuel difference. Soot oxidation shows a higher temperature sensitivity at the low load. The SR fuel shows an overall lower soot level, as well as a faster oxidation rate. Since 25 CAD aTDC is already close to the end of the heat release, it is impossible to conclude if the soot formation is lower in the earlier stage of the combustion from these LEM results.

Table 4.1: Half-life of the calculated $K_{ext}L$. A lower value indicates a faster soot oxidation.

Measurement points	Half-life [CAD]	
	Low load	Medium load
Aged injector + base	3.2	2.36
New injector + base	6	2.39
New injector + SR	4.8	2.21

Due to the fixed location of the LEM laser beam is very close to the ceiling of the combustion chamber, the $K_{ext}L$ value may not be able to reflect the soot level well in the late cycle, when the piston moves further down.

The spatially integrated LII signals (volume above the piston top, excluding the bowl area) are shown in the Figure 4.29 and Figure 4.30 for the low and medium load, respectively. At low load, the aged injector shows the highest soot volume fraction at 25 CAD aTDC but ends with the lowest at 70 CAD aTDC, which again verifies that the extra amount of fuel increases the soot formation while the elevated temperature accelerates the soot oxidation and creates a longer time window for the oxidation. Compared with the baseline fuel, the SR fuel constantly produces less soot during the entire measurement period. Due to the relatively low temperature with the new injector, the soot oxidation slows down significantly after 55 CAD aTDC because the soot volume fraction approaches a plateau (Figure 4.29), which contributes to the difference in the soot half-life as shown in Table 4.2.

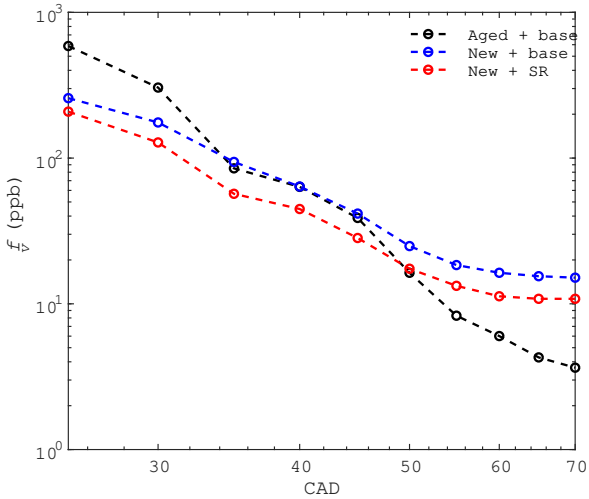

Figure 4.29: Spatially integrated LII signals at low load.

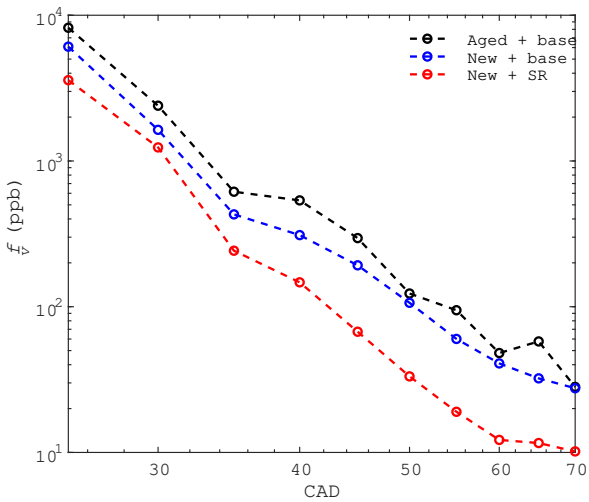

Figure 4.30: Spatially integrated LII signals at medium load.

At medium load, the oxidation rate difference becomes smaller between the cases. Although temperature difference between the new and aged injectors still exists, the temperature sensitivity of the soot oxidation is significantly reduced at this load. The oxidation rate of the soot from the aged injector is very close to that from the new injector (half-life 6 CAD vs 6.1 CAD). Compared with the baseline

fuel, the SR fuel shows a 8% shorter soot half-life at low load while a 14% faster oxidation rate is observed at the medium load condition. This agrees with many other studies that point out the oxygenated fuels are more effective with soot reduction at high engine loads than at low loads [112, 113].

It has to be noted that after around 45 CAD aTDC, the piston is already completely below the LII laser sheet. The volume between the piston and the laser, including the bowl area in the piston, certainly contain unoxidised soot. Thus, the soot volume fraction is inevitably underestimated in the later stage of the LII measurement.

Table 4.2: Half-life of the integrated LII signal. A lower value indicates a faster soot oxidation.

Measurement points	Half-life [CAD]	
	Low load	Medium load
Aged injector + base	6	6
New injector + base	10.3	6.1
New injector + SR	10.18	5.33

Chapter 5

Summary

In this work, an experimental approach is established to investigate the aging effects of injectors and the influences of certain fuel additives on the combustion progress with an focus on the soot process.

One set of new and and one set of aged injectors are first tested on a multi-cylinder engine for general combustion and emission characteristics using real-world operating conditions representing low and medium load application. Four fuels, including a baseline fuel and three of its blends with different fuel additives, are tested. They represent different types of functions to be achieved in the blends. Tri-propylene glycol monomethyl ether (TPGME) is used to represent an oxygenated compound, 2-Ethylhexyl nitrate (2-EHN) is used as an ignition improver, and quaternary ammonium salts (structure confidential) are used as a flow improver.

With exactly the same injection strategies and intake conditions, the aged injectors consistently show a noticeably higher fuel flow rate, which consequently causes a higher power output and affects emissions. Based on this observation, the presence of injector deposits was excluded since they most often cause reduced fuel flow rate and power output. Small soot reduction is observed with the TPGME additive. Ignition delay is reduced with the addition of 2-EHN. The expected flow increase with the flow improver additive is not seen in the selected operating conditions.

One of the new injectors and one of the aged injectors are selected for the following optical diagnostics. X-ray tomography is conducted to investigate whether there is any internal structure difference in the injector nozzle which can lead to this flow rate difference. Only marginal geometry difference can be observed,

which is caused by manufacturing tolerance. Both the nozzle holes and needle heads have smooth surfaces with similar dimensions, indicating that the flow rate difference is very unlikely caused by the difference in the nozzle geometry.

Next, high-speed imaging is conducted on an optically accessible engine using the Mie-scattering in non-reacting conditions. The integrated scattering signals of the aged injector are constantly higher than those of the new injector. Considering both are used in similar ambient conditions, the higher injection rate of the aged injector is demonstrated again. A similar initial response of the fuel injection is observed, meaning the fuel quantity difference is not caused by a timing difference of the SOI. The liquid fuel penetration and spray spreading angles are also similar between the injectors. On the other hand, an apparent prolonged injection is seen with the aged injector, which is considered the main reason of the fuel flow difference. A delayed needle response during the closing stage is suspected to lead to this difference. Although this phenomenon is more obvious during a longer injection event, its impact is larger on the shorter injection events, especially the short pilot injections. Additionally, the aged injector also shows a more serious dribble problem after injection.

Then the combustion process is investigated by analysing the natural luminosity signals and the heat release simultaneously. At low load, the aged injector produces the highest soot luminosity signals simply due to the higher fuel quantity injected. With a lower injection pressure at this point, the soot distribution is less even across the cylinder. The extra amount of fuel also elevates the overall temperature, allowing a longer oxidation window for the soot. The TPGME additive shows little impact on the soot oxidation compared with the baseline fuel at this point. At medium load, the aged injector shows a lower soot luminosity than the new injector. The prolonged injection generates a better fuel-air mixing, which can reduce the soot formation in the early cycle. The higher heat release in the pilot combustion can lead to a more prompt ignition of the fuel from the main injection, leaving less residence time for soot formation in the pyrolysis. The TPGME additive produces a higher soot luminosity at medium load compared with the baseline fuel, likely because the oxygen in the fuel increases the local soot temperature. However, the optical depth can be different if the thickness of the soot cloud differs significantly. The results may also be altered if a broad-band signal is collected instead of this narrow-band signal collection at 452 nm.

Finally combined laser induced incandescence and laser extinction measurements are used to investigate the late cycle soot oxidation. At low load the soot oxidation rate is highly sensitive to temperature variation caused by the fuel quantity difference between the injectors. The TPGME additive shows a smaller impact.

At medium load, however, this fuel quantity sensitivity becomes much smaller. The oxygenated fuel shows a higher soot reduction rate.

5.1 Thesis Contributions

In this thesis, influences of injector aging has been studied along with effects of certain fuel additives. There are different types of injector aging effects. Previous research in the field has mostly focused on effects of injector deposits on the sprays. Studies of drift in injection characteristics due to wear or degradation over time are rare in the literature, especially those conducted in real-world engine conditions. No studies have been found in the literature that investigate aging effects on injection characteristics in light-duty optical engines using multiple injection strategies.

The original findings in this work include:

- An experimental procedure is designed which considers various injector aging effects, which is able to eliminate is able to eliminate unrelated ones.
- A significant delayed needle actuation during closing stage after aging is found to be the major cause of increased injection quantity. Fuel quantity delivered during shorter injection events are more affected than a longer injection event. It is also the first attempt of applying simple light scattering techniques to the liquid part of a fuel jet to estimate fuel quantity and needle responses. The results demonstrates that it works well in this comparative work.
- The TPGME additive is usually found to be able to reduce soot luminosity significantly in the combustion thanks to its oxygen content which reduces the soot formation in the early stage. Several studies conducted on heavy duty optical engine using single injection strategies have verified this finding. However, the part-load operating conditions in this light-duty engine produces a very different combustion mode, leading to a controversial results. Compared with baseline fuel, a higher soot luminosity is observed when using the TPGME additive additive, but the combined LII and LEM measurements indicate an overall lower soot volume fraction when TPGME is added. Most likely the soot temperature is increased by the additive which leads to a stronger soot luminosity that overcomes the effect of a lower soot volume fraction.

Chapter 6

Future Outlook

Some consideration of further extension and improvement of this experimental approach is listed here.

First of all, the operating conditions can be extended to a wider range in the reference tests stage. A more complete set of measurement points which can cover the full engine operating range may help find more interesting points to look at. At different loads or with different injection strategies, the effects of aging and fuel additives could be different. A more complete picture of these influences could provide critical feedback for future design considerations.

Another interesting point would be investigating injectors at different stages of their lifespan from different areas. The fuel quality variation in different markets and the different ways the vehicles are used (for example influences from climate or traffic conditions) may cause different aging problems.

Moving the nozzle (including the needle) and/or the spring from an aged injector to a new injector body would make it possible to isolate the origin of the aged injector's extended injection time – if it is due to changes in the needle, in the spring or if the change has occurred in the injector body. If the problem arises in the injector body, it could for example be due to wear of the solenoid-actuated servo valve that controls the fuel flow to the nozzle area and thereby actuates the opening and closing of the needle.

Some improvements could be done to the optical measurements to get better results. For the Mie-scattering measurement, a better incident light source would be very helpful. It could be an additional light source from the opposite direction of the laser diode, or even four light sources that cover all side windows. If so,

all fuel jets should show equally good scattering signals. Thus, all sprays could be studied and the hole-to-hole variation could be revealed. For the distortion correction process, the absolute value of the natural luminosity in a local area is of less importance since this work is comparative. However, if detailed in-cylinder motion in a local area is critical, a ray-tracing based distortion correction could be used instead of the simple geometric correction applied here. This is because the piston geometry not only causes geometric distortion, but also changes the intensity distribution.

Ignition studies could be added to investigate the early stages of the reaction. Both chemiluminescence imaging and laser induced fluorescence could be used to trace early intermediate products such as OH radicals. Furthermore, early stage soot formation is also interesting to study either by LII or even direct sampling from the cylinder. The engine-out soot close to the exhaust valve position would also be interesting to measure and compare with the in-cylinder soot measurements. The actuation of the injector needle, especially during the closing stage, needs to be further studied to find out the reason of the prolonged injection for the aged injector. High speed X-ray phase-contrast imaging could be ideal for a transient condition when the injector is actuating. Both the needle motion and the internal flow field could then be acquired.

Chapter 7

References

[1] British Petroleum. Energy outlook 2019, 2019. `https://www.bp.com/content/dam/bp/business-sites/en/global/corporate/pdfs/energy-economics/energy-outlook/bp-energy-outlook-2019.pdf`; accessed 25-02-2020.

[2] Carlos Kusano Bucalen Ferrari, Eduardo Luzia Franca, and Adenilda Cristina Honorio-França. Nitric oxide, health and disease. *Journal of Applied Biomedicine*, 7(4):163 – 173, 2009.

[3] Y.P Moodley. The role of inducible nitric oxide in health and disease. *Current Diagnostic Pathology*, 8(5):297 – 304, 2002.

[4] R. Prasad and Venkateswara Bella. A review on diesel soot emission, its effect and control. *Bulletin of Chemical Reaction Engineering Catalysis*, 5(2):69–86, 2011.

[5] T. C. Bond, S. J. Doherty, D. W. Fahey, P. M. Forster, T. Berntsen, B. J. DeAngelo, M. G. Flanner, S. Ghan, B. Kärcher, D. Koch, S. Kinne, Y. Kondo, P. K. Quinn, M. C. Sarofim, M. G. Schultz, M. Schulz, C. Venkataraman, H. Zhang, S. Zhang, N. Bellouin, S. K. Guttikunda, P. K. Hopke, M. Z. Jacobson, J. W. Kaiser, Z. Klimont, U. Lohmann, J. P. Schwarz, D. Shindell, T. Storelvmo, S. G. Warren, and C. S. Zender. Bounding the role of black carbon in the climate system: A scientific assessment. *Journal of Geophysical Research: Atmospheres*, 118(11):5380–5552, 2013.

[6] Robert J Conrado, Chad A Haynes, Brenda E Haendler, and Eric J Toone. Electrofuels: a new paradigm for renewable fuels. In *Advanced Biofuels and Bioproducts*, pages 1037–1064. Springer, 2013.

[7] J.Hagen, O.E.Herrmann, J.Weber, and D.Queck. Diesel combustion potentials by further injector improvement. *MTZ worldwide*, 77, 2016.

[8] Jost Weber, Olaf Herrmann, Ron Puts, Jyun Kawamura, Yasufumi Tomida, and Makoto Mashida. Next improvement potentials for heavy-duty diesel engine - tailor the fuel injection system to the combustion needs, mar 2017.

[9] Dennis Siebers and Brian Higgins. Flame lift-off on direct-injection diesel sprays under quiescent conditions. *SAE Transactions*, 110:400–421, 2001.

[10] Xiangang Wang, Zuohua Huang, Wu Zhang, Olawole Abiola Kuti, and Keiya Nishida. Effects of ultra-high injection pressure and micro-hole nozzle on flame structure and soot formation of impinging diesel spray. *Applied Energy*, 88(5):1620 – 1628, 2011.

[11] Keiya Nishida, Jingyu Zhu, Xianyin Leng, and Zhixia He. Effects of micro-hole nozzle and ultra-high injection pressure on air entrainment, liquid penetration, flame lift-off and soot formation of diesel spray flame. *International Journal of Engine Research*, 18(1-2):51–65, 2017.

[12] Cheolwoong Park, Sanghoon Kook, and Choongsik Bae. Effects of multiple injections in a hsdi diesel engine equipped with common rail injection system. In *SAE 2004 World Congress Exhibition*. SAE International, mar 2004.

[13] Zhiyu Han, Ali Uludogan, Gregory J. Hampson, and Rolf D. Reitz. Mechanism of soot and nox emission reduction using multiple-injection in a diesel engine. *SAE Transactions*, 105:837–852, 1996.

[14] Tomi R. Krogerus, Mika P. Hyvönen, and Kalevi J. Huhtala. A Survey of Analysis, Modeling, and Diagnostics of Diesel Fuel Injection Systems. *Journal of Engineering for Gas Turbines and Power*, 138(8), 02 2016. 081501.

[15] John B Heywood. *Internal Combustion Engine Fundamentals*. New York :McGraw-Hill, 1988.

[16] John E. Dec. A conceptual model of di diesel combustion based on laser-sheet imaging*. In *International Congress Exposition*. SAE International, feb 1997.

[17] H Kosaka, T Aizawa, and T Kamimoto. Two-dimensional imaging of ignition and soot formation processes in a diesel flame. *International Journal of Engine Research*, 6(1):21–42, 2005.

[18] Hidenori Kosaka, Takahiro Nishigaki, Takeyuki Kamimoto, and Shinichi Harada. A study on soot formation and oxidation in an unsteady spray flame via laser induced incandescence and scattering techniques. In *1995 SAE International Fall Fuels and Lubricants Meeting and Exhibition*. SAE International, oct 1995.

[19] Hidenori Kosaka, Takahiro Nishigaki, Takeyuki Kamimoto, Takashi Sano, Akira Matsutani, and Shinichi Harada. Simultaneous 2-d imaging of oh radicals and soot in a diesel flame by laser sheet techniques. In *International Congress Exposition*. SAE International, feb 1996.

[20] Norbert Peters. *Turbulent Combustion*. Cambridge Monographs on Mechanics. Cambridge University Press, 2000.

[21] C. Heimgärtner and A. Leipertz. Investigation of the primary spray breakup close to the nozzle of a common - rail high pressure diesel injection system, jun 2000.

[22] A. Fath, K.-U. Munch, and Alfred Leipertz. Spray break-up process of diesel fuel investigated close to the nozzle. *International Journal of Fluid Mechanics Research*, 24(1-3):251–260, 1997.

[23] Jaclyn E. Johnson, Jeffrey Naber, Seong-Young Lee, Eric Kurtz, Nan Robarge, and Hai-Wen Ge. Investigation of diesel liquid spray penetration fluctuations under vaporizing conditions. In *SAE 2012 World Congress Exhibition*. SAE International, apr 2012.

[24] Dennis L. Siebers. Liquid-phase fuel penetration in diesel sprays. *SAE Transactions*, 107:1205–1227, 1998.

[25] Brian S. Higgins, Charles J. Mueller, and Dennis L. Siebers. Measurements of fuel effects on liquid-phase penetration in dl sprays. *SAE Transactions*, 108:630–643, 1999.

[26] Dennis L. Siebers. Scaling liquid-phase fuel penetration in diesel sprays based on mixing-limited vaporization. *SAE Transactions*, 108:703–728, 1999.

[27] Jeffrey D. Naber and Dennis L. Siebers. Effects of gas density and vaporization on penetration and dispersion of diesel sprays. *SAE Transactions*, 105:82–111, 1996.

[28] Rolf D. Reitz and F. B. Bracco. On the dependence of spray angle and other spray parameters on nozzle design and operating conditions. In *1979*

Automotive Engineering Congress and Exposition. SAE International, feb 1979.

[29] Jang-Heon Kim, Keiya Nishida, Takuo Yoshizaki, and Hiroyuki Hiroyasu. Characterization of flows in the sac chamber and the discharge hole of a d.i. diesel injection nozzle by using a transparent model nozzle. In *International Fuels Lubricants Meeting Exposition*. SAE International, oct 1997.

[30] Dennis L. Siebers. *Recent Developments on Diesel Fuel Jets Under Quiescent Conditions*, pages 257–308. Springer Berlin Heidelberg, Berlin, Heidelberg, 2009.

[31] Lyle M. Pickett and Dennis L. Siebers. Orifice Diameter Effects on Diesel Fuel Jet Flame Structure . *Journal of Engineering for Gas Turbines and Power*, 127(1):187–196, 02 2005.

[32] Dennis Siebers, Brian Higgins, and Lyle Pickett. Flame lift-off on direct-injection diesel fuel jets: Oxygen concentration effects. *SAE Transactions*, 111:1490–1509, 2002.

[33] D. L. Siebers and L. M. Pickett. Injection pressure and orifice diameter effects on soot in di diesel fuel jets. In J. H. Whitelaw, F. Payri, C. Arcoumanis, and J. M. Desantes, editors, *Thermo- and Fluid Dynamic Processes in Diesel Engines 2*, pages 109–132, Berlin, Heidelberg, 2004. Springer Berlin Heidelberg.

[34] Dale R. Tree and Kenth I. Svensson. Soot processes in compression ignition engines. *Progress in Energy and Combustion Science*, 33(3):272–309, 2007.

[35] W. Bartok and A.F. Sarofim. Fossil fuel combustion: A source book. 12 1991.

[36] Randy L. Vander Wal and Aaron J. Tomasek. Soot nanostructure: Dependence upon synthesis conditions. *Combustion and Flame*, 136(1-2):129–140, 2004.

[37] David B Kittelson. Engines and nanoparticles: a review. *Journal of aerosol science*, 29(5-6):575–588, 1998.

[38] Irvin Glassman, Richard A Yetter, and Nick G Glumac. *Combustion*. Academic press, 2014.

[39] Shuichi Matsumoto, Kenji Date, Tooru Taguchi, and Olaf Erik Herrmann. The new denso common rail diesel solenoid injector. *Auto Tech Review*, 2(11):24–29, 2013.

[40] Mikael Lindström. *Injector nozzle hole parameters and their influence on real di diesel performance.* PhD thesis, KTH, 2009.

[41] H Roth, M Gavaises, and C Arcoumanis. Cavitation initiation, its development and link with flow turbulence in diesel injector nozzles. *SAE Transactions*, pages 561–580, 2002.

[42] J. Barker, P. Richard, C. Snape, and W. Meredith. Diesel injector deposits - an issue that has evolved with engine technology. In *SAE International Powertrains, Fuels and Lubricants Meeting.* SAE International, aug 2011.

[43] Jens Tang, Stefan Pischinger, Matthias Lamping, Thomas Körfer, Marek Tatur, and Dean Tomazic. Coking phenomena in nozzle orifices of dl-diesel engines, apr 2009.

[44] Rinaldo Caprotti, Angela Breakspear, Olaf Graupner, Thomas Klaua, and Oliver Kohnen. Diesel injector deposits potential in future fueling systems. Technical report, SAE Technical Paper, 2006.

[45] Robert Quigley, Robert Barbour, Emma Fahey, D Arters, William Wetzel, and James Ray. A study of the internal diesel injector deposit phenomenon. In *TAE Fuels 7th Annual Colloquium*, 2009.

[46] Scott D. Schwab, Joshua J. Bennett, Steven J. Dell, Julie M. Galante-Fox, Alexander M. Kulinowski, and Keith T. Miller. Internal injector deposits in high-pressure common rail diesel engines, oct 2010.

[47] AP Watkinson and DI Wilson. Chemical reaction fouling: A review. *Experimental Thermal and Fluid Science*, 14(4):361–374, 1997.

[48] A. Birgel, N. Ladommatos, P. Aleiferis, S. Zülch, N. Milovanovic, V. Lafon, A. Orlovic, P. Lacey, and Paul Richards. Deposit formation in the holes of diesel injector nozzles: A critical review. In *Powertrains, Fuels and Lubricants Meeting.* SAE International, oct 2008.

[49] Gerhard Lepperhoff and Michael Houben. Mechanisms of deposit formation in internal combustion engines and heat exchangers. In *International Congress Exposition.* SAE International, mar 1993.

[50] Rinaldo Caprotti, Angela Breakspear, Olaf Graupner, Thomas Klaua, and Oliver Kohnen. Diesel injector deposits potential in future fueling systems. In *Powertrain Fluid Systems Conference and Exhibition.* SAE International, oct 2006.

[51] Bruno Argueyrolles, Stephan Dehoux, Patrick Gastaldi, Lysiane Grosjean, Franck Levy, Alexandre Michel, and Daniel Passerel. Influence of injector nozzle design and cavitation on coking phenomenon. In *JSAE/SAE International Fuels Lubricants Meeting*. SAE International, jul 2007.

[52] A Birgel, N Ladommatos, P Aleiferis, S Zülch, N Milovanovic, V Lafon, A Orlovic, P Lacey, and Paul Richards. Deposit formation in the holes of diesel injector nozzles: A critical review. Technical report, SAE Technical Paper, 2008.

[53] J Barker, P Richard, C Snape, and W Meredith. Diesel injector deposits-an issue that has evolved with engine technology. Technical report, SAE Technical Paper, 2011.

[54] Agnese Magno, Ezio Mancaruso, Bianca Maria Vaglieco, Salvatore Florio, Gianmarco Gioco, and Elena Rebesco. Study on spray injection and combustion of fouled and cleaned injectors by means of 2-d digital imaging in a transparent cr diesel engine. In *11th International Conference on Engines Vehicles*. SAE International, sep 2013.

[55] Alessandro Montanaro and Luigi Allocca. Impact of the nozzle coking on spray formation for diesel injectors. In *SAE/KSAE 2013 International Powertrains, Fuels Lubricants Meeting*. SAE International, oct 2013.

[56] Hongming Xu, Chongming Wang, Xiao Ma, Asish K Sarangi, Adam Weall, and Jens Krueger-Venus. Fuel injector deposits in direct-injection spark-ignition engines. *Progress in Energy and Combustion Science*, 50:63–80, 2015.

[57] Yuan Wen, Yinhui Wang, Chenling Fu, Wei Deng, Zhangsong Zhan, Yuhang Tang, Xuefei Li, Haichun Ding, and Shijin Shuai. The impact of injector deposits on spray and particulate emission of advanced gasoline direct injection vehicle. In *SAE 2016 International Powertrains, Fuels Lubricants Meeting*. SAE International, oct 2016.

[58] Jörg Ullmann, Marion Geduldig, Heinz Stutzenberger, Rinaldo Caprotti, and Graham Balfour. Investigation into the formation and prevention of internal diesel injector deposits. In *SAE World Congress Exhibition*. SAE International, apr 2008.

[59] S d'Ambrosio and A Ferrari. Diesel injector coking: optical-chemical analysis of deposits and influence on injected flow-rate, fuel spray and engine performance. *Journal of engineering for gas turbines and power*, 134(6), 2012.

[60] David Greif and Vedanth Srinivasan. Numerical prediction of erosive cavitating flows in injection equipment. In *10th International Conference on Engines Vehicles*. SAE International, sep 2011.

[61] Marco Cristofaro, Wilfried Edelbauer, Phoevos Koukouvinis, and Manolis Gavaises. A numerical study on the effect of cavitation erosion in a diesel injector. *Applied Mathematical Modelling*, 78:200 – 216, 2020.

[62] Florin Mariasiu. Numerical investigation of the effects of biofuel characteristics on the injector nozzle erosion process. *Tribology Transactions*, 56(2):161–168, 2013.

[63] Hisaharu TAKEUCHI, Masaaki KATO, Shuichi KAJITANI, Mizuho YAMAGUCHI, Yuuji AIHARA, and Masaaki TAKAHARA. A study of diesel nozzle tip wear in the case of the fuel dme (erosion). In *The Proceedings of the International Conference on Power Engineering (ICOPE) 2009.2*, pages _2–181_. The Japan Society of Mechanical Engineers, 2009.

[64] Michele Battistoni, Qingluan Xue, Sibendu Som, and Eric Pomraning. Effect of off-axis needle motion on internal nozzle and near exit flow in a multi-hole diesel injector, apr 2014.

[65] X Zhang, J Liu, and J Wang. Effect of fuel and nozzle geometry on the off-axis oscillation of needle in diesel injectors using high-speed x-ray phase contrast imaging. *Journal of Instrumentation*, 11(05):C05015, 2016.

[66] JH Lee, S Cho, Sang Yong Lee, and Choongsik Bae. Bouncing of the diesel injector needle at the closing stage. *Proceedings of the Institution of Mechanical Engineers, Part D: Journal of Automobile Engineering*, 216(8):691–700, 2002.

[67] Nubia M Ribeiro, Angelo C Pinto, Cristina M Quintella, Gisele O da Rocha, Leonardo SG Teixeira, Lílian LN Guarieiro, Maria do Carmo Rangel, Márcia CC Veloso, Michelle JC Rezende, Rosenira Serpa da Cruz, et al. The role of additives for diesel and diesel blended (ethanol or biodiesel) fuels: a review. *Energy & fuels*, 21(4):2433–2445, 2007.

[68] Pin-Chia Chen, Wei-Cheng Wang, William L. Roberts, and Tiegang Fang. Spray and atomization of diesel fuel and its alternatives from a single-hole injector using a common rail fuel injection system. *Fuel*, 103:850 – 861, 2013.

[69] Charles J. Mueller and Glen C. Martin. Effects of oxygenated compounds on combustion and soot evolution in a di diesel engine:broadband natural luminosity imaging. In *Spring Fuels Lubricants Meeting Exhibition*. SAE International, may 2002.

[70] Pierre-Marie Robitaille. Blackbody radiation and the carbon particle. *Progress in Physics*, 3:36, 2008.

[71] HA Michelsen, C Schulz, GJ Smallwood, and S Will. Laser-induced incandescence: Particulate diagnostics for combustion, atmospheric, and industrial applications. *Progress in Energy and Combustion Science*, 51:2–48, 2015.

[72] Max Hofmann, Wolfgang G. Bessler, Christof Schulz, and Helga Jander. Laser-induced incandescence for soot diagnostics at high pressures. *Appl. Opt.*, 42(12):2052–2062, Apr 2003.

[73] P Roth and AV Filippov. In situ ultrafine particle sizing by a combination of pulsed laser heatup and particle thermal emission. *Journal of aerosol science*, 27(1):95–104, 1996.

[74] Henrik Bladh, Jonathan Johnsson, and P-E Bengtsson. On the dependence of the laser-induced incandescence (lii) signal on soot volume fraction for variations in particle size. *Applied Physics B*, 90(1):109–125, 2008.

[75] Boman Axelsson, Robert Collin, and Per-Erik Bengtsson. Laser-induced incandescence for soot particle size measurements in premixed flat flames. *Applied Optics*, 39(21):3683–3690, 2000.

[76] Boman Axelsson, Robert Collin, and Per-Erik Bengtsson. Laser-induced incandescence for soot particle size measurements in premixed flat flames. *Appl. Opt.*, 39(21):3683–3690, Jul 2000.

[77] Hua Zhao and Nicos Ladommatos. Optical diagnostics for soot and temperature measurement in diesel engines. *Progress in Energy and Combustion Science*, 24(3):221–255, 1998.

[78] Craig F Bohren and Donald R Huffman. *Absorption and scattering of light by small particles*. John Wiley & Sons, 2008.

[79] Alan C Eckbreth. *Laser diagnostics for combustion temperature and species*, volume 3. CRC press, 1996.

[80] Chapter 6 - evaluation methods for properties of nanostructured body. In Masuo Hosokawa, Kiyoshi Nogi, Makio Naito, and Toyokazu Yokoyama,

editors, *Nanoparticle Technology Handbook (Second Edition)*, pages 317 – 383. Elsevier, Amsterdam, second edition edition, 2012.

[81] Johan Simonsson, Nils-Erik Olofsson, Sandra Török, Per-Erik Bengtsson, and Henrik Bladh. Wavelength dependence of extinction in sooting flat premixed flames in the visible and near-infrared regimes. *Applied Physics B*, 119(4):657–667, 2015.

[82] AVL. Avl micro soot sensor. `https://www.avl.com/-/mssplus-avl-micro-soot-sensor`; accessed 06-03-2020.

[83] V Macián, V Bermúdez, R Payri, and J Gimeno. New technique for determination of internal geometry of a diesel nozzle with the use of silicone methodology. *Experimental techniques*, 27(2):39–43, 2003.

[84] Alan L Kastengren, F Zak Tilocco, Christopher F Powell, Julien Manin, Lyle M Pickett, Raul Payri, and Tim Bazyn. Engine combustion network (ecn): measurements of nozzle geometry and hydraulic behavior. *Atomization and Sprays*, 22(12):1011–1052, 2012.

[85] Piotr Strek, Daniel Duke, Andrew Swantek, Alan Kastengren, Christopher F. Powell, and David P. Schmidt. X-ray radiography and cfd studies of the spray g injector. In *SAE 2016 World Congress and Exhibition*. SAE International, apr 2016.

[86] Katarzyna E Matusik, Daniel J Duke, Alan L Kastengren, Nicholas Sovis, Andrew B Swantek, and Christopher F Powell. High-resolution x-ray tomography of engine combustion network diesel injectors. *International Journal of Engine Research*, 19(9):963–976, 2018.

[87] Patric Jacobs, Erwin Sevens, and Marc Kunnen. Principles of computerised x-ray tomography and applications to building materials. *Science of the total environment*, 167(1-3):161–170, 1995.

[88] Fred W Bowditch. A new tool for combustion research a quartz piston engine. Technical report, SAE Technical Paper, 1961.

[89] Salma Bejaoui, Xavier Mercier, Pascale Desgroux, and Eric Therssen. Laser induced fluorescence spectroscopy of aromatic species produced in atmospheric sooting flames using uv and visible excitation wavelengths. *Combustion and Flame*, 161(10):2479 – 2491, 2014.

[90] Jessica Dahlstrom, Oivind Andersson, Martin Tuner, and Håkan Persson. Experimental comparison of heat losses in stepped-bowl and re-entrant

combustion chambers in a light duty diesel engine. In *SAE 2016 World Congress and Exhibition*. SAE International, apr 2016.

[91] Silvia Berndt, Ulrike Schümann, Thomas Sadlowski, and Bert Buchholz. Development of a laboratory test for the deposit forming tendency of diesel fuels. *ATZoffhighway worldwide*, 11(1):50–55, 2018.

[92] Charles J. Mueller, William J. Pitz, Lyle M. Pickett, Glen C. Martin, Dennis L. Siebers, and Charles K. Westbrook. Effects of oxygenates on soot processes in di diesel engines: Experiments and numerical simulations. In *2003 JSAE/SAE International Spring Fuels and Lubricants Meeting*. SAE International, may 2003.

[93] Cosmin E. Dumitrescu, A. S. Cheng, Eric Kurtz, and Charles J. Mueller. A Comparison of Methyl Decanoate and Tripropylene Glycol Monomethyl Ether for Soot-Free Combustion in an Optical Direct-Injection Diesel Engine. *Journal of Energy Resources Technology*, 139(4), 04 2017. 042210.

[94] Cosmin E Dumitrescu, Charles J Mueller, and Eric Kurtz. Investigation of a tripropylene-glycol monomethyl ether and diesel blend for soot-free combustion in an optical direct-injection diesel engine. *Applied Thermal Engineering*, 101:639–646, 2016.

[95] Randy L Vander Wal and Aaron J Tomasek. Soot oxidation: dependence upon initial nanostructure. *Combustion and flame*, 134(1-2):1–9, 2003.

[96] Randy L Vander Wal and Aaron J Tomasek. Soot nanostructure: dependence upon synthesis conditions. *Combustion and Flame*, 136(1-2):129–140, 2004.

[97] Holger Bornemann, Friedrich Scheidt, and Wolfram Sander. Thermal decomposition of 2-ethylhexyl nitrate (2-ehn). *International journal of chemical kinetics*, 34(1):34–38, 2002.

[98] PQE Clothier, BD Aguda, A Moise, and HO Pritchard. How do diesel-fuel ignition improvers work? *Chemical Society Reviews*, 22(2):101–108, 1993.

[99] Y Stein, Richard A Yetter, FL Dryer, and A Aradi. The autoignition behavior of surrogate diesel fuel mixtures and the chemical effects of 2-ethylhexyl nitrate (2-ehn) cetane improver. *SAE transactions*, pages 1029–1045, 1999.

[100] Andrew M Ickes, Stanislav V Bohac, and Dennis N Assanis. Effect of 2-ethylhexyl nitrate cetane improver on no x emissions from premixed low-temperature diesel combustion. *Energy & Fuels*, 23(10):4943–4948, 2009.

[101] Scott D Schwab, Gregory H Guinther, Timothy J Henly, and Keith T Miller. The effects of 2-ethylhexyl nitrate and di-tertiary-butyl peroxide on the exhaust emissions from a heavy-duty diesel engine. *SAE transactions*, pages 873–880, 1999.

[102] Megan C Jennings, Kevin PC Minbiole, and William M Wuest. Quaternary ammonium compounds: an antimicrobial mainstay and platform for innovation to address bacterial resistance. *ACS infectious diseases*, 1(7):288–303, 2015.

[103] Chris Zhisheng Chen, Nora C Beck-Tan, Prasad Dhurjati, Tina K van Dyk, Robert A LaRossa, and Stuart L Cooper. Quaternary ammonium functionalized poly (propylene imine) dendrimers as effective antimicrobials: Structure- activity studies. *Biomacromolecules*, 1(3):473–480, 2000.

[104] Charles M Starks. Phase-transfer catalysis. i. heterogeneous reactions involving anion transfer by quaternary ammonium and phosphonium salts. *Journal of the American Chemical Society*, 93(1):195–199, 1971.

[105] IK Karathanassis, K Trickett, P Koukouvinis, J Wang, R Barbour, and M Gavaises. Illustrating the effect of viscoelastic additives on cavitation and turbulence with x-ray imaging. *Scientific reports*, 8(1):1–15, 2018.

[106] Homa Naseri, Kieran Trickett, Nicholas Mitroglou, Ioannis Karathanassis, Phoevos Koukouvinis, Manolis Gavaises, Robert Barbour, Dale Diamond, Sarah E Rogers, Maurizio Santini, et al. Turbulence and cavitation suppression by quaternary ammonium salt additives. *Scientific reports*, 8(1):1–15, 2018.

[107] Michael F.J. Brunt, Harjit Rai, and Andrew L. Emtage. The calculation of heat release energy from engine cylinder pressure data. In *International Congress Exposition*. SAE International, feb 1998.

[108] Tadashi TSURUSHIMA, Long ZHANG, and Yoshinori ISHII. A study of unburnt hydrocarbon emission in small di diesel engines. In *International Congress Exposition*. SAE International, mar 1999.

[109] Jun Kojima, Yuji Ikeda, and Tsuyoshi Nakajima. Spatially resolved measurement of oh*, ch*, and c2* chemiluminescence in the reaction zone of laminar methane/air premixed flames. *Proceedings of the Combustion institute*, 28(2):1757–1764, 2000.

[110] Ansis Upatnieks and Charles J. Mueller. Investigation of the relationship between di diesel combustion processes and engine-out soot using an oxy-

genated fuel. In *SAE 2004 World Congress Exhibition*. SAE International, mar 2004.

[111] Ronald J. Donahue and David E. Foster. Effects of oxygen enhancement on the emissions from a di diesel via manipulation of fuels and combustion chamber gas composition. In *SAE 2000 World Congress*. SAE International, mar 2000.

[112] Juhun Song, Kraipat Cheenkachorn, Jinguo Wang, Joseph Perez, André L Boehman, Philip John Young, and Francis J Waller. Effect of oxygenated fuel on combustion and emissions in a light-duty turbo diesel engine. *Energy & Fuels*, 16(2):294–301, 2002.

[113] A. S. Cheng, Robert W. Dibble, and Bruce A. Buchholz. The effect of oxygenates on diesel engine particulate matter. In *Spring Fuels Lubricants Meeting Exhibition*. SAE International, may 2002.

Scientific publications

Author contributions

Paper I: Performance of New and Aged Injectors with and without Fuel Additives in a Light-Duty Diesel Engine

X. Zhu, Ö. Andersson

I planned and performed the experiments. I processed and analyzed the data. I was responsible for writing the paper.

Paper II: High-Speed Imaging of Spray Formation and Combustion in An Optical Engine: Effects of Injector Aging and TPGME as a Fuel Additive

X. Zhu, M. N. Mannazhi, N. Palazzo, P. E. Bengtsson, Ö. Andersson.

I planned and performed the experiments together with Manu Mannazhi. I processed and analyzed the data. I was responsible for writing the paper. Manu contributed to the data analysis and paper reviewing. Natascia contributes to the paper reviewing.

Paper III: Soot Oxidation Studies in an Optical Diesel Engine Using Laser-Induced Incandescence and Extinction

M. N. Mannazhi, X. Zhu, Ö. Andersson, P. E. Bengtsson.

I planned and performed the experiments together with Manu Mannazhi. Manu finished the data processing and analysis. Manu was responsible for writing the

paper. I contributed to the data processing and paper reviewing.

Paper I

Performance of new and aged injectors with and without fuel additives in a light duty diesel engine

Xinda Zhu (xinda.zhu@energy.lth.se)

Öivind Andersson (oivind.andersson@energy.lth.se)

Department of Energy Sciences
Faculty of Engineering
Lund University
P.O. Box 118
SE-221 00 Lund
Sweden

Abstract

Two sets of diesel injectors are tested in combination with common fuel additives in a multi-cylinder light-duty diesel engine. One set consists of new injectors and the other is aged by 100 000 km use in a vehicle. Four fuels are tested with these injector sets to investigate the impact of fuel additives on combustion and emission characteristics. The results show that the aged injectors consistently deliver larger quantities of fuel for a given injection strategy, leading to a higher power output and deviating emissions. This is hypothesized to be due to drift in the injector actuating characteristics. The fuels tested are a baseline diesel quality, and blends of this fuel with three additives: a cetane number improver (2-ethylhexyl nitrate), a soot reducer (tripropylene-glycol monomethyl ether), and a flow improver consisting of quaternary ammonium salts. At the selected low and medium load operating conditions, these additives had a smaller effect on the emissions than the injector ageing, the most notable effect being that TPGME reduces the soot emissions even at the oxygen-rich conditions studied here. These studies will be followed by optical investigations of the in-cylinder effects on spray and combustion characteristics.

Keywords

Injector aging; fuel additives; TPGME; 2-EHN; Quaternary ammonium salts

Introduction

Diesel engines are the dominant power source for road transports due to their high efficiency, reliability, and application-flexibility. As the overall energy demand is expected to increase in the transportation sector, diesel is likely to remain an important fuel for road transports [1]. Despite these advantages, the diesel engine typically suffers from elevated exhaust emissions of NOx and soot. Due to the adverse health effects of these pollutants, the emission legislations have tightened significantly over past decades and substantial efforts have been made to control them. These efforts include combustion strategies like exhaust gas recirculation (EGR) as well as more advanced aftertreatment systems.

The fuel injection is one of the most important processes affecting the emissions. It is affected both by the injection system hardware and the fuel properties. As fuel injection systems evolve with more precise control, higher injection pressures and finer nozzle holes, the sensitivity to hardware variations increases. For this reason, injector aging could significantly affect the combustion and emission formation processes [2,3,4,5]. Common aging effects include coking phenomena, erosive

damage and worn internal parts [6,7]. These could all cause impaired spray formation and combustion, resulting in increased emissions, for example of soot. It could also cause lowered efficiency and power output by decreasing the effective nozzle discharge rate. Knowledge about aging effects is thus important for engine developers, who are now faced with stricter demands on maintained emissions compliance throughout a vehicle's lifetime. Such knowledge is also important for finding relevant countermeasures to the aging effects.

Another critical factor to the fuel system is the fuel. Diesel fuel consists of thousands of components with a wide range of properties. The complexity increases even more due to the current trend of adding biomass-derived contents to regular diesel. Due to the diverse properties of the individual components, fuel additives are often necessary to achieve ideal fuel properties. Additives are commonly used to modify the fuel to achieve ideal properties, for example for reducing pernicious emissions, improving ignition, improving the viscosity over a wide range of temperature, or preventing deposits [8]. Since a range of additives are added to commercial fuels, it is important to understand how they affect important in-cylinder processes and emissions.

One of the pernicious emissions that can be reduced with fuel additives is soot. Soot is toxic and contributes to climate change [36, 37, 38]. A wealth of research shows that soot emissions can be reduced using oxygenated fuels [9,10,11,12,13]. Some research also reveals that the presence of oxygen in the fuel not only aids the soot oxidation process, but that it changes the structure of the soot in a way that facilitates oxidation [17,18]. Tripropylene-glycol monomethyl ether (TPGME, $C_{10}H_{22}O_4$) is one of the most common oxygenated fuel additives for reducing soot emissions [9,13,14,15,16].

A critical property of diesel which is commonly tuned using additives is the cetane number, which indicates the ignitability of a fuel. It is often enhanced using 2-ethylhexyl nitrate (2-EHN, or EHN, $C_8H_{17}NO_3$). The mechanism through which this additive improves the cetane value is well studied, as well as some side effects such as increased NO_x emissions [19,20,21,22,23]. 2-EHN starts to decompose in the temperature range of 450-550 K which, after a series of reactions, increases the concentration of hydroxyl radicals (OH) which, in turn, prompts the ignition process [33].

In addition to the soot-reducing and cetane-boosting additive types mentioned above, some other fuel properties should also be considered, even though they may not influence performance and emission explicitly. Firstly, for a modern high-pressure fuel injection system, the trend of using finer nozzle holes and higher injection pressures increases the tendency for cavitation inside the nozzle. Cavitation reduces the effective fuel discharge rate and can, over time, result in material erosion. Secondly, to cope with contaminants that could form deposits inside injector nozzle holes, commercial diesel fuel contains detergents. These remove existing deposits and prevent new ones from being formed. Lastly, with increasing levels of bio-content, fuel degradation and bacteria problems also need to be considered. These can be mitigated by additives modifying the fluid properties of the fuel. Quaternary ammonium salts are a new type of fuel additive which is found to be an effective antimicrobial agent as well as detergent [25, 26,27, 28, 29] in the industrial applications. They have recently been found to reduce the turbulence in the orifice and thereby supress cavitation, leading to an improved fuel flow in the nozzles [30,31].

Though effects of injector aging and fuel additives are reported in the literature, their combined effects on combustion and emissions are not well studied, especially not at engine-relevant operating conditions. In this work, we investigate the combined effects of these parameters by testing new and aged injectors on a multi-cylinder, light-duty diesel engine. One set of new injectors and one set of aged injectors were used in combination with four fuels: a neat baseline fuel without

additives, and the baseline fuel combined with the three above-mentioned additive types (a soot reducer, an ignition improver, and a flow-improver). The tests were made to establish the effects of injector aging and fuel additives on the engine's emission and performance characteristics, which are reported here. These tests will be followed by studies in an optically accessible version of the engine, which will be presented in upcoming articles, with the purpose to trace the effects established in this article back to the spray formation and combustion processes in the cylinder.

Experimental set-up

Engine hardware

The reference tests are conducted on a multi-cylinder Volvo D4 engine. A schematic drawing of the engine test bed and gas management system is shown in Figure 1. The engine speed is controlled independently of the engine load by an electrical dynamometer. Engine operating conditions and data acquisition are controlled through an in-house developed LabVIEW-based system and a NI PXI-FPGA hardware combination. High-rate data such as cylinder pressure and common rail pressure are sampled with 0.2 crank angle degree (CAD) resolution, while lower-rate data such as temperature and flow rates are sampled once per engine cycle.

The intake air is supplied from a central air compressor directly to the stock intake manifold. It delivers pressures up to 7 bar and the temperature can be increased to above 100 °C using an electric heater. The low-pressure fuel system generates a stable, circulating 5 bar flow to the high-pressure diesel pump. The high-pressure fuel system is a stock common-rail diesel injection system which can deliver up to 2750 bar injection pressure. Two injector sets consisting of four injectors are used: one new and one aged. The injectors are fourth generation Denso solenoid injectors and the aging consisted in 100 000 km use in a car. The fuel consumption is measured using a high-precision fuel scale and determined from the slope of a straight line fitted to the fuel mass readings which, in stationary operation, decrease linearly with time. The most important engine and injector parameters are given in Table 1.

An AVL AMA i60 exhaust measurement system is used for measuring gaseous emissions and an AVL 483 micro soot sensor is used for measuring exhaust soot. It is based on the photo-acoustic principle and capable of measuring transient soot concentration [43]. Its high sensitivity and wide measurement range make it ideal for exhaust soot measurement.

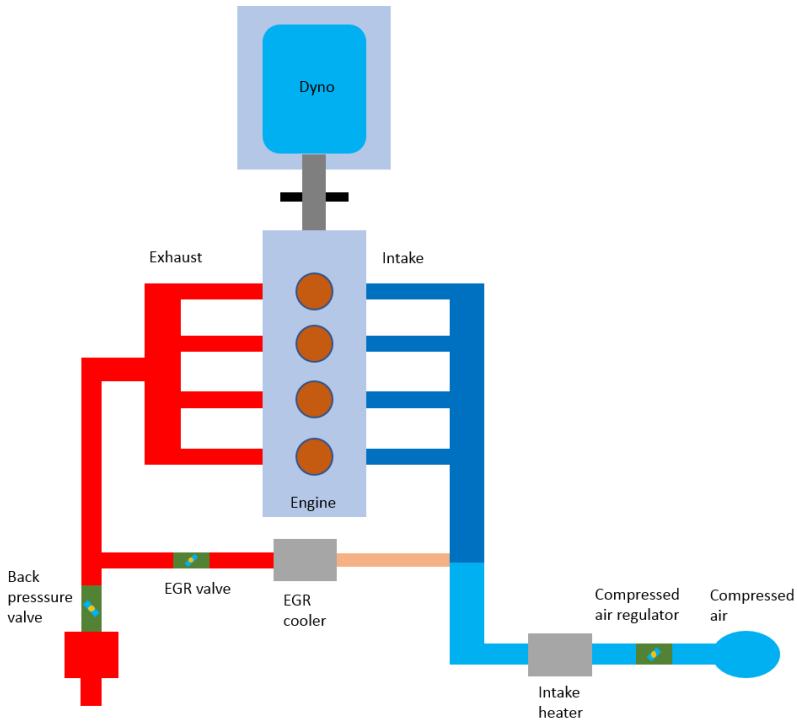

Figure 1. Multi-cylinder Volvo D4 layout.

Table 1. Engine and fuel system parameters.

Stroke [mm]	93.2
Bore [mm]	82
Displacement [L]	2
Connecting Rod [mm]	147
Compression Ratio [-]	15.8
Number of injector nozzle holes [-]	8
Nozzle outlet diameter [um]	125
Nozzle type [-]	Tapered

Operating points

Two reference points adapted from [44] are used in the reference sets. Both apply multiple injection strategies, including two pilot injections, one main injection and one post injection, which are typical for real-world part-load running conditions. The operating conditions are summarized in Table 2. Point 1 has a load of 4 bar IMEPg, while point 2 has 9 bar IMEPg. For simplicity, point 1 is referred to as the low load and point 2 as the medium load in what follows. Due to the hardware limitations of the EGR control system, the actual EGR flow varies continuously even if the engine is running at a stationary point. To maintain stable conditions, therefore, no EGR is applied here, despite the original operating condition using some level of EGR.

Table 2. Operating conditions

	Injection pressure [bar]	Intake pressure [bar]	Intake temperature [degreeC]	Engine speed [RPM]	Engine load IMEPg [bar]	Oxygen concentration [%]
Reference point 1 – low load	450	1.1	30	1500	Approx. 4	20
Reference point 2 – medium load	850	1.6	30	1500	Approx. 9	20

Fuels

Four fuels are tested in this work. The baseline fuel is a pure diesel fuel (CEC RF-79-07) without any additives or FAME. The other three are blends between the baseline fuel and various additives, as shown in Table 3. Unfortunately, for the flow improver (FI), both the constituents and concentration additive are considered confidential by the fuel provider. What is known is that this FI additive is based on salts of quaternary ammonium cations, which are positively charged ions of the structure NR_4^+, R being an alkyl group or an aryl group.

Table 3. Fuels used in this study

Fuel name	Fuel content
Base	Baseline reference fuel
II	Baseline fuel with 0.5%vol. ignition improver (2-ethylhexyl nitrate)
SR	Baseline fuel with 5%vol. soot reducer (Tripropylene-glycol methyl ether)
FI	Baseline fuel with flow improver (Quaternary ammonium salts)

The soot reducer (SR) fuel contains 5 % by volume of Tripropylene-glycol methyl ether ($C_{10}H_{22}O_4$). The measured fuel properties in Table 4 yield an oxygen content of around 1.54 % by weight, assuming there is no oxygen content in the baseline fuel. The additive's flash point of 121 °C is higher than that of diesel, meaning that it is more resistant to autoignition. The presence of oxygen in the structure also indicates the net heating value is much lower than diesel's (27.8 MJ/kg as compared to 43 MJ/kg) [37], leading to a lower heating value for this fuel compared with the other three. Note that the cetane number of the SR fuel is in fact slightly higher than that of the baseline fuel.

The ignition improver (II) fuel contains 0.5 % by volume of 2-ethylhexyl nitrate ($C_8H_{17}NO_3$), which increases its cetane number significantly to around 66.

Table 4. Some properties of the tested fuels

Fuel	Density @ 15C Kg/m^3	Net heating value MJ/kg	Flash point C	Cetane Number -
Base	833.8	43.2	84	53.3
SR	837.6	42.76	84	54.9
II	834.4	43.07	84	66.3
FI	833.8	43.2	84	53.3

Results and analysis

Fuel consumption

Figure 2 shows the total diesel flow rate for the four fuels. The data are grouped according to injector set and load point. The graph demonstrates that the fuel consumption for a given injector set is unaffected by the fuel. The aged injectors show a clear fuel consumption increase of around 0.1 g/s over the new ones in both load points. For this reason, a scaled-down injection duration is introduced for the aged injectors to match the load of the new injectors. In this scaled-down operating point, the main injection duration is shortened to match the load with the new injectors while the pilot and post injection durations are maintained the same. It can be noted that under the conditions tested in this experiment, the flow improver additive does not alter the fuel consumption significantly compared to the other fuels.

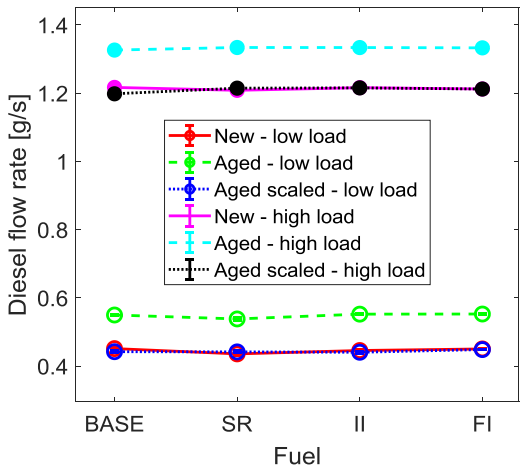

Figure 2. Total diesel flow rates at different loads while using different fuels and injectors.

Cylinder pressure and heat release

Figure 3 and Figure 4 show the heat release rates for the two injector sets in the two load points. In this first comparison, only the baseline fuel is used. The pressure traces and the derived heat release rate curves are averaged over all four cylinders during 150 cycles. The small heat release features before the main peak are contributed by the pilot injections. At the medium load, each pilot injection contributes a separate heat release feature, whereas at the low load, only one pilot heat release feature is observed. This is probably due to a longer ignition delay for the first pilot injection, making the two combustion events blend into one. A typical diesel heat release has an extended mixing-controlled phase, but this is not observed in any of these cases. The shape of the main heat release instead resembles that of a premixed combustion process, with a small additional amount of heat release in the tail contributed by the post injection. Under the conditions studied here, fuel and air are apparently mixed to a relatively high degree before combustion commences.

It can be noted that there is a significant difference between the injector sets in the amount of heat released from the pilot injections. The peak values of the aged injectors are approximately 50 % higher during this phase in both load cases, indicating that they deliver more fuel when using the

same injection pressure and duration. This is observed both in the low and medium load operating points and tallies with the fuel consumption data in Figure 2.

The consecutive main heat release is apparently affected by the amount of heat release from the pilot combustion. The aged injectors display advanced phasing and reduced peak heat release rate, probably due to the extra heat release from the pilot injections. The resulting increase in pressure and temperature advances the ignition of the main injection as compared to the new injectors. This also reduces the peak heat release rate of the main combustion due to a shorter premixing time. This, in turn, should lead to a slightly larger portion of mixing controlled combustion, which can also be seen at the low load, where the fast-decaying heat release rate at the end of the main combustion shows a short, flatter tail. This indicates a short mixing-controlled phase before the post-injection heat release. In the medium load case, the main heat release shows a similar pattern as observed in the low load case, but the difference is smaller, despite a comparable difference in the pilot combustion.

It can be noted that the relative differences in peak heat release rate are greater for the pilot injections than for the main injections. This could be an indication that the additional fuel delivered by the aged injectors is located in the opening and closing flanks of the injection, perhaps due to changes in the needle opening and closing characteristics. Such a behaviour would yield a larger relative increase of the fuel amount for shorter injections, as observed in Figures 3 and 4. If the aged injectors had a greater peak injection rate, on the other hand, the relative increase would be similar for all injections, which is not consistent with the observations in Figures 3 and 4. These hypotheses will be studied using spray imaging in future works.

Figure 5 and Figure 6 shows a comparison of the fuel effects on the combustion performance for the low and medium loads, respectively. Only data from the new injector set are shown in this comparison. Removing the influence of injector aging demonstrates that the heat release is much less affected by the fuel variation. At low load (Figure 5), the pilot heat release shows some phasing variation, indicating that the fuels have different ignition qualities. As expected, the ignition improver (IP) advances the heat release the most in relation to the baseline fuel. The flow improver (FI) has a similar effect, whereas the soot reducer (SR) tends to delay the pilot heat release slightly. The consecutive main heat release, on the other hand, is almost unaffected by the fuel additives, apart from some minor differences in the peak value and the tail. At medium load (Figure 6), the phasing of the pilot combustion is less affected by the fuel than at low load, and the phasing and the shape of the main heat release are almost completely unaffected. This is probably due to the higher in-cylinder temperatures reducing the sensitivity to the fuel's ignition quality.

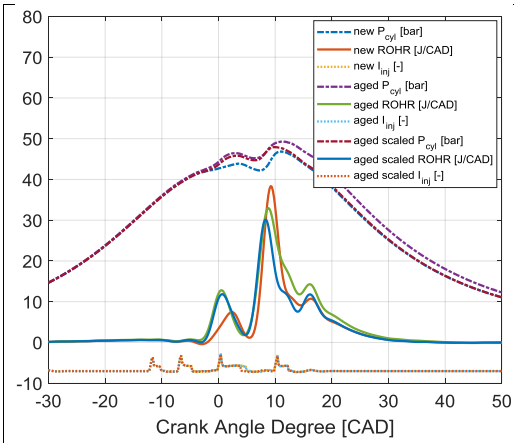

Figure 3. Cylinder pressure, rate of heat release and injector current at low load using different injectors with base line fuel.

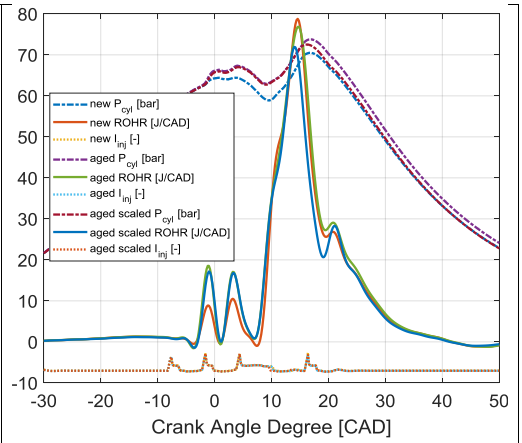

Figure 4. . Cylinder pressure, rate of heat release and injector current at medium load using different injectors with base line fuel.

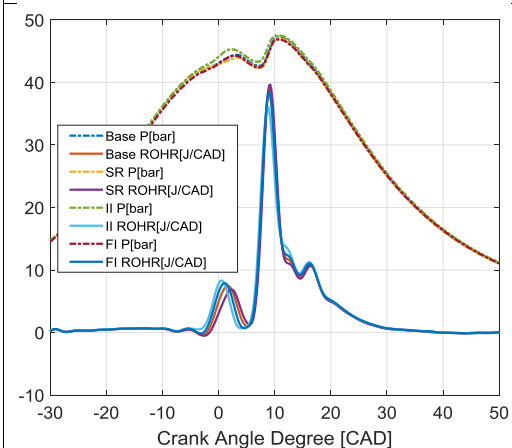

Figure 5. Cylinder pressure, rate of heat release and injector current at low load using different fuels with new injectors.

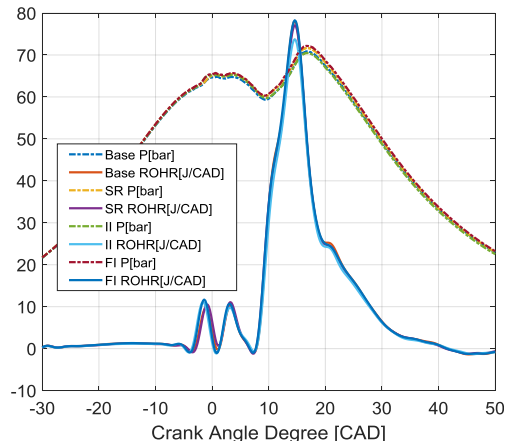

Figure 6. Cylinder pressure, rate of heat release and injector current at medium load using different fuels with new injectors.

Ignition delay

The ignition delay time is defined as the time gap between the start of injection and the start of combustion. The latter is often determined as the point where a specific percentage of the total heat has been released, which depends on the accumulated heat release. However, with multiple pilot injections in the low to medium load range, the aHRR trace is often noisy. This can have great impact on the evaluated ignition delay if the ignition quality difference between fuels is small. Thus, the ignition delay in this work is defined as the time between start of the injection and the first time the aHRR reaches 3 J/CAD. This threshold is based on the noise in the aHRR not surpassing 2 J/CAD before the first pilot combustion in any of the measured points. A threshold value 50 % above this ensured robust detection of the ignition.

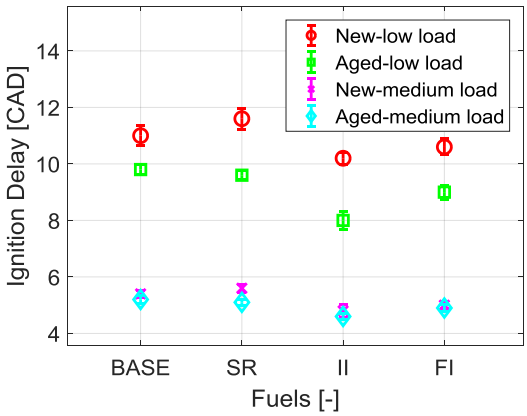

Figure 7. Ignition delay when using different fuels with different injector. The results are from the average of all cylinders.

The aged injectors produce a shorter ignition delay when compared with the new ones as shown in Figure 7. At low load, all four fuels show a clear trend with the II fuel showing the highest auto-ignition propensity, followed by the FI fuel. The ignition delay of the SR fuel is sensitive to the fuel quantity difference. With aged injectors it advances the ignition slightly while with new injectors it delays the ignition slightly. The difference in fuel quantity has a larger effect than the fuel additive. It can also be noticed that the standard deviation is higher for the new injectors than for the aged ones, indicating a larger cycle-to-cycle variation.

At the medium load condition, the overall ignition delay is reduced significantly due to higher temperature and more fuel. A much smaller difference between the injector sets is also observed. The higher in-cylinder temperature reduces the sensitivity to the fuels' ignition quality, which also decreases the cycle-to-cycle variation. The ignition quality of the fuels shows the same trend as observed at the low load condition.

The ignition process of hydrocarbon-air systems is complicated. The difference between the injector sets can be explained by the difference in fuel quantity and the fuel-air mixture preparation. The aged injectors deliver more fuel under the same ambient conditions, which forms a richer fuel-air mixture. The extra liquid fuel may lead to increased cooling of the ambient air. Considering the small pilot injection quantities, however, this cooling should certainly have less impact on the ignition delay than a richer mixture. A richer mixture helps to increase the initial radical pool and the following chain branching reactions since the higher concentration of atomized fuel components and their initial reacting products have less chance to be interrupted by excessive ambient air [42]. Other potential factors are that the fuel droplet size, the injection velocity and flow rate could be different with different injectors, but studies show that these factors have very little impact on the ignition delay under engine conditions [34]. The fuel's physical properties also have limited effects on the ignition process: within a reasonable cetane number range, the volatility and viscosity of a diesel fuel have no significant influence on the ignition delay [35]. Apart from the difference between the injector sets explained above, the 2-EHN additive has the clearest effect, demonstrating its ignition improving effect at these low to medium load conditions even with a very small fraction in the blend.

Emissions

The graphs in Figure 8 show the four legislated emissions versus the fuel types used. The data are grouped according to injector set and load point. The top-left graph shows clear trends in the NOx emissions. Apart from the expected trend that more NOx is produced at the higher load, the aged injector set consistently emits more NOx than the new set. Thermal NOx, which is the dominant formation mechanism in engines, is relatively slow and highly temperature dependent. For this reason, high temperatures early during the cycle tends to increase the NOx emissions. This is the most likely reason why the aged injectors produce more NOx, as they produce higher heat release rates during the pilot combustion phase. Although the scaled-down strategy used with the aged injectors produces the same IMEP as the new injector set, this strategy, too, releases more heat close to TDC. As seen in Figure 9, this leads to higher NOx emissions also for the scaled-down strategy. Comparing the different fuels, on the other hand, no clear NOx trends can be observed, although the ignition improver was expected to show higher NOx emissions. As 2-EHN contains nitrogen, it has previously been reported to increase the NOx emissions [22,23], but this is not observed under the operating conditions investigated here.

The HC measurement results are shown in the top right graph in Figure 8. Generally, they are all in the 60 to 100 ppm range, which is very low. At medium load, the HC emissions are slightly lower because of a higher combustion temperature and a stronger in-cylinder flow field. When using different fuels, no clear interpretation can be made since the variations are maintained within a negligible range of 15 ppm.

The HC emissions of small DI diesel engines are mostly governed by: 1) the impingement of liquid fuel on the combustion chamber wall; 2) asymmetric spray patterns; 3) fuel trapped in the squish area; 4) the nozzle sac volume and the needle behaviour in the injector [44]. Hence, the difference between the new and the aged injectors most likely is caused by spray patterns and nozzle actuation since the injection pressure, timing and ambient air flow are all kept constant at each operating point. Asymmetric spray patterns and fuel dribbling occurring during the needle closing time create local fuel-rich or fuel-lean zones. Under diesel combustion conditions, either too rich or too lean a fuel-air mixture during the early stage of combustion process can cause HC to increase.

The CO emissions are shown in the bottom left graph in Figure 8. The CO emissions from the new injectors surpass those of the aged injectors at both load points, no matter what fuel is used. At low load, an average increase of around 50 ppm of CO is found when using the new injectors, while the gap shrinks to a 20-ppm level at medium load. At medium load, the overall CO level is less than 50 % of the low load level. In terms of the fuel influences, the II fuel and the FI fuel show a slightly lower CO emissions compared with the base and SR fuels at low load. At medium load, no apparent difference can be observed between these fuels. Temperature plays a key role for the CO emissions. The oxidation rate of CO depends on the local temperature, which is higher when the aged injectors deliver more fuel into the cylinder at the same operating condition. At low load, even a minor increase of fuel quantity can make a distinguishable reduction in the CO as the temperature cools down much faster during the expansion stroke.

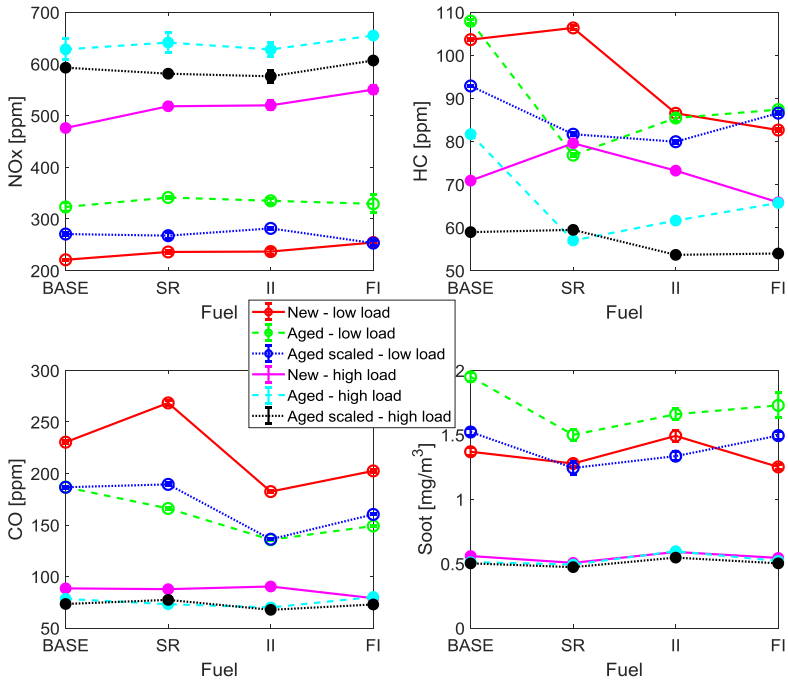

Figure 8. Exhaust mission measurement at different loads with adjusted injection strategies when using different injectors and fuels.

The soot emissions are shown in the bottom right graph in Figure 8. Again, there is a clear separation between the load points, with the low load case emitting at least twice the amount of soot. This probably has the same explanation as the separation between the load cases in NOx and CO emissions, as the soot formation and oxidation processes are strongly temperature dependent. The higher load shows very little difference between the injector sets, whereas there is a marked difference between them at the low load. Here, the aged injector emits most soot, while the scaled down strategy is on par with the new injectors. This is surprising, considering that there is usually a trade-off between soot and NOx. As the aged injectors produce higher temperature and NOx, they would also be expected to produce less soot, which is contrary to the trend in Figure 9. So far, however, the impact of the spray formation remains unknown. In case the aged injectors produce a highly asymmetric spray pattern, for example, the mixing process may be locally aggravated, leading to fuel-rich zones. This could result in both higher soot formation and poorer soot oxidation in these zones and, hence, increased emissions. This potential explanation will be investigated using spray and combustion imaging in an upcoming publication. Few systematic differences in soot emissions are observed between the fuels. The only clear trend is that the soot reducer almost invariably emits the least soot within each combination of injector set and load.

Conclusions

A significant difference of injection quantity between the new and the aged injectors are observed when the same injection strategy is applied. This difference is larger than the difference between individual injectors in the same group. Based on these phenomena, it is hypothesised that the aged injectors do not suffer from coking problem since injector deposits usually decrease the discharge rate of the nozzle, leading to a decreased power output. The higher fuel flow rate delivered by the aged injectors is rather suspected to be related the injectors' nozzle geometry and the needle actuation. Further investigation of the spray behaviour needs to be conducted to find out if the injector needle actuation or the nozzle holes are causing this higher discharge rate.

The four diesel fuel tests in the experiments show very limited impact on combustion and emissions. The selected operating points may also reduce the difference between the fuels due to a high level of premixing and abundance of oxygen. 2-EHN reduces the ignition delay at both load points. However, the ignition is more dependent on the ambient condition and fuel-air mixture formation. TPGME is able to lower the soot emission even in a highly excessive oxygen environment. The reduction effect could be more significant when the ambient oxygen is low, for example during engine transients.

Future work will be conducted on an optical accessible conversion of this engine. The focus will then be on the spray and combustion processes.

Acknowledgement

This work is supported by the MSCA-ITN-ETN of EU H2020 programme, under REA grant agreement no. 675528. The author would like to acknowledge Volvo Cars and Afton Chemical for providing injectors and fuels, respectively, to the project.

Reference

1. 2019 outlook for energy ExxonMobil: https://corporate.exxonmobil.com/-/media/Global/Files/outlook-for-energy/2019-Outlook-for-Energy_v4.pdf. Accessed 25-01-2020

2. D'Ambrosio, S., & Ferrari, A. (2012). Diesel injector coking: Optical-chemical analysis of deposits and influence on injected flow rate, fuel spray and engine performance. Journal of Engineering for Gas Turbines and Power, 134(6). https://doi.org/10.1115/1.4005991

3. Ikemoto, M., Omae, K., Nakai, K., Ueda, R., Kakehashi, N., & Sunami, K. (2011). Injection nozzle coking mechanism in common-rail diesel engine. SAE International Journal of Fuels and Lubricants, 5, 78–87. http://dx.doi.org/10.4271/2011-01-1818. 2011-01- 1818.

4. Smith, A., & Williams, R. (2015). Linking the physical manifestations and performance effects of injecor nozzle deposits in modern diesel engines. SAE International Journal of Fuels and Lubricants, 8(2), 344–357. http://dx.doi.org/10.4271/2015-01-0892.

5. Tang, J. R. A., Pischinger, S. R. A., Lamping, M. F. M. G., Körfer, T. F. M. G., Tatur, M. F. I., & Tomazic, D. F. I. (2009). Coking phenomena in nozzle orifices of dl diesel engines. SAE International Journal of Fuels and Lubricants, 2(1), 259–272. http: //dx.doi.org/10.4271/2009-01-0837.

6. Krogerus, T. R., Hyvönen, M. P., & Huhtala, K. J. (2016). A survey of analysis, modeling, and diagnostics of diesel fuel injection systems. Journal of Engineering for Gas Turbines and Power, 138(8). http://dx.doi.org/10.1115/1.4032417. 081501–1–081501–11.

7. Hofmann, O., Schuckert, S., Wachtmeister, G., & Rixen, D. (2018). Optimal injection strategies to compensate for injector aging in common rail fuel systems. In: SAE Technical Paper 2018-01-1160. https://doi.org/10.4271/2018-01-1160

8. Ribeiro NM, Pinto AC, Quintella CM, da Rocha GO, Teixeira LS, Guarieiro LL, do Carmo Rangel M, Veloso MC, Rezende MJ, Serpa da Cruz R, de Oliveira AM. The role of additives for diesel and diesel blended (ethanol or biodiesel) fuels: a review. Energy & fuels. 2007 Jul 18;21(4):2433-45. https://doi.org/10.1021/ef070060r

9. C.J. Mueller, W.J. Pitz, L.M. Pickett, G.C. Martin, D.L. Siebers, C.K. Westbrook, Effects of oxygenates on soot processes in di diesel engines: experiments and numerical simulations, SAE Paper 2003-01-1791, 2003. https://doi.org/10.4271/2003-01-1791

10. B.E. Hallgren, J.B. Heywood, Effects of oxygenated fuels on di diesel combustion and emissions, SAE Paper 2001-01-0648, 2001. https://doi.org/10.4271/2001-01-0648

11. M. Natarajan, E. Frame, D. Naegeli, et al., Oxygenates screening for advanced petroleum based diesel fuels: part 1. Screening and selection methodology for the oxygenates, SAE Paper 2001-01-3631, 2001. https://doi.org/10.4271/2001-01-3631

12. M. González-D, W. Piel, T. Asmus, et al., Oxygenates screening for advanced petroleum based diesel fuels: part 2. The effect of oxygenate blending compounds on exhaust emissions, SAE Paper 2001-01-3632, 2001. https://doi.org/10.4271/2001-01-3632

13. C.J. Mueller, G.C. Martin, Effects of oxygenated compounds on combustion and soot evolution in a di diesel engine: broadband natural luminosity imaging, SAE Paper 2002-01-1631, 2002. https://doi.org/10.4271/2002-01-1631

14. Manin, J., Skeen, S., Pickett, L., Kurtz, E. et al., "Effects of Oxygenated Fuels on Combustion and Soot Formation/Oxidation Processes," SAE Int. J. Fuels Lubr. 7(3):704-717, 2014. https://doi.org/10.4271/2014-01-2657

15. Park W, Park S, Reitz RD, Kurtz E. The effect of oxygenated fuel properties on diesel spray combustion and soot formation. Combustion and Flame. 2017 Jun 1;180:276-83. https://doi.org/10.1016/j.combustflame

16. Dumitrescu CE, Mueller CJ, Kurtz E. Investigation of a tripropylene-glycol monomethyl ether and diesel blend for soot-free combustion in an optical direct-injection diesel engine. Applied Thermal Engineering. 2016 May 25;101:639-46. https://doi.org/10.1016/j.applthermaleng.2015.12.068

17. Randy L. Vander Wal, Aaron J. Tomasek, Soot oxidation: dependence upon initial nanostructure, Combustion and Flame, Volume 134, Issues 1–2, 2003, Pages 1-9. https://doi.org/10.1016/S0010-2180(03)00084-1

18. Randy L Vander Wal, Aaron J Tomasek, Soot nanostructure: dependence upon synthesis conditions, Combustion and Flame, Volume 136, Issues 1–2, 2004, Pages 129-140. https://doi.org/10.1016/j.combustflame.2003.09.008

19. Bornemann, H., Scheidt, F. and Sander, W., 2002. Thermal decomposition of 2-ethylhexyl nitrate (2-EHN). International journal of chemical kinetics, 34(1), pp.34-38. https://doi.org/10.1002/kin.10017

20. Zaslonko, I.S., Smirnov, V.N., Tereza, A.M. et al. Kinetics of energy liberation during thermal decomposition of nitrates in shock waves. Combust Explos Shock Waves 24, 251–255 (1988). https://doi.org/10.1007/BF00749201

21. Pritchard, H.O., 1989. Thermal decomposition of iso-octyl nitrate. Combustion and Flame, 75(3-4), pp.415-416. https://doi.org/10.1016/0010-2180(89)90052-7

22. Clothier, P.Q.E., Aguda, B.D., Moise, A. and Pritchard, H.O., 1993. How do diesel-fuel ignition improvers work? Chemical Society Reviews, 22(2), pp.101-108. https://doi.org/10.1039/CS9932200101

23. Stein, Y., Yetter, R.A., Dryer, F.L. and Aradi, A., 1999. The autoignition behavior of surrogate diesel fuel mixtures and the chemical effects of 2-ethylhexyl nitrate (2-EHN) cetane improver. SAE transactions, pp.1029-1045. www.jstor.org/stable/44716738

24. Barbour, R., Quigley, R. & Panesar, A. Investigations into fuel additive induced power gain in the CEC F-98-08 DW10B injector fouling engine test. SAE 2014-01–2721, https://doi.org/10.4271/2014-01-2721 (2014).

25. Bento, F. M., & Gaylarde, C. C. (1996). Isolation, characterization and control of micro-organisms isolated from contaminated diesel oil. International Biodeterioration & Biodegradation, 1(37), 117.

26. Barbour, R. H. Method to provide power gain in an engine. US Patent Number US9239000 (2011).

27. Chen CZ, Beck-Tan NC, Dhurjati P, van Dyk TK, LaRossa RA, Cooper SL. Quaternary ammonium functionalized poly (propylene imine) dendrimers as effective antimicrobials: Structure− activity studies. Biomacromolecules. 2000 Sep 12;1(3):473-80. https://doi.org/10.1021/bm0055495

28. Thorsteinsson T, Másson M, Kristinsson KG, Hjálmarsdóttir MA, Hilmarsson H, Loftsson T. Soft antimicrobial agents: synthesis and activity of labile environmentally friendly long chain quaternary ammonium compounds. Journal of medicinal chemistry. 2003 Sep 11;46(19):4173-81. https://doi.org/10.1021/jm030829z

29. Jennings MC, Minbiole KP, Wuest WM. Quaternary ammonium compounds: an antimicrobial mainstay and platform for innovation to address bacterial resistance. ACS infectious diseases. 2015 May 29;1(7):288-303. DOI: 10.1021/acsinfecdis.5b00047

30. Karathanassis, I.K., Trickett, K., Koukouvinis, P. et al. Illustrating the effect of viscoelastic additives on cavitation and turbulence with X-ray imaging. Sci Rep 8, 14968 (2018) doi:10.1038/s41598-018-32996-w

31. Naseri, H., Trickett, K., Mitroglou, N. et al. Turbulence and Cavitation Suppression by Quaternary Ammonium Salt Additives. Sci Rep 8, 7636 (2018) doi:10.1038/s41598-018-25980-x

32. TPGME product data sheet. https://nshosting.dow.com/doc-archive/business/pcm/dowanol/dowanol_tpm/tds/dowanol_tpm.pdf. Accessed 25-01-2020

33. Ickes AM, Bohac SV, Assanis DN. Effect of 2-ethylhexyl nitrate cetane improver on NO x emissions from premixed low-temperature diesel combustion. Energy & Fuels. 2009 Sep 2;23(10):4943-8. https://doi.org/10.1021/ef900408e

34. Higgins B, Siebers D, Aradi A. Diesel-Spray Ignition and Premixed-Bum Behavior, SAE Technical Paper 2000-01-0940. SAE Transactions. 2000;109(3). https://doi.org/10.4271/2000-01-0940

35. Wong CL, Steere DE. The effects of diesel fuel properties and engine operating conditions on ignition delay. SAE transactions. 1982 Jan 1:3873-92. https://doi.org/10.4271/821231

36. Donaldson K, Tran L, Jimenez LA, Duffin R, Newby DE, Mills N, MacNee W, Stone V. Combustion-derived nanoparticles: a review of their toxicology following inhalation exposure. Particle and fibre toxicology. 2005 Dec;2(1):10. DOI: 10.1186/1743-8977-2-10

37. Grahame TJ, Klemm R, Schlesinger RB. Public health and components of particulate matter: the changing assessment of black carbon. Journal of the Air & Waste Management Association. 2014 Jun 3;64(6):620-60. https://doi.org/10.1080/10962247.2014.912692

38. Bond TC, Doherty SJ, Fahey DW, Forster PM, Berntsen T, DeAngelo BJ, Flanner MG, Ghan S, Kärcher B, Koch D, Kinne S. Bounding the role of black carbon in the climate system: A scientific assessment. Journal of Geophysical Research: Atmospheres. 2013 Jun 16;118(11):5380-552. https://doi.org/10.1002/jgrd.50171

39. Tsurushima, T., Zhang, L. and ISHII, Y., 1999. A study of unburnt hydrocarbon emission in small DI diesel engines (No. 1999-01-0512). SAE Technical Paper. https://doi.org/10.4271/1999-01-0512

40. ALV micro soot sensor. 'https://www.avl.com/-/mssplus-avl-micro-soot-sensor'. Accessed on 2020-03-23.

41. Dahlstrom J, Andersson O, Tuner M, Persson H. Experimental comparison of heat losses in stepped-bowl and re-entrant combustion chambers in a light duty diesel engine. SAE Technical Paper; 2016 Apr 5. DOI: https://doi.org/10.4271/2016-01-0732.

42. Glassman I, Yetter RA, Glumac NG. Combustion. Academic press; 2014 Dec 2.

43. ALV micro soot sensor. 'https://www.avl.com/-/mssplus-avl-micro-soot-sensor'. Accessed on 2020-03-23.

44. Dahlstrom J, Andersson O, Tuner M, Persson H. Experimental comparison of heat losses in stepped-bowl and re-entrant combustion chambers in a light duty diesel engine. SAE Technical Paper; 2016 Apr 5.

CRedit

Xinda Zhu: Investigation, Data Curation, Writing - Original Draft, Visualization

Öivind Andersson: Writing - Review & Editing, Supervision

Paper II

High-Speed Imaging of Spray Formation and Combustion in An Optical Engine: Effects of Injector Aging and TPGME as a Fuel Additive

X.Zhu[1], M. N. Mannazhi[2], N. Palazzo[3], P. E. Bengtsson[2], Ö. Andersson[1].

[1]Division of Combustion Engines, Department of Energy Sciences, Lund University, Sweden
[2]Division of Combustion Physics, Department of Physics, Lund University, Sweden
[3]Friedrich-Alexander-University of Erlangen-Nürnberg, Erlangen, Germany

Abstract

High-speed imaging of fuel sprays and combustion is conducted on a light-duty optical engine to investigate the effects of injector aging, with a special focus on soot. The spray behaviours of one new and one aged injector are compared using Mie-scattering. In addition to this, the combustion process of a baseline diesel fuel and a blend with TPGME (Tripropylene Glycol Monomethyl Ether) are compared using natural luminosity (NL) imaging. TPGME is an oxygenated additive which can be used to reduce the soot emissions. X-ray tomography of the two injectors demonstrates that the aging does not lead to significant geometry differences, nor to formation of dense internal nozzle deposits. Both injectors show similar liquid penetration and spreading angle. However, the aged injector shows a prolonged injection and more fuel dribbling after the injection events, leading to a higher injection quantity. The fuel quantity difference shows a larger impact on the NL at low load than the TPGME additive, indicating that the in-cylinder temperature is more important for soot oxidation than oxygen concentration under these conditions. At medium load, the NL is much less sensitive to small temperature variations, while the TPGME is more effective for soot reduction.

Introduction

Modern day diesel injection systems usually consist of high-pressure fuel pump, common rail and fast-response diesel injectors. The combination of high injection pressure, fine nozzle holes and fast injector actuation enables precise control of multiple fuel injection events within one cycle. Injection timing, quantity and the fuel distribution are all key factors for an ideal combustion process. Effective efficiency improvement and in-cylinder emission reduction can be achieved simultaneously by optimizing fuel injections (1, 2, 3, 5).

However, with such high level of fuel injection precision, deviation from the ideal fuel injection could have major influences. Relatively consistent fuel injection characteristics through the lifespan of the engine is critical to maintain a good engine performance and restricted emissions.

Faulty or aged injectors can impact the spray patterns and combustion process, leading to reduced efficiency, power loss and high emissions, etc (4). Injector faults and injection related engine faults are the most common problems in diesel engines. Some common injector problems are: 1) clogged nozzle holes; 2) injector needle and control valve stiction; 3) eroded/worn injector nozzles; 4) injector needle actuation related opening/closing/leaking problems and faulty solenoids.

The formation of deposits and influences of injector deposits on the fuel injection are the most studied topics among those injector problems. A primary and commonly agreed indication of injector fouling is a reduced flow rate and associated power loss (10, 11). Deposits built up on the injector tip can reduce the spray cone angle and disrupt the atomization (12, 13). The spray penetration speed

and length usually decrease as well (14, 15, 16). However, the deposits' effects on the spray penetration might depend on the fuel properties, the form of the deposits and the injector geometry since a longer spray penetration is found when coking occurs in some gasoline direct injection researches (10, 13, 17). Cylinder-to-cylinder and cycle-to-cycle variation due to asymmetric spray patterns is usually increase as well.

Consequently, emissions are also affected by the disturbed sprays. While the HC and NOx emissions are often marginally influenced, the soot emissions show significant increase when the injector is coked due to a degraded air-fuel mixing (13, 15).

Few studies about the influences of nozzle erosion on sprays can be found in the literature. Most of them are cavitation-related numerical researches on erosion-induced geometry damage, affecting the discharge rate and the flow field (18, 19, 20). A nozzle hole with erosion is locally widened and rough surfaces are formed due to material loss, which can cause a reduced discharge rate, narrower spray cone angle and shorter spray penetration by increased turbulence in these areas.

The injector needle motion is another important factor that can affect the fuel injection, especially during the lifting and closing phases. The needle oscillation is found to have a certain impact on the internal flow dynamics. The off-axis motion at low and medium lift position has a direct impact on the mass flow rate and hole-to-hole variations (24, 25). Needle bouncing during the closing stage is confirmed to be a major cause of after-injection (fuel dribbles). An increase of the needle valve spring stiffness or an increase of the gap between the needle and the nozzle body can worsen the needle bouncing problem (26). In addition to the after-injection problem, leakage can also be caused by needle tip wear (27).

In addition to the analysis of various physical influences of aging components, control strategies which focus on identifying and compensating for the aging effects of injectors are also studied in several researches (21, 22, 23). Such efforts on the research of injector aging all serve the same purpose: ensuring an ideal fuel injection to achieve high efficiency, low emissions and low noise.

One of the targets of optimizing the fuel injection is soot reduction. Soot has been a research focus in the past decades. Both its toxicity to health and impact on the environment have been revealed (28, 29) and in-cylinder soot processes have been extensively studied in compression ignition engines (30). In addition to the evolution of the fuel injection systems and the after-treatment system, oxygenated fuels are also considered to have clear soot reduction effects compared with non-oxygenated fuels (31, 32). Among many candidates, tripropylene-glycol monomethyl ether (TPGME, $C_{10}H_{22}O_4$) shows good performance (31, 33).

A recent study conducted on a light-duty diesel engine at our laboratories found that a set of aged injectors yielded higher flow rates than a set of new injectors when using the same injection strategies and injection pressure (41). It was hypothesized that the geometry and/or the needle actuation could be the major causes of the phenomenon while the presence of deposits were less likely. However, the spray formation of these injectors and combustion process remain unknown. Hence, a more detailed in-cylinder investigation is carried out in this study to explain the observation. It was also found that the TPGME, as a soot reducer additive, works well even in an environment with excessive oxygen, but its impact on the combustion process, especially the in-cylinder soot formation and oxidation, remains to be revealed.

Previous research about injector aging has mostly focused on deposits. Few studies are found regarding the needle actuation. None of them has done so in optical diesel engines with real-world multiple injection strategies.

In this work, optical diagnostics are performed to trace the difference between the aged and the new injectors. X-ray tomography is performed first to investigate the internal nozzle geometry of the injectors. After this, the liquid fuel spray development is studied using high-speed Mie scattering imaging. Finally, the natural luminosity is imaged to investigate influences of different injectors and the effects of the TPGME additive.

This work will also provide a basis for a combined laser induced incandescence (LII) and laser extinction measurements of in-cylinder soot processes with these injectors and additive in the future.

Methodology

Optical engine set-up

The high-speed imaging experiments are conducted on a single-cylinder light-duty Volvo diesel engine. The design of this optical engine is illustrated in Figure 1. The construction of the engine applies a Bowditch design, maintaining the stock engine block, crank shaft and pistons as a base. A single cylinder head which contains identical valve and intake systems to the stock engine is specially built. A quartz liner holds four quartz windows, providing optical access from the side in four directions of the combustion chamber. The quartz piston is mounted on a piston extension, which is connected with the stock piston in the engine block. The geometry of the quartz piston is identical to the stock piston to ensure a realistic flow field in the cylinder. A mirror reflects the light passing down through the quartz piston and provides a bottom view of the combustion chamber. The quartz material is non-crystalline fused silica, which provides high transmission in the UV region. Some of the key dimensions of the engine are shown in Table 1.

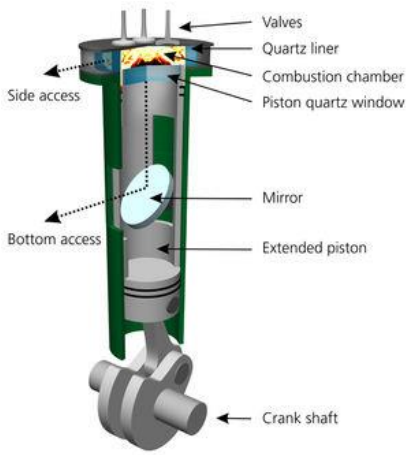

Figure 1. Three-dimensional view of a research engine equipped with optical access from below via an elongated piston (the Bowditch design) and from the sides via a cylinder quartz ring inserted as part of the cylinder liner.

The engine is equipped with an external intake system which contains two compressors and a heater. One compressor takes ambient air from the test cell and the other takes EGR gas from an external diesel burner. The gases are mixed to obtain the required oxygen concentration in the final mixture.

A minimum level of around 5 % oxygen is achievable. Combustion is supressed at this low oxygen level, avoiding any flame luminosity that could disturb the spray imaging.

Table 1. Key dimensions of the engine and its injector.

Displaced volume	492 cc
Bore	82 mm
Stroke	93 mm
Connecting rod length	147 mm
Compression ratio	13.5
Injector nozzle holes outlet diameter	125 µm
Number of nozzle hole	8
Nozzle shape	Tapered
Spray umbrella angle	155 °

The injectors tested are the Denso G4S solenoid injectors. One is from a new batch (only used for brief tests) and one is from an aged batch (after over 100 000 km of usage). In a previous reference test, it was found that the aged injectors deliver significantly more fuel when using the same injection strategy and the difference between the new and the aged set is bigger that the difference between the individuals in the same set. In this work, one aged injector that shows the most substantial difference is selected.

Operating points and fuels

Two reference points are adapted from (39). They both implement two pilot injections, one main injection and one post injection, which represent real-world part-load operating points. The operating conditions are summarized in Table 2.

Table 2. Operating points and their estimated TDC conditions.

	Reference point 1 – low load	Reference point 2 – medium load
Injection pressure [bar]	450	850
Intake pressure [bar]	1.27	1.83
Intake temperature [degreeC]	75	75
Engine speed [RPM]	1200	1200
Engine load IMEPg [bar]	Approx. 4	Approx. 9
Oxygen concentration [%]	20	20
Estimated TDC density [kg/m^3]	Approx. 15	Approx. 22
Estimated TDC temperature [K]	Approx. 880	Approx. 890

Two fuels are tested in this work. One is a baseline reference diesel CEC RF-79-07. It doesn't contain any additives or FAME, making it ideal for additive testing. The other fuel is a blend of the baseline fuel and a 5 % by volume of soot reducer (Tripropylene-glycol methyl ether, TPGME, $C_{10}H_{22}O_4$). Thus, the blend has a calculated 1.54 weight percentage of oxygen, assuming that there is no oxygen in the baseline fuel. The TPGME additive has similar physical properties to diesel, despite its slightly higher density. This means it can be blended with regular diesel without changing much of the overall physical properties. Two of the most notable difference in the chemical properties are: 1) a higher flash point at 121 °C; 2) a lower net heating value of just 27.8 MJ/kg (5) compared with diesel at

around 43 MJ/kg. Some of the measured fuel properties provided by the supplier are listed in Table 3.

Table 3.Some properties of the tested fuels.

Fuel names	Content	Density @ 15C Kg/m^3	Net heating value MJ/kg	Flash point °C
Base	CEC RF-79-07 Pure diesel	833.8	43.2	84
SR	Base fuel + 5%vol. TPGME	837.6	42.76	84

Optical set-up

Mie scattering is used to study the spray formation in a non-reacting environment. This technique is based on elastic scattering of light from particles or droplets that have a diameter similar to or larger than the wavelength of the incident light. The Mie signal is proportional to the square of the particle/droplet diameter, meaning it is suitable for characterizing initial liquid phase sprays. A 452 nm continuous wave laser diode is used as the incident light source. The laser is aimed directly at one of the side windows. With two cylindrical lenses shaping the laser, it covers the entire entrance of the window. The purpose is to make the incident light as even as possible at the entrance. Because of the shape of the side window and the bowl shape of the piston, the laser light is heavily distorted by refraction before encountering the spray near TDC. Strong reflection is also observed from the cylinder head. To minimize this interference, graphite spray is applied to the cylinder head.

The camera used is a Photron FASTCAM SA5. It has a monochrome sensor which can capture 12-bit uncompressed data. The recording speed is set at 25 000 fps with a shutter time of 39754 ns. The resolution is 512 x 512 pixels, which is the maximum setting at this speed. A 100 mm focal length, f/2 fixed aperture B. Halle lens is used for imaging. A band-pass 452 nm (+/- 22 nm) filter is placed in front of the objective lens.

Natural luminosity (NL) imaging is performed to characterize the general features of the combustion process. Diesel combustion emits high intensity thermal radiation. Thus, in addition to the 452 nm bandpass filter, ND05 and ND07 filters are used for reducing the NL at low load and at medium load, respectively, to prevent sensor saturation. The rest of the optical set-up remains the same as the set-up for the spray imaging. The ND factors are multiplied to the recorded signals to retrieve the original ones.

A grid image with 2x2 mm squares is used for the focusing adjustment of the camera. It is attached on top of the optical piston. Then the piston is cranked to 5 CAD after TDC, which is approximately in the middle of the injection events. When the piston is close to the TDC position, a couple of degrees of movement doesn't affect the focusing significantly since the piston only travels a short distance. For the NL imaging, it is difficult to get good focusing in the late cycle when the piston is moving away from the TDC. This is not considered problematic, however, as only the soot luminosity is of importance in the late cycle in this comparative work.

X-ray tomography

There are several methods to obtain the internal geometry of the injector nozzles. The 3D nozzle hole dimensions can be obtained by using silicone moulding (6). However, this method is limited to

the nozzle region. For 2D imaging, optical microscopy can provide direct visualization of the orifice exit while phase-contrast X-ray imaging can reveal the internal structure very well. Phase-contrast can also be coupled with high speed imaging to determine the needle motions (7).

3D X-ray tomography can characterize the internal 3D shape very well and it has been used for extracting the internal structure of fuel injectors (7, 8, 9). The principle can be found in (40). In this work, X-ray tomography is performed in a ZEISS Xradia 520 3D X-ray microscope. A maximum X-ray source voltage of 160 kV and a power of 10 W are used for the dense metal material on the injectors. Approximate 5 mm of the nozzle tip region is scanned, in which the nozzle holes and a certain part of the needle tip and the needle seat surface are covered in the imaging. The voxels are set to cubic with 8 micron, meaning there is an 8 micron distance between two neighbouring slices and the pixels in each slice are square with 8 micron sides. Around 680 slices are acquired for each case. Then a 3D reconstruction is performed using the slices of the tomography results in the 3D Slicer software. Since the material density of the injector nozzle tip and the needle are different, the different levels of X-ray absorption lead to different intensities in the tomography images. The geometry of these two components can thus be extracted by a proper thresholding. Finally, the surface conditions of the nozzle orifices, needles and needle seats can be observed through the reconstructed surfaces.

Image processing

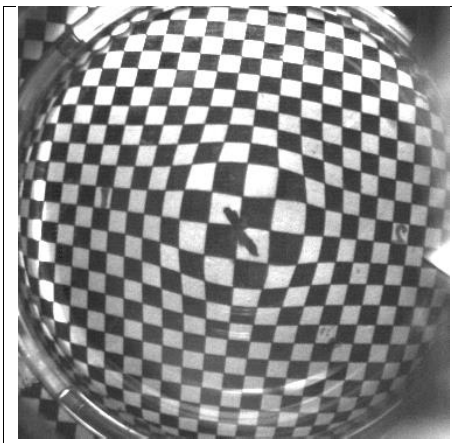

Figure 2.Recorded target image without correction.

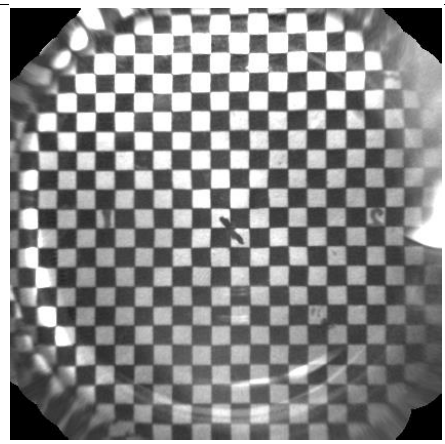

Figure 3. Recorded target image after correction.

An image correction process is necessary since the bowl shape of the piston causes severe distortion. A distorted image and a corrected image are shown in Figure 1 and Figure 2, respectively. The procedure is performed in MATLAB by fitting geometric transformation to control points using the local weighted mean method. This method works well for distortion that varies locally. Due to the larger distortion in the middle, some tiny distortions can still show in the centre area in the corrected image. But the influence is considered small enough to be neglected. When looking up from the bottom of the optical piston, the boundary of the bowl area causes accumulated distortion in a small ring area which is barely possible to be corrected. Thus, the effective measurement area is limited in the piston bowl region, a circle with a diameter of around 45 mm in the centre. The corrected images have a spatial resolution of 10 pixels per millimetre.

Due to the geometry of the bowl shape and the side-entering laser light, severe beam steering occurs, causing non-uniform illumination of the sprays. Additionally, the incident light only covers one side window, meaning that some sprays are less illuminated than others. Thus, only the spray that gives the highest scattering signals is used for the spray analysis.

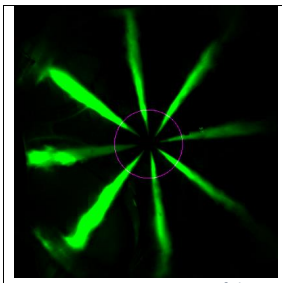

Figure 4. Start position of the circular mask for sampling intensity.

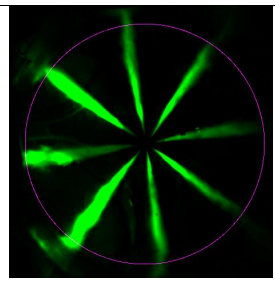

Figure 5. Stop position of the circular mask for sampling intensity.

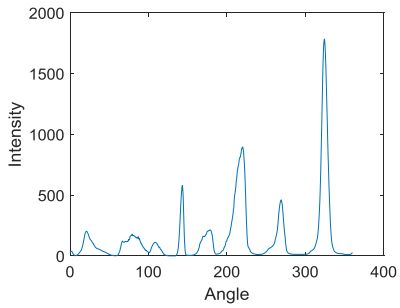

Figure 6. Averaged intensity single from the sampling of a series of circular masks to find the strongest scattering spray and its angular position.

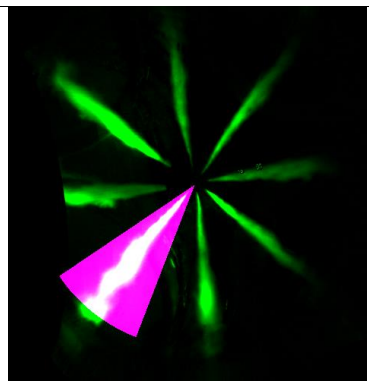

Figure 7. Illustration of the relative position of the pie-shaped mask and the spray to be selected.

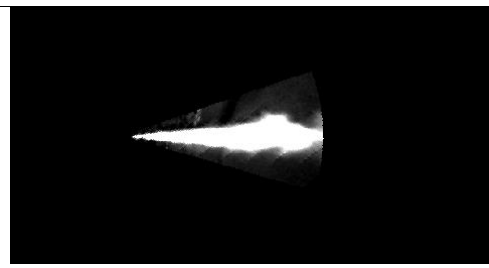

Figure 8. Illustration of a final region of interest created for further analysis.

The measured signals are first processed by background subtraction and distortion correction. Then the location of the nozzle tip is determined and a serials of concentric circle masks separated by 2 pixels are made to sample the pixel intensity on the circles. The minimum radius of the circles is 50 pixels and the maximum radius of the circles is 210 pixels. A frame of a fully developed spray which reaches the bowl boundary is selected from each measurement cycle for the calculation. The intensity-angular position relation is hence revealed. This procedure is illustrated in Figure 4, Figure 5 and Figure 6, in which the start position of the sampling, the end position of the sampling and the final results are shown respectively. Therefore, the spray with the strongest scattering signal can be identified along with its angular position.

Next, to prepare the spray for the analysis, a pie-shaped mask which can cover the entire spray in all frames is made as a region of interest as shown in Figure 7. To avoid the reflection at the curved

bowl boundary when the scattering spray is approaching, the radius of the pie-shaped mask is controlled at 220 pixels, just slightly shorter than the bowl radius. Finally, this selected region of interest is rotated to a horizontal position using the angle information retrieved before as illustrated in Figure 8.

Natural luminosity analysis

Before diving into the analysis of the natural luminosity (NL) of the combustion progresses, the major factors that can influence the NL signal are discussed briefly to clarify the interpretation of the signals in this work. The NL luminosity mainly consists of soot incandescence and chemiluminescence. In a diesel combustion mode, soot incandescence is a strong broadband thermal radiation from hydrocarbon combustion, while chemiluminescence is a weaker, narrowband non-thermal radiation mostly emitted by gaseous intermediate combustion products. The NL is mainly dependent on soot volume fraction and soot temperature and can therefore be used as a qualitative indicator in the combustion analysis. It is difficult to use NL as a quantitative soot diagnostic because there are many interferences (37): 1) interference from chemiluminescence; 2) soot particle size, spectral emittance, refractive index, and temperature; 3) quantum efficiency and linearity of the detection systems; 4) adiabatic flame temperature; 5) in-cylinder temperature; 6) spatial distribution of luminous soot; 7) optical thickness effects.

The chemiluminescence emission is usually in the 300 to 600 nm region and often much weaker than the soot luminosity (37). Additionally, the 452 nm bandpass filter can effectively block most of the typical chemiluminescence emissions such as OH*, CH* and C2* (38). Thus, the chemiluminescence contribution can be neglected in this work.

The use of different ND filters at each load point ensures there is no saturation of the camera sensor in the measurement. Although the linearity of the camera response is not verified, it is assumed to be linear in this work. The wavelength-dependent quantum efficiency of the camera is also neglected since no intensifier is used and the narrow-band incoming signal after the band-pass filter.

The difference of adiabatic flame temperature between the two fuels can also be considered negligible as the SR fuel only contains a limited amount of additive. The fuel property change is thereby small and the overall air-fuel ratio is not affected when comparing the fuels.

The difference in the optical thickness needs to be considered in line-of-sight measurement. Any medium between the signal source and the detection system that can absorb and/or scatter the radiation affects the recorded results. If a flame is thick, the burning soot signal on the far side from the camera is attenuated when it passes the flame, while the soot on the close side is not affected.

Results and discussion

Injector geometry analysis

Figure 9 and Figure 10 show the cross-sections and the reconstructed 3D surfaces of the nozzles and the needle tip areas of the new and the aged injector, respectively. It can be noted that all orifice surfaces are smooth as well as the transition area from the sac volume to the nozzle channel. The needle tips and the needle seat surfaces show a good match without any gap.

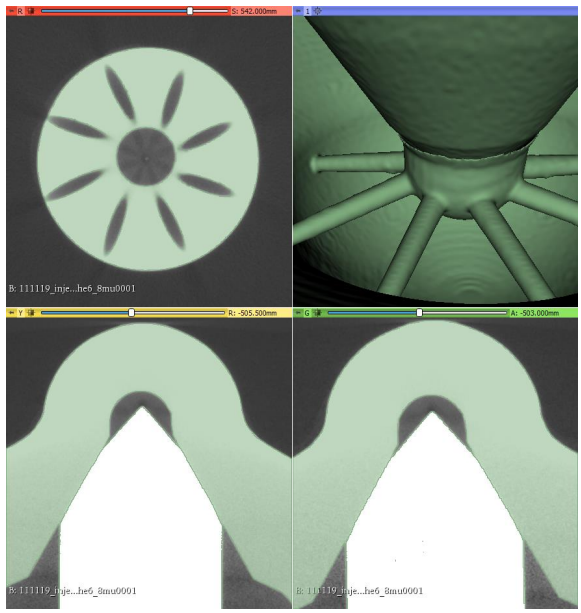

Figure 9. Cross section views of the new injector's nozzle tip and a reconstructed 3D model representing the needle and the nozzle surfaces.

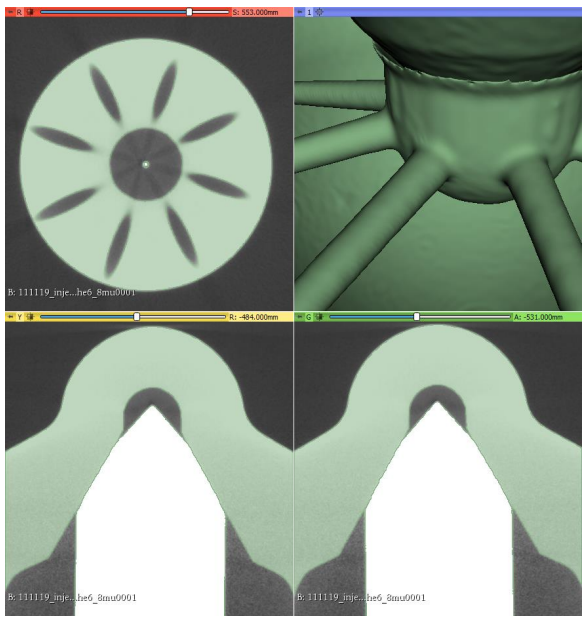

Figure 10. Cross section views of the aged injector's nozzle tip and a reconstructed 3D model representing the needle and the nozzle surfaces.

Figure 11 shows an overlapped cross-section view comparison at different positions in the nozzles from both the new and the aged injectors. It demonstrates that the geometry is similar in both injectors. Despite some small variation, most likely caused by manufacturing tolerance, there is no substantial geometry difference. Thus, it can be concluded that the nozzle geometry of the aged injector does not explain the increased fuel injection quantity. The spray pattern is also unlikely affected. The hypotheses of deposits or nozzle wearing can be thus eliminated.

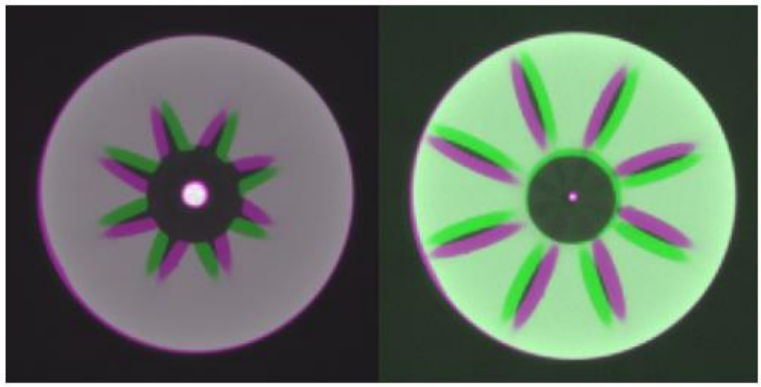

Figure 11. Overlapped cross section views of the nozzle area from the new and the aged injectors at different distance from nozzle tip.

Spray analysis

Injection quantity

The total intensity in the ROI is calculated by just summing the signal in all the pixels in an image. Though there is some background noise, the scattering signal is generally much stronger. Thus, the addition of the noise is considered negligible. The results at low load and medium load are shown in Figure 12 and Figure 13, respectively. At low load, all four injections show an approximately Gaussian intensity profile, meaning that the fuel injection is mostly in a transient condition (i.e. the needle does not reach its fully open position). The scattering signal from the aged injector is significantly higher, especially during the two pilot injections. This supports the previous observation that the aged injectors deliver more fuel than the new ones do, as the higher signal indicates that more liquid fuel is present in the cylinder.

At medium load, the main injections show a top-hat profile, which means the needles are fully lifted and the fuel injection reaches a quasi-steady state. The peak scattering values during the main injection are similar for both injectors, meaning that the discharge rates when the needle is fully lifted are similar for the two injectors. As the integrated signal doesn't increase despite the ongoing fuel injection during this period indicates that the fuel injection rate equals the evaporation rate. Note that although this total scattering signal can be used as an indicator of the fuel quantity, the actual amount of fuel is not directly proportional to the scattering signal due to the occurrence of multiple scattering.

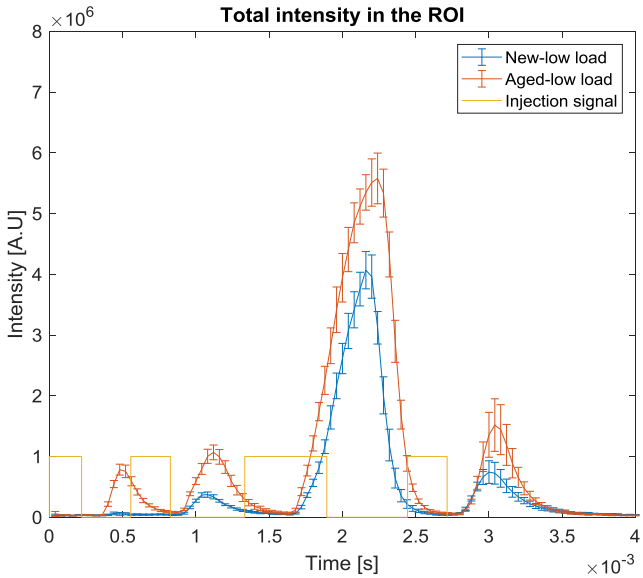

Figure 12. Mie-scattering signal at low load using different injectors.

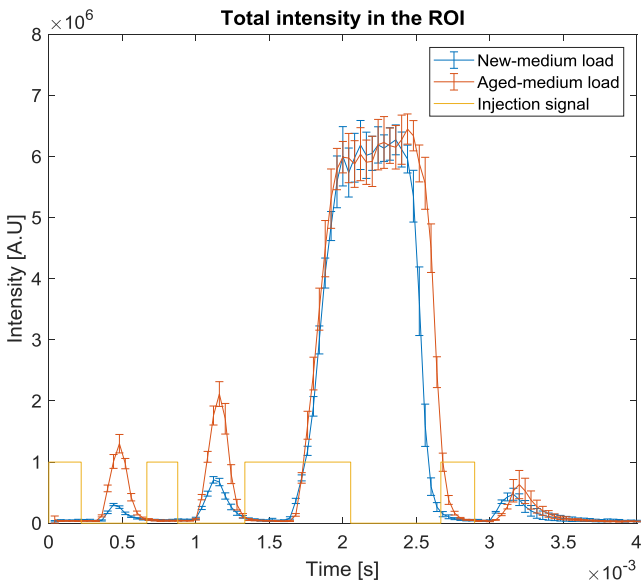

Figure 13. Mie-scattering signal at medium load using different injectors.

By calculating the time derivatives of the total scattering signals, the intensity change rate is obtained, which is shown in Figure 14 and Figure 15 for the low and medium load cases, respectively. The instants where the change rate starts to increase above zero are very close for both injectors,

which means the delay between the injection current and the actual fuel injection is similar. The response of the needle in the lifting stage is thus similar. However, there is a time gap between the instants where the scattering signals start to decrease (the derivative goes from positive to negative). Since the ambient conditions are similar, the liquid fuel length cannot be affected considerably by different evaporation rates. It is most likely that the needle closing is having a lag with the aged injector, especially during the main injection. This therefore seems to be the main reason why the aged injector shows a higher injection quantity. If the delay between the closing command signal and the actual needle closing is constant, the percentual increase will be larger for a short injection than for a longer.

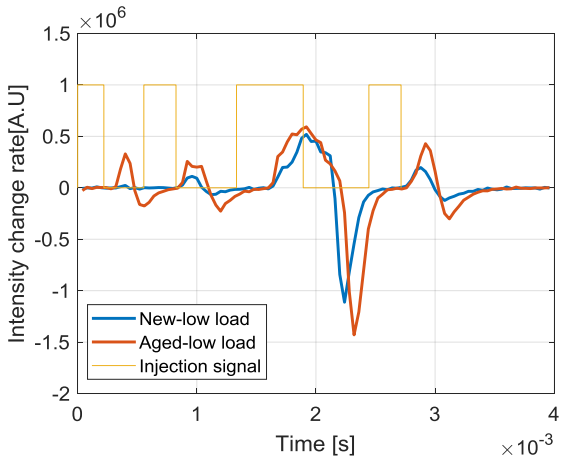

Figure 14. Total scattering signal change rate at low load.

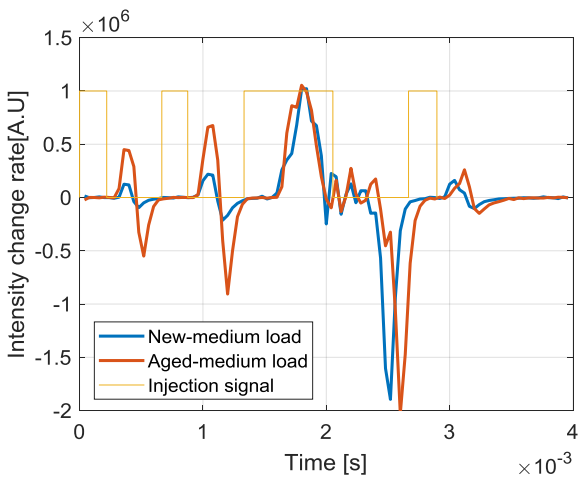

Figure 15. Total scattering signal change rate at medium load.

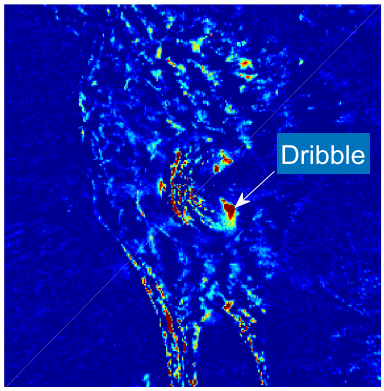

Figure 16. Near nozzle area right after the first pilot injection when the new injector is used, with contrast enhancing.

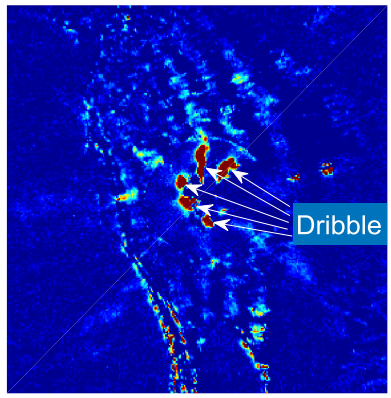

Figure 17. Near nozzle area right after the first pilot injection when the aged injector is used, with contrast enhancing.

A close look at the nozzle area after the fuel injection events, especially the pilot injections, shows that there is more fuel dribbling after injections from the aged injector. An example is shown in Figure 16 and Figure 17 for the new and the aged injector at medium load, respectively. The near nozzle area of the new injector shows small fuel dribbles from one orifice while there are five obvious fuel dribbles from the aged injector. These dribbles contribute to the fuel flow difference between the injectors. They are induced by the evacuating fuel flow right after the needle closing which means the dribbling process is primarily governed by the needle closing speed and not the injection velocity (34). It is also pointed out that the injection pressure plays an insignificant role if the needle closing speed is the same (34). Whether the dribbling is caused by severe needle bouncing in the end of injection requires further investigation.

Spray penetration length

The spray length is calculated by sampling the pixel intensity along the spray axis to obtain an intensity-position curve. A threshold of 5 % of the maximum intensity is applied to obtain the spray length. Finally, an actual distance can be calculated by multiplying the spatial resolution with the pixel count.

Figure 18 and Figure 19 present the spray penetration at low load and medium load, respectively. The liquid spray length in the pilot injections from the aged injector is significantly longer than that from the new injector, mainly due to the prolonged injection duration. In the main injection, both liquid lengths can approximately reach the bowl wall and thus their maximum penetration distances are inherently limited. Large cycle-to-cycle variation can be observed in the main injection at medium load because of spray tip fluctuations caused by turbulence. In that case, the fuel injection rate is equal to the evaporation rate. Since the hot air is mainly entrained upstream and the liquid fuel is mostly evaporated downstream, the liquid fuel droplets close to the spray tip are highly sensitive to turbulence, leading to larger fluctuations.

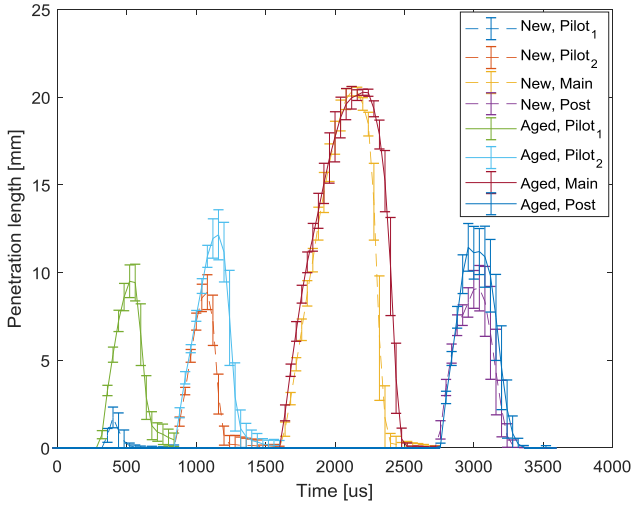

Figure 18. Spray penetration at low load using new and aged injectors.

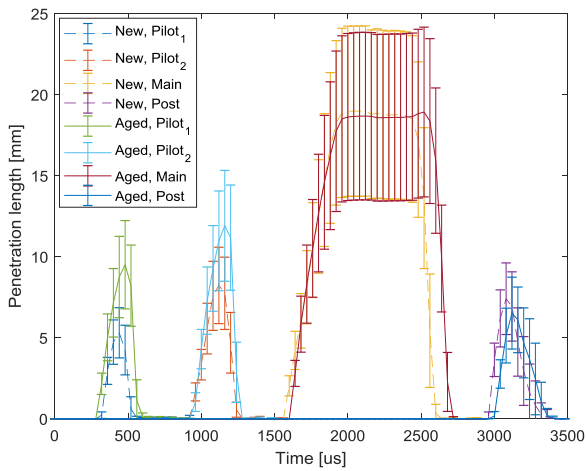

Figure 19. Spray penetration at medium load using new and aged injectors.

Spray penetration speed

The fuel spray penetration speed during the injection can be derived by calculating the time derivatives of the liquid spray lengths. Figure 20 shows the results at low load and Figure 21 shows the results at medium load. No significant penetration speed difference can be found between the two injectors in the main injection events. This matches what is observed in the total intensity change rate, where the needle response during the lifting stage is similar between the two injectors. Due to the limited time resolution of the imaging system, the liquid spray may have travelled a different distance between the the first image with clear scattering signals and its previous frame.

This leads to a relatively large variation in the initial spray speed estimation. In the later liquid spray development phase, both the mean values and the standard deviations are close.

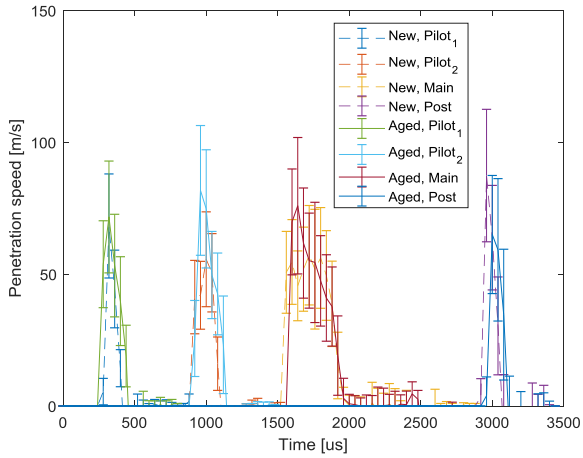

Figure 20. Spray penetration speed at low load with different injectors.

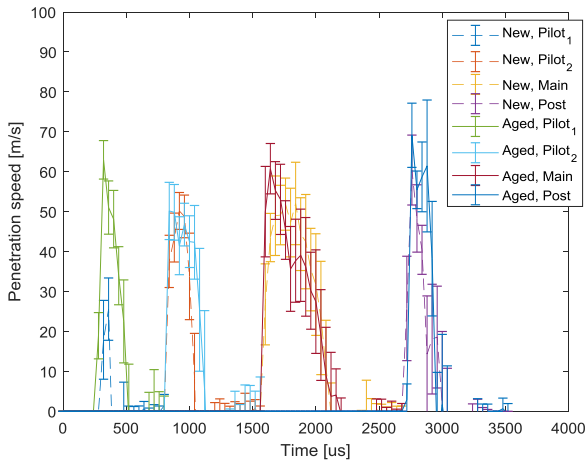

Figure 21. Spray penetration speed at medium load with different injectors.

Fuel spray spreading angle

The spray spreading angle is a function of the ratio of the fuel and the ambient gas density, orifice geometry parameters and the effects of the injector needle and tip design on flow through orifice (35). The spray spreading angle and the general spray morphology can be used as indicators for identifying problems such as asymmetric sprays or large shot-to-shot variations. There are different ways of defining the spray spreading angle (36). For comparing the spray morphology between the

two injectors, the spray width is calculated at different locations. The intensities on axes perpendicular to the spray axis are sampled at different downstream locations. Pixels on each axis that have higher intensities than 5 % of the maximum are counted as the spray width at this position. A frame of a fully developed spray during the main injections is selected for the width estimation. Then the average of all measured cycles is calculated.

The results are shown in Figure 22 and Figure 23 for low load and medium load case, respectively. Generally, the spray widths are very similar between the injectors at both load points. There is strong reflection at around 7 to 8 mm downstream of the injector nozzle during the measurement of the new injector, leading to a large overestimation of the spray width. The standard deviation increases with the increasing distance from the nozzle. As the atomization of the liquid spray increases downstream the nozzle, multiple scattering increases. This can cause overestimated spray widths and the influences form turbulence in the far end are increased, which generates a larger fluctuation. No consistent asymmetric spray patterns are observed. Thus, the conclusion is drawn that the air entrainment rates during the injections are similar for both injectors since both the liquid spray penetration and spray spreading angles are similar.

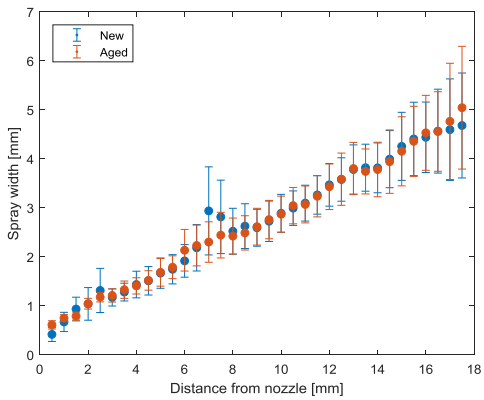

Figure 22. Spray width comparison at low load when using the new and the aged injector.

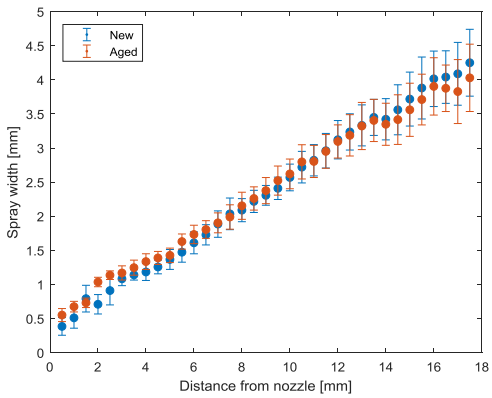

Figure 23.Spray width comparison at medium load when using the new and the aged injector.

Combustion analysis

Figure 24 shows a sequence of NL images, while Figure 25 shows the corresponding cylinder pressure, heat release, and the spatially integrated NL signals. The first soot luminosity appears at around 3 CAD with weak and unevenly distributed signals. These arise from soot luminosity in the rich premixed pilot combustion. Just after 7 CAD, the main injection occurs and the cool fuel jets are injected into the combusting areas, getting ignited by the heat released in the pilot combustion. Eight individual reacting plumes are formed and the integrated NL increases sharply to a peak just after 10 CAD (Figure 25).

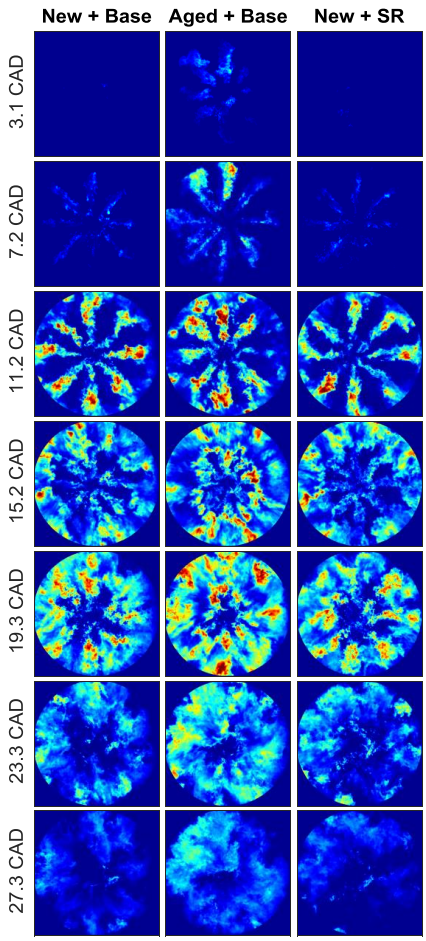

Figure 24. Natural luminosity signal during combustion processes at low load when using different fuels with different injectors.

As the piston goes down, a small part of the combusting products expands into the squish volume while the majority gets redirected along the bowl wall towards the centre of the piston. The soot oxidation continues while the combined effects of diffusion and post injection help redistribute the unoxidized soot more evenly in the cylinder. After the short post injection, the second NL peak occurs at around 19 CAD as the added heat release from the post injection increases the temperature again.

The momentum of the injection also boosts the mixing of unoxidized soot and oxygen. This peak is most likely contributed by the mixing of remaining oxygen in the central area which is not previously consumed. After this peak point the signal has a fast decay since most soot is oxidized.

All three cases at low load show a similar in-cylinder process. The integrated intensity is very close when comparing the fuels for the new injector (Figure 24). On the other hand, the aged injector shows a significantly stronger soot luminosity during the entire combustion process. This could simply be caused by the difference in the fuel quantity, which elevates both soot volume fraction and in-cylinder temperature. It is more obvious at the second NL peak when the soot clouds get redirected into the centre and more oxygen is entrained for further oxidation. Because of the elevated temperature, there is a larger soot oxidation window. Thus, the NL signal observed with the aged injector continues its decay to the later parts of the cycle.

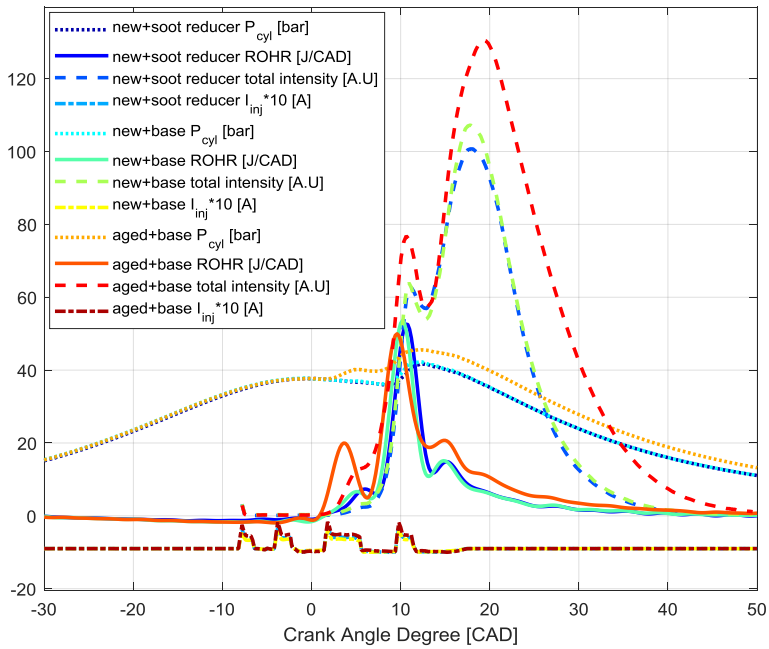

Figure 25. Pressure, heat release rate and spatial integration of natural luminosity signal during combustion at low load.

At medium load, the very first NL signal starts at around 3 CAD when the first pilot injection is ignited (Figure 27). Rich premixed combustion appears more clearly just after the second pilot injection at around 5 CAD (Figure 26). These are the soot particles from the second pilot injection being oxidized. They keep travelling towards the bowl boundary and growing larger until about 8 CAD, as evidenced by the increasing signals. Then the main injection starts. This time, the cool fuel jets shoot into the already reacting products and lead to a small reduction in the NL by partially quenching the reactants as shown in Figure 26 at around 9.6 CAD.

The fuel jets from the main injection get ignited quickly, which leads to the sharp increase of the main combustion heat release just after 10 CAD (Figure 27). The main combustion heat release still appears to be highly premixed. When the reacting jets reach the bowl wall, they impinge on it until the end of main injection. During this time, soot particles may not have sufficient temperature to be oxidized due to heat losses to the wall. The wall also limits the access to oxygen, which limits the oxidation rate and leads to a decreased temperature. Cold soot is driven and redirected by the fuel injection towards the central area. The NL only starts to climb sharply after 15 CAD and peaks at around 22 CAD. The peak NL is higher at the medium load when using the new injector, with the SR fuel being the highest. The aged injector shows the lowest NL, but it still has a longer decay time. Compared with the low load case, the soot is more evenly distributed in the cylinder volume after the main injection (Figure 26).

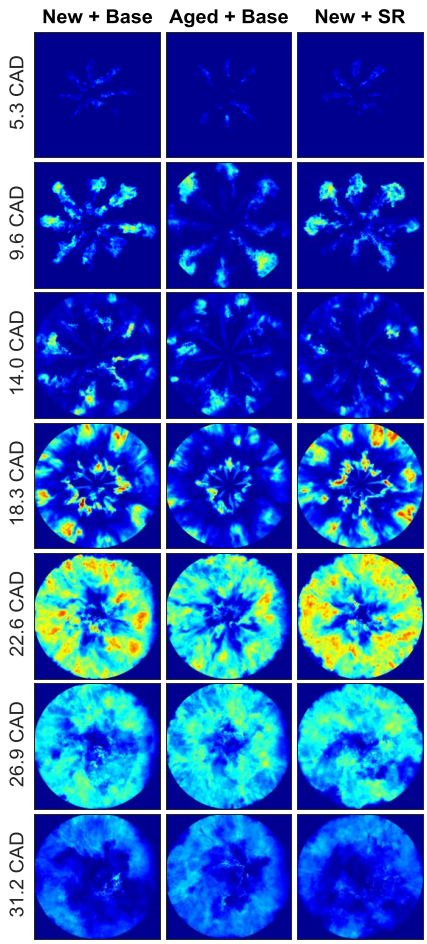

Figure 26. Natural luminosity signal during combustion processes at medium load when using different fuels with different injectors.

One possible reason for this is that the aged injector's longer injection duration provides both a higher fuel quantity and more momentum exchange, which provides a better mixing and higher temperature. The initial heat release from the aged injector's pilot combustion is significantly higher than that from the new injector, leading to a slightly advanced ignition of the main injection. Thus, the overall combustion process of the aged injector tends to be a more even and prompt. Less soot is formed thanks to the improved mixing and hence less soot luminosity is shown in the late cycle. Another possible reason is that there is in fact more soot formed by the aged injector due to the higher fuel quantity injected. A thicker cool soot cloud along to the bowl wall could be formed due to heat loss and restricted oxygen access, leading to significantly attenuated NL signals in the imaging plane. The total soot luminosity could be higher because of a slightly higher temperature and increased soot volume fraction. But in this case the difference of the optical thickness between the combustion cases becomes too large to provide a proper estimation of the soot volume fraction.

As for the fuel comparison, the SR fuel gives a stronger NL signal compared with the baseline fuel, indicating either that more soot is formed in the early stages or that the soot temperature in the late cycle is boosted by the added oxygen in the fuel. It is noteworthy that the integrated NL intensity might be different for broadband signal collection, since relatively cold soot emits much less. Only high temperature burning soot is then observed in the images, while the size and volume fraction of cold soot particles remains unknown. Also, as the piston goes down during the expansion stroke, the temperature decreases fast and the remaining cooled soot is not visible anymore.

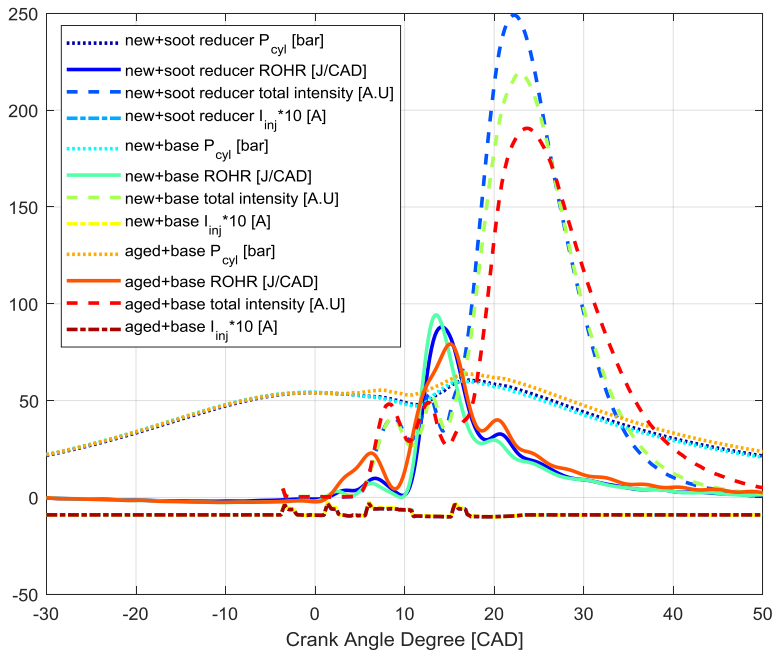

Figure 27. Pressure, heat release rate and spatial integration of natural luminosity signal during combustion at medium load.

Conclusions

In this work, the effects of injector aging on the spray formation and combustion are studied using optical diagnostics, where one new injector and one aged injector are compared. The combustion process of the TPGME soot reducer is also investigated against a baseline reference fuel.

An X-ray tomography of the injectors eliminates the hypothesis that the aging leads to significant geometric differences in the injector nozzle and needle areas. The high-speed Mie-scattering imaging of fuel injection under non-reacting conditions demonstrates that the sprays from both injectors are even and symmetric. The liquid fuel penetration and jet spreading angles are also similar. However, the aged injector shows a longer injection duration when using the same injection strategy, as well as a much more obvious fuel dribbling after the injection. This means that the needle actuation of the aged injector is behaving differently in the close stage, which is considered as the main reason of the fuel quantity difference between the two injectors.

Natural luminosity imaging of the combustion processes reveals differences in the in-cylinder soot processes. At low load, the difference in fuel quantity dominates the total luminosity signal. More soot is formed with more fuel and the oxidation also lasts longer with a longer high temperature window. No significant difference is observed between the two fuels. At medium load, the TPGME fuel shows stronger soot luminosity than the base fuel, while the aged injector using base fuel gives the lowest. Enhanced mixing and higher temperature lead to an overall prompter combustion, which restricts the time for soot formation while the oxidation rate is boosted drastically. The strong soot luminosity from the SR fuel might be caused by a higher soot volume fraction or elevated temperature due to the oxygen content.

This work will be followed by combined measurements using laser induced incandescence and laser extinction for further clarifying the late cycle oxidation process of the soot.

Acknowledgement

This project is funded by the MSCA-ITN-ETN of EU H2020 programme under REA grant agreement no. 675528 and by the Swedish Energy Agency through the KCFP engine research centre. The author would like to acknowledge Volvo Cars and Afton Chemicals for providing injectors and fuels, respectively, to the project. Special thanks to the solid mechanics department at Lund University for helping with the X-ray tomography of the injectors.

References

1. Ma S, Zheng Z, Liu H, Zhang Q, Yao M. Experimental investigation of the effects of diesel injection strategy on gasoline/diesel dual-fuel combustion. Applied Energy. 2013 Sep 1;109:202-12.
2. Park C, Kook S, Bae C. Effects of multiple injections in a HSDI diesel engine equipped with common rail injection system. SAE Technical Paper; 2004 Mar 8.
3. Han Z, Uludogan A, Hampson GJ, Reitz RD. Mechanism of soot and NOx emission reduction using multiple-injection in a diesel engine. SAE transactions. 1996 Jan 1:837-52.

4. Krogerus, T. R., Hyvönen, M. P., and Huhtala, K. J. (February 23, 2016). "A Survey of Analysis, Modeling, and Diagnostics of Diesel Fuel Injection Systems." ASME. J. Eng. Gas Turbines Power. August 2016; 138(8): 081501. https://doi.org/10.1115/1.4032417
5. Payri F, Luján JM, Guardiola C, Rizzoni G. Injection diagnosis through common-rail pressure measurement. Proceedings of the Institution of Mechanical Engineers, Part D: Journal of Automobile Engineering. 2006 Mar 1;220(3):347-57.
6. Macián V, Bermúdez V, Payri R, Gimeno J. New technique for determination of internal geometry of a diesel nozzle with the use of silicone methodology. Experimental techniques. 2003 Mar 1;27(2):39-43.
7. Kastengren AL, Tilocco FZ, Powell CF, Manin J, Pickett LM, Payri R, Bazyn T. Engine combustion network (ECN): measurements of nozzle geometry and hydraulic behavior. Atomization and Sprays. 2012 Jan 1;22(12):1011-52.
8. Strek P, Duke D, Swantek A, Kastengren A, Powell CF, Schmidt DP. X-ray radiography and CFD studies of the Spray G injector. SAE Technical Paper; 2016 Apr 5.
9. Matusik KE, Duke DJ, Kastengren AL, Sovis N, Swantek AB, Powell CF. High-resolution X-ray tomography of Engine Combustion Network diesel injectors. International Journal of Engine Research. 2018 Nov;19(9):963-76.
10. Xu H, Wang C, Ma X, Sarangi AK, Weall A, Krueger-Venus J. Fuel injector deposits in direct-injection spark-ignition engines. Progress in Energy and Combustion Science. 2015 Oct 1;50:63-80.
11. Birgel A, Ladommatos N, Aleiferis P, Zülch S, Milovanovic N, Lafon V, Orlovic A, Lacey P, Richards P. Deposit formation in the holes of diesel injector nozzles: A critical review. SAE Technical Paper; 2008 Oct 6.
12. Barker J, Richard P, Snape C, Meredith W. Diesel injector deposits-an issue that has evolved with engine technology. SAE Technical Paper; 2011 Aug 30.
13. Wen Y, Wang Y, Fu C, Deng W, Zhan Z, Tang Y, Li X, Ding H, Shuai S. The impact of injector deposits on spray and particulate emission of advanced gasoline direct injection vehicle. SAE Technical Paper; 2016 Oct 17.
14. Magno A, Mancaruso E, Vaglieco BM, Florio S, Gioco G, Rebesco E. Study on spray injection and combustion of fouled and cleaned injectors by means of 2-D digital imaging in a transparent CR diesel engine. SAE Technical Paper; 2013 Sep 8.
15. d'Ambrosio S, Ferrari A. Diesel injector coking: optical-chemical analysis of deposits and influence on injected flow-rate, fuel spray and engine performance. Journal of engineering for gas turbines and power. 2012 Jun 1;134(6).
16. Montanaro A, Allocca L. Impact of the Nozzle Coking on Spray Formation for Diesel Injectors. SAE Technical Paper; 2013 Oct 14.
17. Wang Z, Ma X, Jiang Y, Li Y, Xu H. Influence of deposit on spray behaviour under flash boiling condition with the application of closely coupled split injection strategy. Fuel. 2017 Feb 15;190:67-78.
18. Cristofaro, Marco & Edelbauer, Wilfried & Koukouvinis, Phoevos & Gavaises, Manolis. (2019). A numerical study on the effect of cavitation erosion in a Diesel injector. Applied Mathematical Modelling. 78. 10.1016/j.apm.2019.09.002.
19. Greif D, Srinivasan V. Numerical prediction of erosive cavitating flows in injection equipment. SAE Technical Paper; 2011 Sep 11.
20. Mariasiu F. Numerical investigation of the effects of biofuel characteristics on the injector nozzle erosion process. Tribology transactions. 2013 Mar 1;56(2):161-8.
21. Hofmann O, Strauß P, Schuckert S, Huber B, Rixen D, Wachtmeister G. Identification of aging effects in common rail diesel injectors using geometric classifiers and neural networks. SAE Technical Paper; 2016 Apr 5.
22. Hofmann O, Schuckert S, Wachtmeister G, Rixen DJ. Optimal Injection Strategies to Compensate for Injector Aging in Common Rail Fuel Systems. SAE International Journal of Engines. 2018 Jan 1;11(6):1083-92.

23. Hofmann O, Rixen DJ. Aging tolerant control of direct injection engines. Control Engineering Practice. 2018 Aug 1;77:201-12.
24. Battistoni M, Xue Q, Som S, Pomraning E. Effect of off-axis needle motion on internal nozzle and near exit flow in a multi-hole diesel injector. SAE international Journal of Fuels and Lubricants. 2014 Apr 1;7(1):167-82.
25. Zhang X, Liu J, Wang J. Effect of fuel and nozzle geometry on the off-axis oscillation of needle in diesel injectors using high-speed X-ray phase contrast imaging. Journal of Instrumentation. 2016 May 16;11(05):C05015.
26. Lee JH, Cho S, Lee SY, Bae C. Bouncing of the diesel injector needle at the closing stage. Proceedings of the Institution of Mechanical Engineers, Part D: Journal of Automobile Engineering. 2002 Aug 1;216(8):691-700.
27. TAKEUCHI H, KATO M, KAJITANI S, YAMAGUCHI M, AIHARA Y, TAKAHARA M. C201 A STUDY OF DIESEL NOZZLE TIP WEAR IN THE CASE OF THE FUEL DME (Erosion). InThe Proceedings of the International Conference on Power Engineering (ICOPE) 2009.2 2009 Nov 16 (pp. _2-181_). The Japan Society of Mechanical Engineers.
28. Donaldson K, Tran L, Jimenez LA, Duffin R, Newby DE, Mills N, MacNee W, Stone V. Combustion-derived nanoparticles: a review of their toxicology following inhalation exposure. Particle and fibre toxicology. 2005 Dec;2(1):10.
29. Bond TC, Doherty SJ, Fahey DW, Forster PM, Berntsen T, DeAngelo BJ, Flanner MG, Ghan S, Kärcher B, Koch D, Kinne S. Bounding the role of black carbon in the climate system: A scientific assessment. Journal of Geophysical Research: Atmospheres. 2013 Jun 16;118(11):5380-552.
30. Tree DR, Svensson KI. Soot processes in compression ignition engines. Progress in Energy and Combustion Science. 2007 Jun 1;33(3):272-309.
31. C.J. Mueller, W.J. Pitz, L.M. Pickett, G.C. Martin, D.L. Siebers, C.K. Westbrook, Effects of oxygenates on soot processes in di diesel engines: experiments and numerical simulations, SAE Paper 2003-01-1791, 2003.
32. B.E. Hallgren, J.B. Heywood, Effects of oxygenated fuels on di diesel combustion and emissions, SAE Paper 2001-01-0648, 2001.
33. Manin, J., Skeen, S., Pickett, L., Kurtz, E. et al., "Effects of Oxygenated Fuels on Combustion and Soot Formation/Oxidation Processes," *SAE Int. J. Fuels Lubr.* 7(3):704-717, 2014
34. Moon S, Huang W, Li Z, Wang J. End-of-injection fuel dribble of multi-hole diesel injector: comprehensive investigation of phenomenon and discussion on control strategy. Applied Energy. 2016 Oct 1;179:7-16.
35. Siebers DL. Recent developments on diesel fuel jets under quiescent conditions. InFlow and combustion in reciprocating engines 2008 (pp. 257-308). Springer, Berlin, Heidelberg.
36. Johnson JE, Naber JD, Lee SY. Characterizing diesel fuel spray cone angle from back-scattered imaging by fitting Gaussian profiles to radial spray intensity distributions. Journal of engineering for gas turbines and power. 2012 Jun 1;134(6).
37. Mueller CJ, Martin GC. Effects of oxygenated compounds on combustion and soot evolution in a DI diesel engine: broadband natural luminosity imaging. SAE Transactions. 2002 Jan 1:518-37.
38. Kojima J, Ikeda Y, Nakajima T. Spatially resolved measurement of OH*, CH*, and C2* chemiluminescence in the reaction zone of laminar methane/air premixed flames. Proceedings of the Combustion institute. 2000 Jan 1;28(2):1757-64.
39. Dahlstrom J, Andersson O, Tuner M, Persson H. Experimental comparison of heat losses in stepped-bowl and re-entrant combustion chambers in a light duty diesel engine. SAE Technical Paper; 2016 Apr 5.
40. Jacobs P, Sevens E, Kunnen M. Principles of computerised X-ray tomography and applications to building materials. Science of the total environment. 1995 May 1;167(1-3):161-70.

41. Zhu X, Andersson Ö. Performance of new and aged injectors with and without fuel additives in a light duty diesel engine. (Submitted to Transportation Engineering Journal, under review).

Paper III

Soot oxidation studies in an optical diesel engine using laser-induced incandescence and extinction:

the effects of injector ageing and TPGME fuel additive

Manu Mannazhi[1], Xinda Zhu[2], Öivind Andersson[2], Per-Erik Bengtsson[1]

[1]Division of Combustion Physics, Department of Physics, Lund University, Sweden
[2]Division of Combustion Engines, Department of Energy Sciences, Lund University, Sweden

Abstract

Previous studies have shown that ageing of injectors adversely affects the performance of a diesel engine in terms of the spray formation and combustion. It has also been shown that the presence of oxygenated additive tripropylene glycol monomethyl ether (TPGME) in the fuel can lower soot emissions. In this study, the effects of injector ageing and TPGME fuel additive on the late cycle oxidation of soot was investigated using laser diagnostic techniques in a light-duty optical diesel engine at two load conditions. The optical engine was equipped with a quartz piston with the same complex piston geometry as a production engine. Planar laser-induced incandescence (LII) was used to obtain in-cylinder 2D soot volume fraction (f_v) distributions, which were quantified using semi-simultaneous extinction measurements. The soot oxidation rate was estimated from the decay rate of the in-cylinder soot concentration for differently aged injectors and for the cases with and without the presence of TPGME in the fuel. The aged injector produced higher soot concentrations in the cycle at both load conditions in comparison with the new injector. Also, the aged injector showed higher soot oxidation rates at low load condition compared to the new injector. Addition of TPGME resulted in lower soot concentrations in the cycle at both load conditions and faster oxidation rates especially at mid load conditions.

1. Introduction

Reducing particulate matter (PM) emissions from diesel engines has been a persistent struggle for several decades due to its harmful effects on human health and the environment [1]. Increasingly stricter regulations are being implemented in the automobile sector to control PM emissions from internal combustion engines. Soot emissions, the dominant part of the PM emissions (> 40 % [1]) from a diesel engine, are influenced by several factors such as fuel composition, chamber geometry, fuel injection characteristics such as ageing of injectors, and after-treatment systems. Thus, further investigations are motivated and in this study, we focus on the effects of ageing of injector and soot reducer additive on late cycle soot oxidation.

Ageing of the injectors has been shown to adversely affect the combustion process in a diesel engine in several ways. Injector ageing has been found to result in the formation of deposits, either on or inside the nozzle tips, known as injector coking. Coking has a major impact on the durability of the engine performance. It leads not only to an increase in the injected fuel flow rate, but also to a deterioration in the spray quality in terms of atomization, symmetry and penetration. Such effects influence the fuel-air mixing and hence the combustion leading to an increase in soot emissions [2].

There have been many studies on injector coking or ageing of injectors in diesel engines [2-6]. Aged injectors have been found to have slower needle dynamic [5] and smaller spray penetration [3], and have been shown to produce dribbles at the end of fuel injection [7]. A study in an optical engine using high speed spray imaging measurements showed lower fuel injection for the aged injector compared to the clean or new injector [5]. Contrary to this observation, a multi-cylinder Volvo D4 engine using the exact same nozzles as in the present study showed a higher fuel injection for the aged injector [XX – ref tests]. This behavior of high fuel injection was also observed in our previous high speed imaging measurements using the same injectors and the optical engine used in the present study, where the aged injector produced longer injection durations compared to the new injector [7]. These effects of ageing of injectors on fuel injection and spray formation influence the combustion and subsequent emissions. Combustion in aged injectors has shown to have a larger area of high temperature regions compared to the new injector [5]. Aged injectors also produce higher amount of in-cylinder soot and result in higher exhaust emissions [5], such as hydrocarbon [3] and soot emissions [XX – ref tests].

While ageing of injectors results in elevated soot emissions, there are many ways to reduce these emissions. One way to do this is to use oxygenated fuel additives, which lower the soot emissions by the oxidation of soot formed in the combustion cycle. The additives tripropylene glycol monomethyl ether (TPGME) and dibutyl maleate (DBM) have been found to be the most effective ones on reducing soot emissions based on studies performed in a light duty diesel engine using eight different oxygenated fuels [8]. The effect of TPGME in reducing engine-out soot emissions compared to the baseline diesel fuel for the same engine operating conditions was also observed in another study [XX – ref tests]. However, two main disadvantages of the studies based on engine-out emission measurements are their lack of spatial resolution and inability to investigate the transient phenomena in a combustion cycle. This has led to the application of optical diagnostic techniques in constant volume chambers and optical engines. A study in an optical engine using spatially integrated natural luminosity (SINL) imaging showed that TPGME and DBM reduced the SINL signals by 1/7 and 1/3 respectively [9]. The SINL signal represents average in-cylinder soot concentration to an approximation and hence TPGME is found to be more effective than DBM in reducing soot levels. This has been demonstrated again in another study in an optically accessible constant volume chamber using natural luminosity and extinction measurements [10]. Several investigations using line-of-sight averaged high speed imaging measurements of natural luminosity [7, 11-13], OH chemiluminescence[11-13] and back-illuminated extinction [13] have indicated that TPGME can be a good candidate for a fuel additive that reduces soot emissions.

In spite of the fact that the effects of ageing of injector and TPGME additive on soot formation and emission has been investigated by several research groups, there is still more work to be done. All of the investigations mentioned above have certain disadvantages that fall in at least one of these four categories. First, there are some studies that have been performed in metal engines with no optical access [XX- ref tests] [8]. Second, there are various investigations using emission measurements that lack spatial resolution, and for which it is impossible to attain information on transient processes [XX-ref tests] [3, 8]. Third category belongs to the studies in a constant volume chamber [10, 13] or an optical engine with a simplified piston geometry [3, 5, 9-12]. The flow structures developed using a flat piston are different from the one with a curved piston used in a production engine, and hence leads to differences in fuel-air mixing and late-cycle soot oxidation behavior in comparison with the real production engine. Fourth category is related to the application of line-of-sight averaged techniques, such as OH chemiluminescence and natural luminosity measurements, which lack spatial resolution along the imaging direction [5, 7, 9-13]. Additionally, these studies in the optical engines are mostly qualitative measurements and it would be advantageous to have quantitative information on parameters such as soot concentration. It is important to have a detailed understanding about the

effects of ageing of injectors or TPGME additive on the soot formation and oxidation. For example, a good understanding on how injector ageing affects PM emissions is vital, as this could give valuable information about how manufacturers could maintain emission level compliance throughout the vehicle's lifetime. Planar quantitative measurements performed in an optical engine with the geometry of the piston as close to the production engine as possible could be instrumental in this regard.

In this study, laser-induced incandescence (LII) [14] was used for in-cylinder soot concentration measurements. LII can provide quantitative two-dimensional (2D) soot concentrations when calibrated using another technique, such as extinction. The LII technique is based on the heating of soot particles to high temperatures (~3500-4000 K) using a pulsed laser beam resulting in an enhanced Planck radiation from these particles. This radiation, called the LII signal, is found to be proportional to the soot volume fraction (f_v) to a first approximation [15]. Laser extinction [16], the previously mentioned calibration technique, is another diagnostic technique where evaluating the attenuation of laser energy when it traverses a soot-laden medium provides the soot concentration (more details in section 3.2). LII has been extensively applied in laboratory as well as practical systems to study sooting flames [14]. Several investigations have also been made in diesel engines using LII to study soot formation and oxidation [17-19]. Extinction has also been used as a stand-alone technique to study soot oxidation in optical diesel engines [20-22]. However, the use of a combination of LII and extinction to study soot oxidation in a diesel engine has been limited, especially with respect to the effects of injector ageing or TPGME additive. A combination of 2D LII and extinction has been employed in a constant volume chamber to study the effects of TPGME on soot formation and oxidation [23]. However, as pointed out before, there should be several differences in the behavior of combustion in a diesel engine and a constant volume chamber.

In this study, the effects of injector ageing and TPGME additive on late-cycle soot oxidation have been investigated in an optical engine derived from a multi-cylinder light duty Volvo diesel engine. The optical engine was equipped with a quartz piston with the exact geometry as the production engine. Laser diagnostic techniques 2D LII and extinction have been applied at two different load conditions to obtain 2D soot volume fraction (f_v) distributions and soot oxidation rates. This study is a continuation of our previous investigation of injector ageing and TPGME additive using high speed imaging measurements of soot luminosity and Mie scattering [7].

2. Experimental setup

2.1 Information on the engine and operating conditions

A multi-cylinder light duty Volvo diesel engine has been operated as a single-cylinder optical engine using a Bowditch design. The optical engine has four quartz windows in the cylinder liner providing optical access from the sides of the top volume of the cylinder. It has also been equipped with a transparent quartz piston mounted on a piston extension. A plane mirror mounted on the piston extension at an angle of 45° assists in the visualization of the combustion chamber through the piston. In this work, visualization has mainly been made from the side window. Key parameters related to the engine and injector geometry are given in Table 1.

Table 1. Key parameters representing the geometry of the engine and injector.

Bore	82 mm
Stroke	93 mm
Displaced volume	492 cc
Compression ratio	13.5

Connecting rod length	147 mm
Number of nozzle holes	8
Outlet diameter of injector nozzle holes	125 µm
Nozzle shape	Tapered
Spray umbrella angle	155°

Two sets of investigations were performed in this work. Firstly, the effects of injector ageing on soot formation and oxidation were studied. For this case, measurements were performed in the optical engine using a new injector (operated only for some reference tests before) and an aged injector (with over 100,000 km on-field usage). For comparing data from measurements using different injectors, the alignment of the sprays for all the injectors with respect to the incoming laser beam/sheet was set identical. This was checked using a high speed camera (Photron FASTCAM SA-Z) by performing high-speed imaging measurements of spray and soot luminosity through the bottom side of the quartz piston. The second set of investigations dealt with the effect of the additive tripropylene glycol monomethyl ether (TPGME) on soot formation and oxidation. For this, two fuel blends were used. The first one termed as baseline diesel meets the CEC RF-79-07 standard. The second fuel is a blend of the baseline diesel and a 5 % vol. TPGME ($C_{10}H_{22}O_4$). The fuel blend with TPGME has a calculated 1.5 % oxygen concentration by weight while the baseline fuel is assumed to have 0 %. Other important properties of the tested fuels are given in Table 2.

Table 2: Properties of the baseline fuel (BL) and the blend with TPGME additive.

	Baseline (BL)	**TPGME**
Composition	CEC RF-79-07 Pure diesel	Baseline fuel + 5 % vol. TPGME
Density @ 15 °C (kg/m^3)	833.8	837.6
Net heating value (MJ/kg)	43.2	42.76
Flash point (° C)	84	84

The engine was operated without EGR and at a speed of 1200 rpm, which accommodates the 10 Hz frequency of the laser system. Moreover, a 1:9 skip fire sequence was incorporated for the measurements. The operating points of the optical engine were developed by adapting the two reference points provided by Volvo for metal engines. Both of the reference points involve four injections per cycle, i.e., two pilot injections followed by one main injection and one post injection. The reference points 1 and 2 will be termed low and mid load conditions from now on. Table 3 summarizes the operating conditions of the optical engine for both loads. More details on the engine operating conditions can be found in our previous work [7].

Table 3: Operating conditions of the optial engine for both loads used in this study.

	Low load	**Mid load**
Injection pressure [bar]	450	850
Intake pressure [bar]	1.27	1.83
Intake temperature [°C]	75	75
Engine speed [RPM]	1200	1200
Engine load $IMEP_g$ [bar]	~ 4	~ 9
Oxygen concentration [%]	20	20
Estimated TDC density [kg/m^3]	~ 15	~ 22
Estimated TDC temperature [K]	~ 850	~ 860

2.2 Optical setup

A schematic representation of the optical setup is given in Fig. 1. Laser-induced incandescence (LII) measurements were performed using a Nd:YAG laser operated at 10 Hz at its fundamental wavelength 1064 nm. A laser wavelength of 1064 nm was selected for LII as it does not induce fluorescence from polycyclic aromatic hydrocarbon (PAH) molecules to cause interferences to the LII signal [14]. The laser beam was transformed into a vertical laser sheet of height 16 mm and made to pass through the optical windows, while being focused at the centre of the combustion chamber using a combination of cylindrical lenses. To decide on the laser fluence (laser energy per unit area of cross-section) to be used in the optical engine measurements, LII measurements using fluences ranging from 0.1 to 1.0 J/cm^2 were performed in premixed ethylene-air flames (ϕ = 2.3) on a flat-flame burner. It is recommended to use a laser fluence, which lies in the so called *plateau region* of the fluence curve (variation of LII signal with laser fluence) where the LII signal is rather insensitive to variations in laser intensity [24]. As a result of this, a laser fluence of 0.7 J/cm^2 at the centre of the combustion chamber was chosen for the LII measurements.

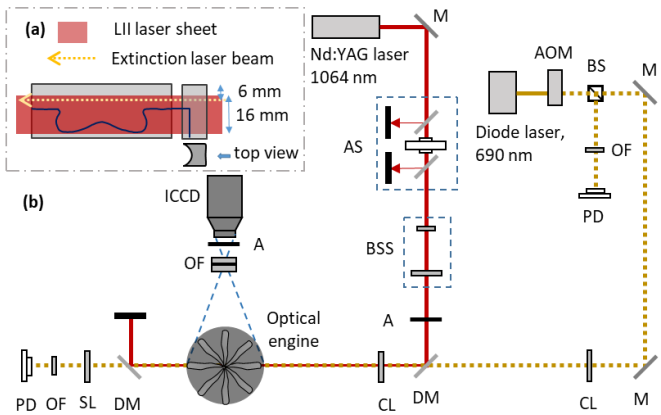

Figure 1: **a)** Schematic representation showing the propagation of LII and extinction laser beams through the optical engine. Note the irregular shape of the piston head. The refraction of the laser sheet through the engine chamber is extremely complex and has not been detailed. **b)** Schematic representation of the experimental setup focusing on the laser-induced incandescence (LII) and extinction measurements. A – Aperture, AOM – Acousto Optic Modulator, AS – Attenuation System, BS – Beam Splitter, BSS – Beam Shaping System, CL – Cylindrical Lens, DM – Dichroic Mirror, M – Mirror, OF – Optical Filter, PD – Photodiode, SL – Spherical Lens.

An ICCD camera (PIMAX IV, Princeton Instruments) equipped with an f = 100 mm f#2.0 UV lens was placed orthogonal to the path of the laser sheet and used for acquiring the two-dimensional LII signals. As the curvature of the quartz piston warps the focal plane, it was difficult to achieve sharp images of the whole imaged area, especially using a large aperture for the objective lens (f#2.0). To improve the depth of focus, an additional aperture of 12 mm diameter was placed in front of the objective lens, resulting in an overall f-number of ~ f#8, which considerably improved the image quality. However, reducing the aperture came with a reduction in the light intake and thus the signal intensity. Two short-pass filters with cut-off wavelength 450 nm were placed in front of the detector to reduce the background flame luminosity contribution to the LII signal. As a short gate width is recommended for signal acquisition for high-pressure applications, a prompt and short gate width of 20 ns was selected [15]. Additionally, a background flame luminosity image was captured ~2.4 µs before the frame with

the LII signal for each individual laser pulse, and this image was used for background subtraction on a single-shot basis.

A diode laser operating at 690 nm was used for extinction measurements. It has been reported that PAHs have very low absorption at wavelengths greater than around 700 nm [25]. The wavelength 690 nm was strategically chosen in this work for the extinction measurements as, firstly, the PAH absorption at this wavelength in comparison with soot absorption can be neglected and, secondly, laser alignment is easily made since the wavelength is in the upper edge of the visible spectral range. An acousto-optic modulator (AOM) operating at 72 kHz created laser beam modulations to enable the recording of background signals in between the laser pulses for subsequent background subtraction. Additionally, interference filters with a central wavelength of 690 ± 2 nm (FWHM 10 nm) were placed in front of the photodiodes to filter out unwanted radiation, mainly the broadband flame luminosity.

3. Methodology

3.1 Distortion correction

The complex geometry of the piston is detailed in Fig. 1a. As the 2D LII signal traverses through the quartz piston and the optical window on its way to the detector, severe distortions are introduced in the detected signal image, although the detection aperture was reduced as described previously. A procedure was developed for correcting this distortion. Two target grids were fabricated in the shape of the piston bowl and were illuminated using LED arrays. These two grids correspond to the left and right halves of the piston bowl. They were placed one after the other along the same plane of propagation of the laser sheet. The undistorted image of the left-side target grid is shown in Fig. 2a. Once the target grid is imaged through the quartz piston and the optical window using the same imaging optics, the image gets distorted as shown in Fig. 2b. To correct for this distortion, the whole image is split into three sections. These sections are the right and left halves of the piston bowl and the region above the piston top. Each section is then separately corrected for the distortion by transforming the points in the distorted image using a local weighted mean transformation with reference to the corresponding points in the undistorted image. This procedure is done for all the three sections of the image and the resulting distortion corrected sections are stitched together afterwards. The distortion-corrected target image of the left-side target is shown in Fig. 2c. Similar procedure is applied for the distortion correction of the mean LII signal images. The distorted and distortion-corrected 2D LII signal image at 30° crank angle after top dead centre (CA aTDC) for the case of the aged injector with baseline fuel at mid load condition is shown in Fig. 2d and 2e, respectively. Distortion-corrected LII images are used for all the analyses presented in this work.

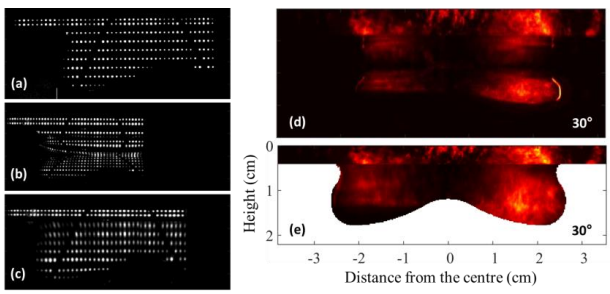

Figure 2: Image distortion correction procedure. **a)** Undistorted target grid. **b)** Distorted target grid viewed through the piston and the optical window. **c)** Distortion-corrected target grid. **d)** Distorted LII image at 30° CA aTDC for the aged injector with baseline fuel at mid load. **e)** Distortion-corrected LII image.

3.2 Calibration of LII signal into soot volume fraction (f_v)

Laser extinction measurements have been used for calibration of LII signals into absolute soot volume fractions in several studies [14, 26]. In this technique, a laser beam is sent through the soot-laden medium. The net decrease of the laser intensity across the beam path, caused due to soot in the medium, is used to evaluate line-of-sight averaged soot volume fractions. The extinction coefficient K_{ext} can be extracted using Beer-Lambert law,

$$I_t = I_0 e^{-K_{ext}L}, \tag{1}$$

where I_0 and I_t represent the initial and transmitted laser intensities and L is the absorption length. Assuming that the measurements are in the Rayleigh limit, i.e. where the particles are much smaller than the laser wavelength, the scattering contribution of the particles to the extinction was neglected [16]. The laser wavelength used for extinction in this study was 690 nm to simplify laser beam alignment in the visible spectral region, while still keeping absorption by PAH molecules at a negligible level. Under these assumptions, the soot volume fraction can be calculated using

$$f_v = \frac{K_{ext}\lambda}{6\pi\, E(m)}, \tag{2}$$

where λ is the laser wavelength and $E(m)$ is the soot absorption function represented as a function of the complex refractive index of soot m as,

$$E(m) = -Im\left[\frac{m^2-1}{m^2+2}\right] \text{ [27]}. \tag{3}$$

The procedure of calibrating the 2D LII signal intensities into 2D f_v distributions is shown in Fig. 3. The extinction laser beam was directed through the optical engine at a distance of approximately 9 mm from the cylinder head co-planar to the 1064 nm laser sheet used for LII measurements. At first, measurements of the initial and transmitted beam intensities were performed for motored cycles where the engine was operated without any fuel injection and hence without combustion. However, all the other operating conditions for the motored cycles were the same as for the fired cycles (cycles involving combustion). The reference intensity values were registered for motored cycles for which no soot was present in the combustion chamber.

As previously described, the extinction laser beam was modulated using an AOM. The modulations in the signal intensities I_0 and I_t for the motored case and the fired case are shown in Fig. 3a and 3b, respectively. It can be seen that the peak intensities of $I_{t,fired}$ varies with time due to the presence of soot in the combustion chamber. It can also be observed that the minimum intensities of $I_{t,fired}$ have a variation unlike that of $I_{t,motored}$. This is due to transmission of flame luminosity to the photodiode through the IF690 filter. The modulation of the extinction laser beam intensity enables subtraction of this background flame luminosity from the transmitted beam intensity. As there were 10 modulations per crank angle degree, after background subtraction, a resolution of 0.1° CA was achieved in the extinction measurements. The background subtracted intensities for one motored cycle and one fired cycle from 25° to 100° CA aTDC are shown in Fig. 3c. This corresponds to the case of new injector with baseline fuel at mid load condition. Crank angle resolved $K_{ext}L$ values were obtained using the Beer-Lambert law. Figure 3d shows the crank angle resolved $K_{ext}L$ values averaged over 150 cycles for this

case. Meanwhile, the product $K_{ext}L$ represents the line-integrated f_v. Based on the $K_{ext}L$ values, the LII signal images at CADs are calibrated in terms of absolute soot volume fractions (f_v).

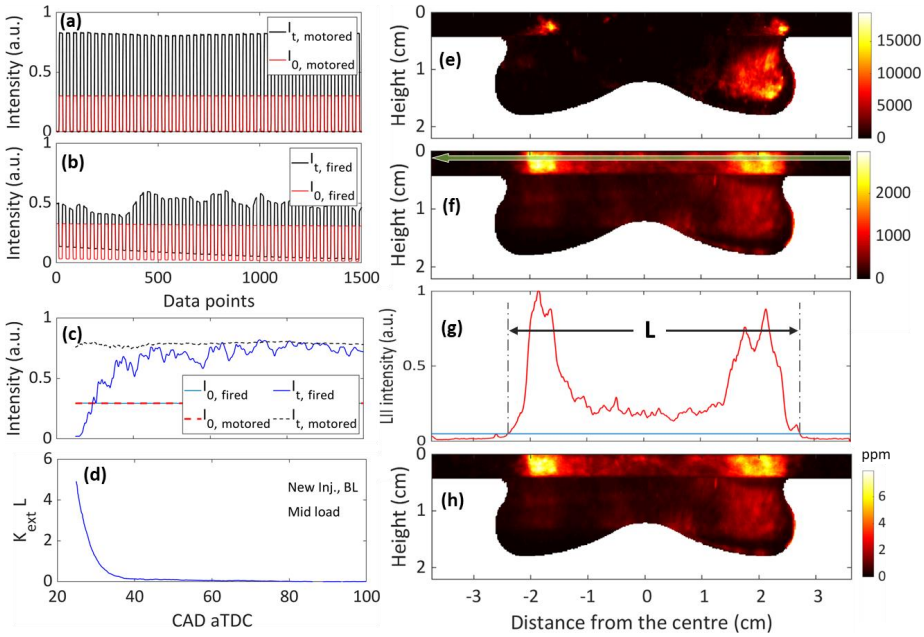

Figure 3: Calibration procedure for soot concentration measurements. Signal intensities for extinction measurements acquired in one motored cycle **(a)** and one fired cycle **(b). c)** Background-subtracted intensities for one motored and one fired cycle. **d)** $K_{ext}L$ for the new injector with baseline fuel at mid load condition averaged over 150 fired cycles. Background-subtracted distortion-corrected 2D LII signal at 30° CA aTDC; a single-shot **(e)** and the mean of 70 single-shots **(f)**. **g)** LII signal profile of the mean image along the extinction laser beam path, where *L* is the absorption length used for f_v evaluation. **h)** 2D f_v distribution in ppm for the new injector with baseline fuel for the mid load case at 30° CA aTDC.

Figure 3e shows a single-shot background-subtracted and distortion-corrected 2D LII signal at 30° CA aTDC for the case of new injector with baseline fuel at mid load condition. During the operation, soot deposits were formed on the optical components of the engine, mainly on the quartz piston and to some extent on the optical windows, which attenuated the LII signal. These optical components had to be regularly cleaned by dismounting the engine, and this cleaning was performed after 10-20 fired cycles. To achieve representative average data, around 70 cycles were needed and hence this value was chosen for the average data presented in this work. An example of an average LII signal image is shown in Fig. 3f. The detected LII signal is lower from regions within the bowl than above it due to multiple reasons. Firstly, more soot deposits are formed on the piston surface compared to the optical windows. The piston was cleaned after 10-20 cycles, but since there was some soot deposit building up during these 10 cycles, the signal transmission to the detector was reduced for the later cycles. Secondly, due to the curvature of the piston, some of the LII signal intensity originating from the piston bowl region is lost due to refraction. Thirdly, and probably the most important reason, is the difference in laser fluence between the regions above and below the piston bowl. The curvature of the piston leads to refraction of the incident laser beam and consequently to lower and more uncertain laser

fluences in regions inside the piston bowl resulting in lower LII signals. This is the reason why the region inside the piston bowl is not selected for quantitative analysis.

The spatial position of the extinction laser beam has been marked in Fig. 3f. The LII signal profile at this spatial position for the same case has been plotted in Fig. 3g. A cut-off at 5% of the maximum LII signal intensity was used to estimate the effective absorption length, L. The $K_{ext}L$ value for this case at 30° CA aTDC was obtained from Fig. 3d. Equation (2) was used to evaluate the soot volume fraction along this spatial position and later to obtain calibration constants for conversion of the LII signal intensity to absolute soot volume fraction f_v. The $K_{ext}L$ values for 25°, 30° and 35° CA aTDC were used to calibrate the LII images at the corresponding locations in the cycle for individual cases. However, as the accuracy of extinction measurements decreases at lower levels of extinctions (i.e. low soot concentrations), the calibration constant at CAD35 was used to also calibrate the LII images from 40° - 70° CA aTDC for each case. Figure 3h shows a 2D f_v distribution at 30° CA aTDC for the case of new injector with baseline fuel at the mid load condition. The colour-bar represents f_v in ppm.

4. Results

As mentioned in the previous section, the laser diagnostic data from LII and extinction measurements have been measured on a plane and along a line, respectively. This raises the question whether such data is representative of the combustion processes occurring in the engine chamber, which may be rather inhomogeneous. However, in this study we measure late in the cycle where the soot is fairly uniformly distributed in the azimuthal direction. This can be observed in Fig. 4 where the natural luminosity distribution imaged through the bottom of the quartz piston is shown at a few cycle locations late in the cycle. It can be seen that the soot is fairly uniformly distributed along the azimuthal direction. Hence, the planar soot volume fraction data has been treated as a representation of the entire combustion chamber during late cycle (CAs > 25° CA aTDC).

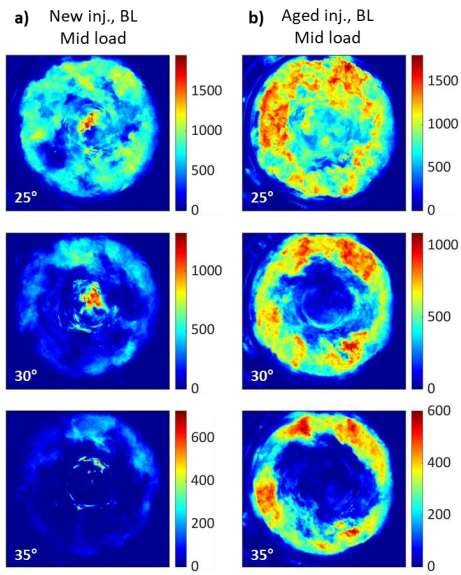

Figure 4: Natural flame luminosity (a.u) distribution imaged through the bottom of the quartz piston at the mid load conditions for new **(a)** and aged **(b)** injectors with baseline diesel fuel. The specific locations in the cycle in terms of CAD aTDC are marked in the respective sub-figures.

4.1 Soot oxidation from extinction

As discussed in section 3.2, $K_{ext}L$ is a measure of line-integrated soot concentration along the beam path of the extinction laser. Figure 5 shows the CA resolved $K_{ext}L$ values evaluated using extinction measurements for 3 cases at both low and mid load conditions: a) aged injector with baseline fuel, b) new injector using baseline fuel and c) new injector using the fuel with TPGME. Each individual curve is obtained after averaging 150 fired cycles. From these curves, one can observe how the soot concentration is decreasing with increase in CA. The CA resolved extinction data has been utilized in extracting soot oxidation rates in some previous studies [22, 28]. The strategy has been to use the evaluated half-lives of the exponential fits to the $K_{ext}L$ vs CAD aTDC curves to represent the rate of soot oxidation. Hence, shorter half-life value represents faster soot oxidation and vice versa. In the present study, it was found that the $K_{ext}L$ vs CAD aTDC curves deviate from the exponential behavior after around 35° CA aTDC, mainly due to poor signal-to-noise ratio at low extinction levels. Hence, exponential fits were generated for each curve until 35° CA aTDC and half-lives were extracted. The evaluated half-lives using the extinction data for all the cases are given in Table 4.

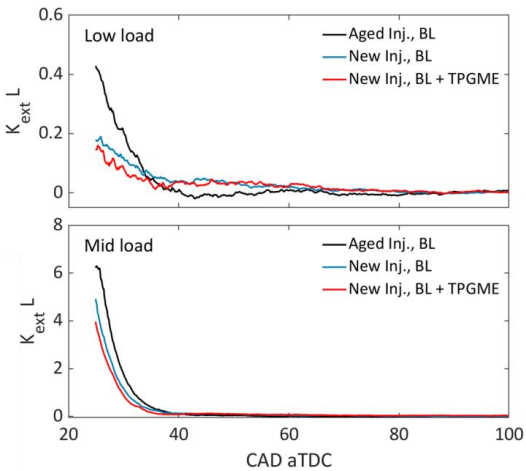

Figure 5: $K_{ext}L$ derived from extinction measurement vs crank angle degree after top dead centre (CAD aTDC) for low load and mid load conditions for three cases; (1) aged injector, baseline (BL) fuel, (2) new injector, baseline (BL) fuel, (3) new injector, TPGME additive.

Table 4: Half-lives (CAD) of soot oxidation rate evaluated from the extinction data for the low and mid load conditions for all the three cases.

Case	**Half-life (CAD)**	
	Low load	Mid load
Aged Inj., BL	3.2	2.36
New Inj., BL	6.0	2.39
New Inj., TPGME	4.8	2.21

The data was split into two sets for ease of comparison. In set one, the effect of injector ageing was studied while in set two, the effect of addition of TPGME was studied. Figure 5 shows that $K_{ext}L$ values of all the cases tend to approach zero for late in the cycle (higher values of CA) irrespective of the loads. The accuracy of extinction measurements was low late in the cycle as the transmitted signal intensity (I_t) during the fired cycle was close to the value of transmitted signal intensity during the motored cycle. This results in a low signal-to-noise ratio thus compromising the accuracy of the extinction technique. Hence the $K_{ext}L$ values later in the cycle are used neither to estimate net emissions nor for comparisons between the two sets mentioned above.

4.1.1 Effect of ageing of injectors

In Fig. 5, at low load conditions, the aged injector shows higher values of $K_{ext}L$ until around 32° CA aTDC compared to the new injector. This indicates that a higher amount of soot was formed in the case with the aged injector early in the cycle. This was also observed in another work where the aged injector consistently produced higher amount of soot compared to the new injector [5]. However, the case with the aged injector shows a faster decay and demonstrates an 82 % increase in the oxidation rate compared to the new injector. This behavior could be due to two main reasons. Firstly, it has been shown that the aged injector has a ~ 25 % higher load compared to the new injector at the same low load conditions [XX ref tests]. This higher load transpires into a slightly higher temperature which should increase both the soot formation and oxidation. Also, it has been shown that an aged injector produces a larger high-temperature region compared to a new injector [5]. Additionally, from our previous study, the aged injector has been seen to produce dribbles towards the end of injection [7]. Such dribbles generally lead to the formation of unburned hydrocarbons, but could also form soot.

In Fig. 5, at mid load conditions, the case with the aged injector produced higher amount of soot early in the cycle and showed soot concentrations higher than the new injector case throughout the cycle. The oxidation rates are generally faster for the mid load conditions compared to the low load conditions for the corresponding injectors. However, the oxidation rate for the aged injector case is similar to that of the new injector at the mid load condition, which can be explained in relation to the relative increase in the load for the aged injector case at both low load and mid load conditions. The low load case has a 25 % increase in the load for the aged injector compared to the new injector whereas, this increase is only 12 % at the mid load conditions [XX – ref tests]. Soot oxidation in diesel engines generally relies on late cycle mixing which is driven by air motion. At higher loads, the higher overall fuel amount will impart more momentum on the gas. If this is sufficient to provide adequate conditions for mixing, a small variation in the fuel amount (aged/new) may not have a large impact. At low loads, on the other hand, where a much smaller amount of fuel is injected, the gas motion becomes more critical, hence a small variation in fuel amount could have a relatively larger impact on the late cycle mixing. A 25 % increase in the amount of fuel injected thereby triggers more fuel-air mixing and hence a larger difference in the oxidation rate between aged and new injectors is seen at the low load conditions compared to the mid load conditions.

4.1.2 Effect of TPGME additive

Among the cases with the new injector being operated using baseline fuel and TPGME, a first interesting observation in Fig. 5 is that TPGME consistently produce lower $K_{ext}L$ values for both load conditions. Both load conditions also produce a similar drop of ~ 20 % in the peak $K_{ext}L$ values (at 25° CA aTDC) for the case with TPGME compared to the baseline fuel. Additionally, the case with TPGME has higher soot oxidation rates (corresponding to shorter half-lives in Table 4) compared to the one with baseline fuel for both loads. However, there is a larger increase in the soot oxidation rate for the fuel blend with TPGME at the low load condition compared to the mid load condition. This is contrary

to what is expected as oxygenated additives are found to perform better at higher load conditions [9]. This is discussed later in section 4.3 in conjunction with the analysis of the LII data. In a numerical study by Mueller et al. [10], it was found that all of the oxygen in the TPGME molecule is available for soot oxidation and TPGME does not form much unsaturated species that can lead to soot. The efficiency of the additive was also verified in their study using measurements in a constant-volume combustion vessel and an optical engine.

4.2 2D soot volume fraction distributions

Distortion-corrected 2D LII images were calibrated to absolute soot volume fraction (f_v) distributions using extinction measurements. These 2D f_v distributions for 25° – 70° CA aTDC for the aged injector with baseline fuel at mid load condition are shown in Fig. 6. The colour bars represent f_v in ppm. Due to the high curvature of the piston bowl geometry, the laser fluence at all points inside the piston bowl was not uniform and it cannot be certified that the fluence at all spatial positions was on the plateau of the fluence curve. As mentioned before in section 2.2, this condition is important for quantitative LII measurements. Hence, in this study, the region inside the piston bowl is discussed qualitatively, and the quantitative analysis is restricted to the region above the piston top where illumination of the soot by the laser sheet is fairly homogeneous. In this study, as the piston moves down from the laser sheet for certain duration in the late cycle (35° - 70° CA aTDC), it is not possible to image the full region inside the piston bowl late in the cycle. Reverse-squish flow, the flow from inside the piston bowl region outwards to the squish region is caused by the momentum transfer of the spray and the swirling gas motion. This brings the soot formed inside the piston bowl towards the squish region late in the cycle. Thus, the reverse-squish flow causes a more even distribution of soot in the whole combustion chamber and makes sure that the information in the squish region can be used as a representative of the whole combustion chamber. A general decrease in peak soot concentration can also be observed late in the cycle. This is attributed mainly to soot oxidation.

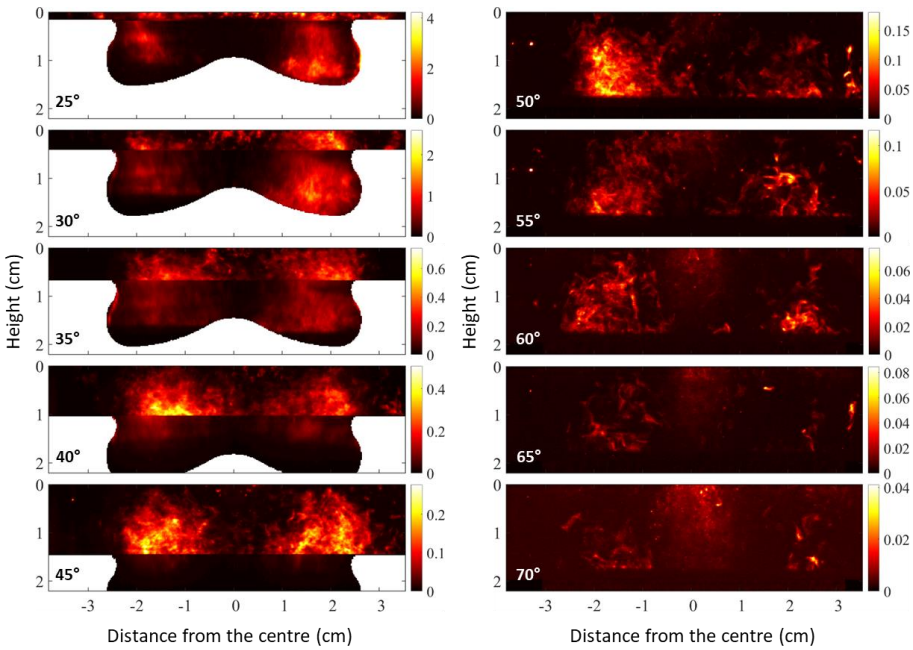

Figure 6: 2D soot volume fraction (ppm) distributions for 25° – 70° CA aTDC at mid load condition for the aged injector with baseline fuel.

4.3 Soot oxidation from calibrated LII images

Figure 7 shows the mean f_v at the region along the plane of the laser sheet above the piston top in a log-log plot. As pointed out earlier in this section, high-speed imaging measurements showed that the soot cloud becomes fairly evenly distributed in the cylinder late in the cycle [7]. Hence, this region may be assumed to be representative of the whole combustion chamber. Similar to the analysis of the $K_{ext}L$ data, half-lives (shown in Table 5) were evaluated by fitting exponential curves to the mean f_v vs CA curves. Soot oxidation rates can also be extracted from the slopes of the log-log plots shown in Fig. 7.

The 2D LII images represent a larger portion of the combustion chamber than the extinction data, making them more representative of the overall situation. Additionally, LII measurements were found to be ~ 80 times more sensitive than the extinction measurements, i.e. much lower soot concentrations could be measured with LII. Hence, the f_v values at 70° CA aTDC shown here can be used to draw parallels to the engine-out emissions. The $K_{ext}L$ curves in Fig. 5 also cement this argument as the variation in the $K_{ext}L$ values after 70° CA aTDC is very miniscule for both load conditions. Additionally, the $K_{ext}L$ curves in Fig. 5 have smaller half-lives compared to their respective counterparts obtained from evaluating the LII data. This could be due to larger area being covered by the LII images when compared to the extinction measurements which are line-of-sight averaged 1D measurements. However, the results from extinction and LII correlate very well with each other.

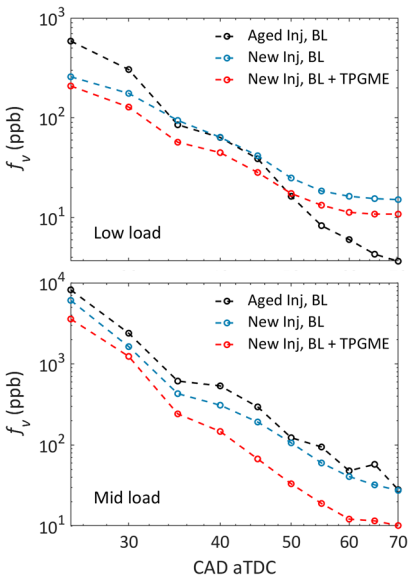

Figure 7: Mean f_v evaluated from LII measurements along the region of the laser sheet over the piston top vs CAD aTDC at mid and low load conditions for all the three cases.

Table 5: Half-lives (CAD) of soot oxidation rate evaluated from the LII data for the low and mid load conditions for all the three cases.

Case	Half-life (CAD)	
	Low load	Mid load
Aged Inj., BL	6.0	6.0
New Inj., BL	10.3	6.1
New Inj., TPGME	10.2	5.3

4.3.1 Effect of ageing of injectors

At low load conditions, similar to the extinction data, the aged injector show higher values of $K_{ext}L$ for 25° CA aTDC and 30° CA aTDC compared to the new injector. This underlines a higher soot formation for aged injector early in the cycle. There is an increase of 70 % in the oxidation rate for the aged injector compared to the new injector. It is apparent from the slopes of the curves in Fig. 7 that the aged injector case has a higher slope (in magnitude) compared to the new injector at low load condition. As mentioned before, the faster oxidation rate could be due to the higher fuel injection in the aged injector compared to the new injector resulting in higher temperatures. There is also a 76 % decrease in the final soot concentration at 70° CA aTDC for the aged injector compared to the new injector due to the faster oxidation rate for the aged injector case.

At mid load conditions, the aged injector still produced higher amount of soot early in the cycle. However, the oxidation rates are rather similar for the aged and the new injectors. As mentioned before in section 4.1.1, the relative increase in load for the aged injector compared to the new injector at mid load is only 12 % compared to the 25 % at the low load condition. This results in a smaller effect in mixing at the mid load condition compared to the low load condition. Additionally, there is little to no difference in the final soot concentrations at 70° CA aTDC for both the injector cases. So, the aged injector produced higher amount of soot early in the cycle for both load conditions. However, a faster oxidation rate was demonstrated by the aged injector only in the low load conditions resulting in lower soot very late in the cycle.

4.3.2 Effect of TPGME

When analysing the effect of soot reducer, it can be seen that like extinction data, the case with the soot reducer always produces lower amount of soot compared to the baseline fuel. At low load condition, it can be seen from Table 5 that the difference between the soot oxidation rates of both the cases are minimal. There is only a 29 % reduction in the soot concentration at 70° CA aTDC for the TPGME case at low load condition while there is a 63 % reduction for the mid load case. This could be due to the faster oxidation rates shown by the aged injector at mid load condition compared to the low load condition. Mueller et al. [9] states that studies from non-optical engines showed that addition of oxygenates in the fuel produced significantly less PM emissions, especially at higher load conditions. Hence it was seen that the soot reducer additive TPGME was more effective at mid load conditions compared to low load conditions.

5. Conclusions

In this study, the effects of ageing of injectors and presence of the oxygenated fuel additive, tripropylene glycol monomethyl ether (TPGME) on the combustion and the subsequent soot emissions in a light duty optical diesel engine were investigated. The laser diagnostic techniques laser-induced incandescence (LII) and extinction were used to study the effects of these parameters in an optical engine having the same piston geometry as a production engine. Measurements were performed at two load conditions on a set of aged and new injectors using baseline diesel fuel, and on the same new injector using a blend of baseline diesel with TPGME additive. LII data being two-dimensional and having a higher sensitivity compared to extinction data provide more accurate estimations of soot oxidation rates late in the cycle. The main conclusions are:

1. The aged injector produced higher soot concentration compared to the new injector for both of the loads. From our previous study [XX-ref tests] it was shown that the aged injector injects more fuel compared to the new injector for the same injection conditions. This leads to that the aged injector case showing higher soot formation.
2. The aged injector displayed a higher soot oxidation rate compared to the new injector at low load condition. It has been shown in our previous study that for the aged injector, the percentage increase in the fuel injection was higher at the low load condition compared to the mid load condition [XX - ref tests]. As a result of this larger percentage increase at the low load condition, late cycle mixing driven by the increased momentum transfer should be more predominant resulting in faster soot oxidation.
3. The fuel blend with TPGME produced lower soot concentrations compared to the baseline fuel for both of the loads.
4. The soot oxidation rate was higher for the TPGME case at the mid load condition, while at low load both the baseline and TPGME cases displayed rather similar oxidation rates.

6. Acknowledgements

This project has received funding from the European Union's Horizon 2020 research and innovation programme under the Marie Sklodowska-Curie grant agreement No 675528. It has also partly been funded by the Swedish Energy Agency through the KCFP Engine Research Center. The authors gratefully acknowledge Volvo Car Corporation and Afton Chemicals for providing injectors and fuels, respectively, for these studies.

7. References

1. R. Prasad, V.R. Bella, A review on diesel soot emission, its effect and control, Bulletin of Chemical Reaction Engineering & Catalysis 5 (2) (2010) 69.
2. S. d'Ambrosio, A. Ferrari, Diesel injector coking: optical-chemical analysis of deposits and influence on injected flow-rate, fuel spray and engine performance, Journal of engineering for gas turbines and power 134 (6) (2012).
3. P. Richards, R. Walker, D. Williams. Fouling of two stage injectors-an investigation into some causes and effects. SAE Technical Paper; 1997. Report No.: 0148-7191.
4. E. Mancaruso, L. Sequino, B.M. Vaglieco, C. Ciaravino. Coking effect of different fn nozzles on injection and combustion in an optically accessible diesel engine. SAE Technical Paper; 2013. Report No.: 0148-7191.

5. A. Magno, E. Mancaruso, B.M. Vaglieco, S. Florio, G. Gioco, E. Rebesco. Study on spray injection and combustion of fouled and cleaned injectors by means of 2-D digital imaging in a transparent CR diesel engine. SAE Technical Paper; 2013. Report No.: 0148-7191.
6. F. Königsson, P. Risberg, H.-E. Angstrom. Nozzle Coking in CNG-Diesel Dual Fuel Engines. SAE Technical Paper; 2014. Report No.: 0148-7191.
7. X. Zhu, Soot oxidation studies in an optical diesel engine using high speed imaging of soot luminosity and Mie scattering, (2020).
8. M.A. González D, W. Piel, T. Asmus, W. Clark, J. Garbak, E. Liney, M. Natarajan, D.W. Naegeli, D. Yost, E.A. Frame, Oxygenates screening for AdvancedPetroleum-Based Diesel Fuels: Part 2. The Effect of Oxygenate Blending Compounds on Exhaust Emissions, SAE Transactions (2001) 2246-55.
9. C.J. Mueller, G.C. Martin, Effects of oxygenated compounds on combustion and soot evolution in a DI diesel engine: broadband natural luminosity imaging, SAE Transactions (2002) 518-37.
10. C.J. Mueller, W.J. Pitz, L.M. Pickett, G.C. Martin, D.L. Siebers, C.K. Westbrook, Effects of oxygenates on soot processes in DI diesel engines: experiments and numerical simulations, SAE transactions (2003) 964-82.
11. C.E. Dumitrescu, A. Cheng, E. Kurtz, C.J. Mueller, A Comparison of Methyl Decanoate and Tripropylene Glycol Monomethyl Ether for Soot-Free Combustion in an Optical Direct-Injection Diesel Engine, Journal of Energy Resources Technology 139 (4) (2017).
12. C.E. Dumitrescu, C.J. Mueller, E. Kurtz, Investigation of a tripropylene-glycol monomethyl ether and diesel blend for soot-free combustion in an optical direct-injection diesel engine, Applied Thermal Engineering 101 (2016) 639-46.
13. J. Manin, S. Skeen, L. Pickett, E. Kurtz, J.E. Anderson, Effects of oxygenated fuels on combustion and soot formation/oxidation processes, SAE International Journal of Fuels and Lubricants 7 (3) (2014) 704-17.
14. H. Michelsen, C. Schulz, G. Smallwood, S. Will, Laser-induced incandescence: Particulate diagnostics for combustion, atmospheric, and industrial applications, Prog. Energy Combust. Sci. 51 (2015) 2-48.
15. H. Bladh, J. Johnsson, P.-E. Bengtsson, On the dependence of the laser-induced incandescence (LII) signal on soot volume fraction for variations in particle size, Appl. Phys. B 90 (1) (2008) 109-25.
16. J. Simonsson, N.-E. Olofsson, S. Török, P.-E. Bengtsson, H. Bladh, Wavelength dependence of extinction in sooting flat premixed flames in the visible and near-infrared regimes, Appl. Phys. B 119 (4) (2015) 657-67.
17. I. Boxx, O. Heinold, K. Geigle, Laser-induced incandescence measurements in a fired diesel engine at 3 kHz, Experiments in Fluids 56 (1) (2015) 3.
18. P.C. Miles, R. Collin, L. Hildingsson, A. Hultqvist, Ö. Andersson, Combined measurements of flow structure, partially oxidized fuel, and soot in a high-speed, direct-injection diesel engine, Proc. Combust. Inst. 31 (2) (2007) 2963-70.
19. J. Sjöholm, R. Wellander, H. Bladh, M. Richter, P.-E. Bengtsson, M. Alden, U. Aronsson, C. Chartier, O. Andersson, B. Johansson, Challenges for in-cylinder high-speed two-dimensional laser-induced incandescence measurements of soot, SAE International Journal of Engines 4 (1) (2011) 1607-22.
20. D.R. Tree, J.E. Dec, Extinction measurements of in-cylinder soot deposition in a heavy-duty DI diesel engine, SAE Transactions (2001) 1618-34.
21. W. Hentschel, J.-U. Richter, Time-resolved analysis of soot formation and oxidation in a direct-injection diesel engine for different EGR-rates by an extinction method, SAE transactions (1995) 1873-86.
22. Y. Gallo, J. Simonsson, T. Lind, P.-E. Bengtsson, H. Bladh, O. Andersson. A study of in-cylinder soot oxidation by laser extinction measurements during an EGR-sweep in an optical diesel engine. SAE Technical Paper; 2015. Report No.: 0148-7191.

23. L.M. Pickett, D.L. Siebers, Fuel effects on soot processes of fuel jets at DI diesel conditions, SAE transactions (2003) 2044-66.
24. H. Bladh, P.-E. Bengtsson, Characteristics of laser-induced incandescence from soot in studies of a time-dependent heat-and mass-transfer model, Appl. Phys. B 78 (2) (2004) 241-8.
25. S. Bejaoui, X. Mercier, P. Desgroux, E. Therssen, Laser induced fluorescence spectroscopy of aromatic species produced in atmospheric sooting flames using UV and visible excitation wavelengths, Combust. Flame 161 (10) (2014) 2479-91.
26. J. Simonsson, A. Gunnarsson, M.N. Mannazhi, D. Bäckström, K. Andersson, P.-E. Bengtsson, In-situ soot characterization of propane flames and influence of additives in a 100 kW oxy-fuel furnace using two-dimensional laser-induced incandescence, Proc. Combust. Inst. 37 (1) (2019) 833-40.
27. F. Liu, J. Yon, A. Fuentes, P. Lobo, G.J. Smallwood, J.C. Corbin, Review of recent literature on the light absorption properties of black carbon: Refractive index, mass absorption cross section, and absorption function, Aerosol Sci. Technol. 54 (1) (2020) 33-51.
28. G. Lequien, Ö. Andersson, P. Tunestal, M. Lewander. A Correlation Analysis of the Roles of Soot Formation and Oxidation in a Heavy-Duty Diesel Engine. SAE Technical Paper; 2013. Report No.: 0148-7191.